Lake hydrochemistry and aquatic plant diversity across permafrost landscapes of Yakutia, Eastern Siberia

Izabella Baisheva*[1§], Birgit Heim*[1§], Jorge García Molinos[2], Amelie Stieg[1], Hanno Meyer[1], Ramesh Glückler[1,3], Kathleen R. Stoof-Leichsenring[1], Antje Eulenburg[4], Pier P. Overduin[4], Evgenii S. Zakharov[5], Aital V. Egorov[5], Paraskovya V. Davydova[5], Lena A. Ushnitskaya[5], Sardana N. Levina[5], Ruslan M. Gorodnichev[5], Robert Jackisch[6], Antonie Haas[7], Nikolai V. Torgovkin[8,9], Stefan Kruse[1], Luidmila A. Pestryakova[5], Ulrike Herzschuh[1,10,11]

[1] Polar Terrestrial Environmental Systems, Alfred Wegener Institute Helmholtz Centre for Polar and Marine Research, 14473 Potsdam, Germany
[2] Arctic Research Center, Hokkaido University, 001-0021 Sapporo, Japan
[3] Department of Physical Geography, Utrecht University, 3584CB Utrecht, Netherlands
[4] Section of Permafrost Research, Alfred Wegener Institute Helmholtz Centre for Polar and Marine Research, 14473 Potsdam, Germany
[5] Institute of Natural Sciences, North-Eastern Federal University of Yakutsk, 677007 Yakutsk, Russia
[6] Institute of Landscape Architecture and Environmental Planning, Technical University Berlin, 10623 Berlin, Germany
[7] Computing and Data Centre, Alfred Wegener Institute Helmholtz Centre for Polar and Marine Research, 27570 Bremerhaven, Germany
[8] Melnikov Permafrost Institute, 677010 Yakutsk, Russia
[9] Northeast Forestry University, 150040 Harbin, China
[10] Institute for Environmental Science and Geography, University of Potsdam, 14476 Potsdam, Germany
[11] Institute for Biochemistry and Biology, University of Potsdam, 14476 Potsdam, Germany
* *Equal contributions:* Izabella Baisheva and Birgit Heim
§ *Correspondence to*: Izabella Baisheva (izabaiant@gmail.com) and Birgit Heim (birgit.heim@awi.de)

Abstract. Freshwater ecosystems are a major feature of northern landscapes that are expected to experience significant future changes due to climate change and land-use alterations. To undertake an assessment of lake characteristics and drivers, we analysed lake hydrochemistry (ion hydrochemistry, stable water isotopes, dissolved organic carbon (DOC)) and sedimentary DNA (sedDNA)-derived aquatic and terrestrial plant diversity from a wide range of lakes sampled in summer 2021 in Eastern Siberia. There in the Central Yakutian lowland, abundant lakes in topographic permafrost-thaw depressions, named alaas, and larch dominated boreal forests define the traditional cultural landscape that is home to the indigenous Sakha people, with critical ecosystem services like freshwater supply, meadows for cattle breeding, as well as fishing and hunting grounds. We classified the sampled thermokarst lakes into three successional thermokarst lake stages: new thermokarst lakes, old alaas lakes and connected alaas lakes. In contrast to lakes of the Yakutian lowland alaas-dominated landscape, lakes on the Verkhoyansk Oymyakon high mountain plateau represent deeper and more oligotrophic lake systems much less used as human resources. SedDNA-derived macrophyte diversity in lake surface sediments reflects the different lake types that we could distinguish using lake morphology and hydrochemistry. It also reveals a dominance of brackish water-tolerant cosmopolitan submerged macrophytes, particularly *Stuckenia* and *Potamogeton*, across all lakes. In contrast, the macrophytes *Myriophyllum* and *M. verticillatum* are exclusively found in mountain lakes and in freshwater lakes in the lowlands, supporting their indicator value for freshwater conditions. The hydrochemical analysis reveals a clear distinction between low-mineralised mountain lakes and the highly variable hydrochemistry of the lowland lakes with much higher mineral content. Mountain lake hydrochemistry seems to be mainly determined by the climate, whereas the environmental drivers of hydrochemistry in the lowland thermokarst lakes are more diverse. The lake developmental stage within the thermokarst lake sequence (new thermokarst lakes, alaas lakes, connected alaas lakes) most likely is a key driver for anorganic, isotopic and organic lake hydrochemistry of the lakes in the Central Yakutian lowland. Specifically, the thermokarst lake's developmental stage is reflected by DOC, pH, its stable water isotopic composition and the hydrochemistry of alkali and earth alkali elements.

Several new thermokarst lakes show a lighter stable water isotopic composition than alaas lakes and connected alaas lakes, possibly due to contributions from meltwater of adjacent old permafrost ground-ice. New thermokarst lakes are also characterised by high DOC and mainly located in forest. In contrast, connected alaas lakes that are typically located in large alaas systems where settlements and managed land use is located show lower DOC and lower mineralisation despite their location close to anthropogenic influence. We assume that temporary high discharge, such as the snowmelt, enables dilution, lowering organic and mineral contents in these lakes. In contrast to the more diluted connected alaas lakes, old alaas lakes show a heavier oxygen isotope composition and high mineral content due to contemporary evaporation in summer highlighting their vulnerability to future warming. However, some of the sampled high-salinity lakes show low chloride despite high salinities and enriched isotopic composition and are characterised by elevated fluoride concentrations. As these sampled lakes are far from settlements and managed land use, human influence cannot cause the high fluoride levels. This points to an additional process beyond the current evaporation for these specific lakes, such as leakage from older lacustrine sediments or salt deposits in permafrost.

Our results provide a detailed examination of lake systems in modern conditions within highly climate-sensitive lowland and mountain permafrost landscapes. Future warming and prolonged exposure to evaporation may lead to more extreme evaporation. On the other hand, enhanced permafrost degradation and rising surface water discharge as it is already observed in Eastern Siberia may also lead to higher hydrological connectivity and an increase of connected alaas lakes, this case providing more freshwater to the region. New thermokarst lakes also provide good water quality supporting traditional land uses such as fishing and drinking water resources for humans and forest wildlife.

Keywords:

Lakes, ion hydrochemistry, sedDNA, macrophytes, stable water isotopes, alaas, thermokarst lakes, land cover, permafrost

1 Introduction

Climate change is occurring at an accelerated rate particularly at high latitudes (Bekryaev et al., 2010; Serreze and Barry, 2011; Walsh, 2014; IPCC, 2022; Rantanen et al., 2022). Global warming has profound consequences, including the rapid warming and degradation of permafrost (Romanovsky et al., 2010; Nitze et al., 2018; Biskaborn et al., 2019; Smith et al., 2022; Miner et al., 2022), especially in areas with sedimentary Yedoma deposits rich in ground-ice, which are particularly vulnerable to permafrost degradation in the future (Strauss et al., 2017; Nitzbon et al., 2020). In this context, boreal forests and permafrost are recognised as critical tipping elements in the planetary climate system (Wang et al., 2023; Rockström et al., 2024), potentially acting as environmental drivers of change in high-latitude surface waters. The Conservation of Arctic Flora and Fauna (CAFF) working group of the Arctic Council has already reported changes in freshwater chemistry across the Northern Hemisphere with a major data gap located in Eastern Siberia (Lento et al., 2019, 2022; Huser et al., 2020; Aronsson et al., 2021). In the Republic of Sakha (Yakutia) in Eastern Siberia, lakes are a dominant landscape form with an estimation of over 700000 lakes (Rumyantsev et al., 2012) and a human population of less than a million unevenly distributed over a vast territory of 3084 million km^2 (Sukneva, 2021). Access to running water and sewage services is limited (Dudarev, 2018), also in the populated Central Yakutia region. Lakes are the main source of drinking water for humans and livestock, and provide other resources such as fishing (Crate et al., 2017; Naumov et al., 2020; Desyatkin et al., 2021).

Deciduous needleleaf boreal forests represent the dominant land cover across the Eastern Siberian boreal region leading to enhanced ion content and alkalinity input into the lakes (Herzschuh et al., 2013), which are predominantly shallow and eutrophic (Pestryakova et al., 2012). Future changes in lake hydrochemistry, lake and lake catchment geomorphology, and surrounding ecosystems are expected to have a large impact on the local population, making it crucial to understand the current state and drivers of these Northern lakes that are expected to undergo significant changes in response to climate change.

In Central Yakutia, lakes mainly occur as residual lakes in large thermokarst basins and as comparatively young permafrost thaw lakes on the larch forest covered uplands (e.g., Pestryakova et al., 2012; Ullrich et al. 2017a,b, 2019). The formation and development of thermokarst lakes is the most abundant form of permafrost degradation (Grosse et al., 2013) with different evolutionary stages (e.g., Marsh et al. 2009; Jones et al. 2011; Kokelj and Jorgenson, 2013; Bouchard et al., 2017). As thermokarst lakes follow a complex sequential development, lake stages may show distinct initial and secondary lake stages and different lake stages can co-exist within a region (Jorgenson and Shur, 2007; Manasypov et al., 2014; Bouchard et al., 2014, 2017; Ullrich et al. 2017b, 2019). The unique permafrost landscape of the central Yakutian lowland was formed by intense thermokarst processes in ice-rich permafrost starting during the Holocene warming (12–11 cal ka BP), which subsequently developed into an “alaas” (in Sakha language Алаас) landscape initiated in the Holocene Thermal Maximum (8.2–5 cal ka BP) (Katamura et al., 2006; Biskaborn et al., 2012; Pestryakova et al., 2012; Biskaborn et al., 2016; Ulrich et al. 2017a) with alaases representing remnant depressions from successive permafrost degradation due to ponding and the successive development of larger lakes and their recession. The different evolutionary lake types in this continuous permafrost landscape can be classified according to the Central Yakutian thermokarst lake chronosequence (Bosikov, 1991; Soloviev, 1959; Desyatkin and Desyatkin, 2006; Desyatkin, 2009; Fig. A18). The first stage called "byllar" (in Sakha language Быллар) starts with the formation of small depressions and ponding due to the melting of ground-ice, specifically of low-center polygons and ice wedges. Eventually, the system moves into the next stage where several ponds form a "dyede" lake (in Sakha language Дүөдэ/Дьүөдьэ); a semi-rounded shallow lake with an ice-wedge derived polygonal pattern on the bottom and steep banks (Soloviev, 1959). The next lake stage, the "tyympy" lake (in Sakha language Тыымпы) forms when the water bodies further enlarge by thermal and mechanical erosion into the surrounding ice-rich permafrost, resulting in further basin subsidence and increasing water volume (Bosikov, 1991). More recently, new thermokarst lakes are forming much more rapidly, in just a few decades, initiated by human land use or fire disturbance (Fedorov et al., 2014; Ulrich et al., 2017a) and after agricultural land has been abandoned and in settlement areas (Lytkin et al., 2021; Zhirkov et al., 2023; Suleymanov et al., 2023). In this study, we refer to lakes of both, dyede and tyympy stage in the following as ‘new thermokarst lakes’. The hydrochemical properties

of these newly forming thermokarst lakes remain so far largely uncharacterised in the literature. Consequently, their potential to develop into viable habitats or resource bases for the Yakut people is not yet understood.

Continuing with the thermokarst lake chronosequence, the larger and deeper mature lakes develop an underlying talik (i.e. a thaw bulb) characteristic for the continuous permafrost zone (Grosse et al., 2013). Finally, in this mature thermokarst lake stage, evaporation or draining may cause a thermokarst lake to recede, resulting in residual lakes at the lowest points of topographic depressions with refreezing processes of the underlying lake talik (Soloviev, 1959; Desyatkin, 2008; Ulrich et al., 2019). Residual alaas lakes are usually shallow, although they also may reach depths of several meters, and are called in the following 'old alaas lakes'. In a further stage, lakes can further become hydrologically connected in strongly degraded and interconnected alaas systems, eventually only temporally during high discharge events when water levels are high, such as during the annually occurring snow melt. These lakes, in the following called 'connected alaas lakes', are larger in lake area and often more elongated and irregular in shape and deeper and are described as a thermokarst lake type typical for the Central Yakutian alaas landscape (Ulrich et al., 2017b; Hughes-Allen et al., 2023).

Hydrochemistry such as the concentrations of major and minor ions and dissolved organic carbon (DOC) can reflect natural environmental and climatic processes as well as land cover and human activities in the lake environments (Hu et al., 2020; Du et al., 2023). Previous studies of contemporary lake hydrochemistry in Yakutia (Kumke et al., 2007; Pestryakova et al., 2012) investigated hydrochemistry related to specific lake types, however, could not yet link it to different lake types as a potential driver, with the notable exception of less mineralised sand-dune lakes in contrast to all other sampled lowland thermokarst lakes.

In this study, we sampled and investigated a wide range of lakes across two contrasting permafrost landscapes: the eastern Central Yakutian lowland (hereafter Central Yakutia) and the Verkhoyansk Oymyakon high mountain plateau (hereafter Verkhoyansk mountain region). In contrast to the sampled Central Yakutian lowland lakes that we can link to the Yakutian thermokarst lake chronosequence, the sampled mountain lakes in the Verkhoyansk Mountain region represent different aquatic ecosystems. These lakes are partly glacial lakes, partly thermokarst lakes and characterised by cold and deep water bodies with low nutrient and mineral contents, in the following 'mountain lakes'.

We examined a comprehensive dataset of lake hydrochemistry on ion chemistry, stable water isotopes, hydrophysics and aquatic plant diversity derived from sedimentary DNA (sedDNA) from lake surface-sediments of the sampled lakes. DNA-derived data on vegetation and animals are powerful tools for biodiversity monitoring, also enabling the reconstruction of aquatic and terrestrial organisms (Thomsen et al., 2015; Taberlet et al., 2018). SedDNA-derived lake macrophyte abundance is potentially linked to hydrochemical and morphological characteristics of lakes (Stoof-Leichsenring et al., 2022; Revéret et al., 2023a,b; Li et al., 2024; Różańska-Boczula and Sender, 2025). Furthermore, the Directive 2000/60/EC of the European Parliament (2000) proposes macrophyte composition, particularly submerged macrophytes, as indicator for water quality because aquatic macrophyte diversity, including richness and composition, can indicate lake trophic states (Bennion et al., 2000). In their extensive SedDNA dataset from surface sediments in lakes in Eastern Siberia and the high Tibetan Plateau, Stoof-Leichsenring et al. (2022) identified lake depth, specific electrical conductivity (EC), and July mean temperature as the main environmental drivers of macrophyte diversity.

Our objectives are, therefore, to (i) assess the inorganic, organic, and stable water isotopic lake hydrochemical diversity and sedDNA-derived macrophyte diversity from our 2021 field work for mountain lakes in the Verkhoyansk mountain region and lowland thermokarst lakes of Central Yakutia, and (ii) identify potential environmental drivers of lake hydrochemistry and lake-specific aquatic plant diversity, with a particular focus on the role of land cover and the lowland thermokarst lake sequence.

2 Data and methods

2.1 Study area

The study area spans a substantial region of over 700 km from west to east, extending from Central Yakutia between the Lena, Aldan, and Amga rivers to the Oymyakon high mountain plateau in the Yakutian Verkhoyansk mountain region (Fig. 1). Central Yakutia is characterised by an extreme subarctic continental climate, with long cold and dry winters (mean monthly temperature in January −41.3 °C) and warm summers (mean monthly temperature in July +19.3 °C) (Yakutsk city, 62.01°N, 129.43°E, 98 m a.s.l.). The Central Yakutian lowlands feature a unique, lake-rich alaas landscape with a relatively high population density and land-use management contributing to a predominance of grassland around lakes within the alaas systems (Zakharova et al., 2018). The main settlements east of the Lena River include Nizhny Bestyakh, Maya, Churapcha, and Ytyk-Kyuyel (Fig. 1D). The main settlement in the Yakutian Verkhoyansk mountain region is Oymyakon (Fig. 1C).

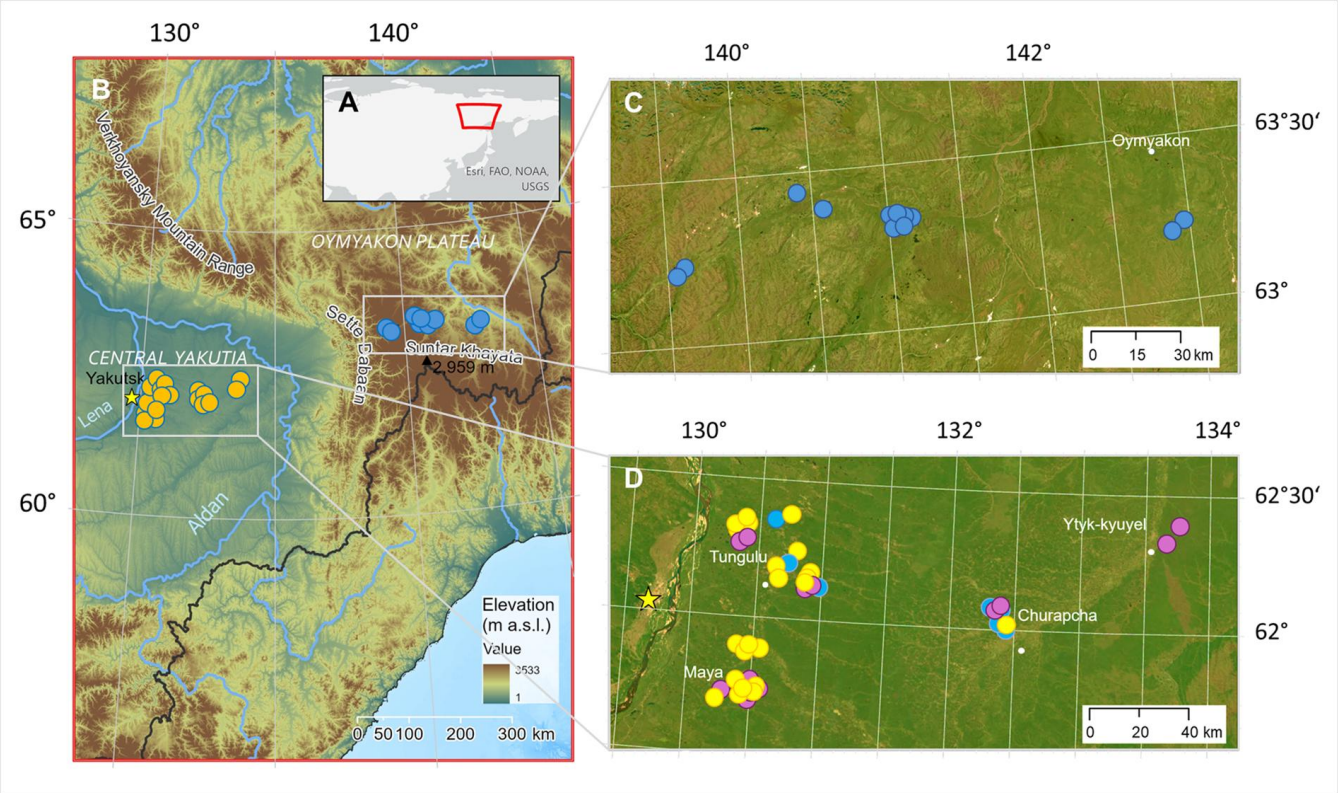


Figure 1: (A) Map overview on Asia with the image border of map B in Eastern Siberia. (B) Map overview on the sampled lakes of the Yakutia 2021 expedition covering the eastern Central Yakutian lowland in the West and the Oymyakon high mountain plateau in the Verkhoyansk mountains in the East. The yellow star shows Yakutsk, the capital of the Republic of Sakha. Background topography is the colour-coded GEBCO Compilation Group 2021. GEBCO Grid. Source: Esri, Maxar, Earthstar Geographics, and the GIS User Community. (C) Overview of the sampled Verkhoyansk mountain lakes (dark blue circles), and the settlement Oymyakon (white circle). (D) Overview of the sampled lakes in the Central Yakutian lowland are colour-coded per lake type (connected alaas lakes (light blue circles), old alaas lakes (yellow circles), new thermokarst lakes (violet circles). The settlements Maya, Tungulu, Churapcha and Ytyk-Kyuyel are marked with white circles, the yellow star marks the city Yakutsk. Background images are ©ESRI World Imagery (C,D).

Central Yakutia is characterised by extensive summergreen needleleaf larch forests, transitioning from pure larch stands in Eastern Central Yakutia westwards into a belt of mixed forests with stands of evergreen needleleaf tree species along the western and the eastern banks of the Lena River due to deeper thaw depths on sandy lithologies (Troeva et al., 2010; Kruse et al. 2018, 2020; Miesner et al., 2022; van Geffen et al., 2022, 2025; Enguehard et al., 2024). The alaases are non-forested, mainly covered by meadow, but also steppe, and semi-desert herbaceous plant communities occur there (Danilov, 2005) and few agricultural sites, the majority of them abandoned since the Soviet Union times. In Central Yakutia, ultra ice-rich sediments widely occur as part of the Pleistocene to Early Holocene Ice Complex (Romanovsky, 1993; Brouchkov et al., 2004), respectively, Yedoma (Strauss et al., 2017). They are the lithologically dominant units under the forested uplands, whereas

the topographical depressions of the alaases are covered by younger Holocene sediment infilling and more recent deposits due to anthropogenic activities such as agriculture (e.g., Windirsch et al., 2020; Ulrich et al., 2021).

The sampled lakes in the Central Yakutian lowland are distributed across four morphologically defined terraces described in Soloviev (1959) and Zakharova et al. (2018). In the west are the younger and lower terraces, getting older and higher towards the east. From west to east, the Bestyakh terrace, a non-dated terrace with mainly alluvial sand and gravel deposits located along the eastern bank of the Lena River, gives place to the Tungulu terrace (22–14 cal ka BP), with mainly loamy sand, loess and lacustrine/bog sediments, while the Abalakh terrace (56–45 cal ka BP) with silt and loamy deposits gives place to the Magan terrace with the highest elevation and a stratigraphy of mostly loamy deposits of Middle Pleistocene origin. The Tungulu and Abalakh terraces' are specifically characterised by the abundance of Yedoma with a very high concentration of ground-ice together with its high degradation potential.

East of the Central Yakutian lowland, the Verkhoyansk mountain range rises as part of the western segment of the Verkhoyansk fold-and-thrust belt (Khudoley and Prokopiev, 2007) composed of terrigenous and carbonate sedimentary rock from the Riphean, Palaeozoic and Mesozoic. The Suntar Khayata mountain range, with Muus-Khaya ("Ice Mountain" in Sakha) as its highest peak (2959 m a.s.l.), and the Oymyakon high mountain plateau (around 1200 m a.s.l) are located within the southernmost part of the Verkhoyansk mountains. The Oymyakon high mountain plateau is also known as the cold pole of the Earth because of its extreme continentality, with extremely low minimum winter temperatures (-67.7 °C) due to the permanent position of the winter Siberian High, which is further exacerbated by the strong topographic temperature inversions in winter (Shahgedanova, 2003). The landscapes of the Oymyakon high mountain plateau are characterised by wide braided river valleys punctuated by small lakes, while a high number of lakes are also located in mountainous terrain on rock or in glacial moraine belts. These mountain slopes are covered by open larch forests, which give way to mountain tundra as elevation increases, at around 2000 m a.s.l.. Lakes in this region remain ice-covered for most of the year, representing oligotrophic aquatic ecosystems, and are largely unaffected by human activity apart from sparse settlements and occasional fishing and hunting.

2.2 Fieldwork

In August 2021, we sampled 66 lakes in the Central Yakutian lowland and the Verkhoyansk mountain region (Fig. 1, Table A1) with fieldwork described in detail in Morgenstern et al. (2023). For the Yakutian lowland region, we pre-selected lakes according to the different terraces, land cover, lake area and forms, including recommendations from Sakha scholars. For the mountain region, we pre-selected lakes according to different land cover, altitude and lake area and recommendations from Sakha scholars. We assigned name codes (EN21401 to EN21467) according to the temporal order of the sampling, as the majority of the smaller sampled lakes have no officially recognised names. Of the 66 sampled lakes, 15 lakes (EN21401 to EN21415) are located within the Verkhoyansk mountain range at elevations ranging from 789 m to 1310 m a.s.l., primarily on the Oymyakon high mountain plateau (Fig. 1B,C) and 51 lakes in the Central Yakutian lowland at elevations between 115 m to 307 m a.s.l. (Fig. 1B,D). In the pre-selection, we methodologically could not robustly determine the thermokarst lake stages, and opted to capture a large variety of lakes in different land cover settings across climate gradients.

The geographic coordinates and elevation according to the World Geodetic System 1984 (WGS 84) of the sampling locations in the central parts of the lakes were recorded with GPS devices (Garmin, GPSMAP67i) from an inflatable boat. We measured lake-water depth, transparency, hydrophysical properties, and collected water and surface-sediment samples at the deepest part of the lakes (Fig. A1). Lake depth was measured across the lakes using a handheld Echo-Sounder (Hondex PS-7) and lake transparency with a Secchi disk that was lowered on the shady side of the boat until the white part of the disk was no longer visible. Physical parameters, such as EC and pH, were measured using a Multi-340i device (WTW, Germany) directly in the upper water layer in the Verkhoyansk mountain range. In the Central Yakutian expedition part, EC and pH were measured at the camp field laboratory on the same day of water sampling. The water samples were collected from the boat from the upper water layer at a sampling depth of 0.5 m into sterile 2 L sample containers (Whirl-Pak®).

The fieldwork treatment of water samples for anions and cations involved a filtration step using 0.45 µm pore-size pre-syringe cellulose-acetate filters. Filtrated anion samples were directly stored in 8 mL wide-mouth bottles (Nalgene), while filtrated cation samples were placed in 15 mL tubes (Falcon) and preserved by adding suprapure 65 % HNO_3. Water samples for DOC were filtered through 0.7 µm pore-size pre-syringe glass fibre filters and stored in 20 mL glass vials (Scientific Fisher) with 30% HCl solution added for preservation. Water samples for stable water isotope analysis were collected either directly from the lake into 30 mL narrow-mouth polyethylene bottles or transferred from the water sample container, filled to the top and sealed tightly. Additionally, a single rain event that occurred during the field work time on 22 August 2021 was sampled for stable water isotope measurements at the Tungulu campsite in Central Yakutia. Except for the isotopic samples that were collected with three separate bottles, all water samples prepared for the specific analyses were sampled and prepared as one sample. Lake surface-sediment was collected from a HYDRO-BIOS grabber, subsampled with sterile spoons and stored in 250 mL bottles (Nalgene). All samples were stored and transported in cool and dark conditions until analysis.

During the fieldwork, we conversed with local Sakha people on lakes as a resource for the local population and included excerpts of their knowledge in our study according to the recommendations of McCartney et al. (2022). We also included traditional indigenous knowledge from the author team, Izabella A. Baisheva, Evgenii S. Zakharov, Aital V. Egorov, Paraskovya V. Davydova, Lena A. Ushnitskaya, Sardana N. Levina, and Luidmila A. Pestryakova, who were born in the Republic of Sakha (Yakutia; Sakha Sire, Ksenofontov et al., 2025) and identify themselves as Sakha scholars.

2.3 Laboratory analysis

Dissolved inorganic and organic hydrochemistry

The dissolved ionic water composition and DOC was measured at the Hydrochemistry Laboratory of the Alfred Wegener Institute Helmholtz Centre for Polar and Marine Research, Potsdam, Germany (AWI). Major cations (magnesium (Mg^{2+}), calcium (Ca^{2+}), sodium (Na^{+}), potassium (K^{+})) and metals (aluminium (Al^{3+}), iron (Fe^{2+}), manganese (Mn^{2+}), strontium (Sr^{2+})), were measured using inductively coupled plasma optical emission spectrometry (ICP-OES; Perkin-Elmer, Optima 8300 DV). Major anions (chloride (Cl^{-}), fluoride (F^{-}), sulfate (SO_4^{2-})) and minor ions (barium (Ba^{2+}), bromide (Br^{-})) were measured using ion chromatography (ICS; Thermo Scientific, Dionex ICS-2100). Hydrogen carbonate (HCO_3^{-}) was analysed by potentiometric pH endpoint titration up to pH 4.3. Total dissolved solids (TDS) were calculated using the sum of major cations and major anions. DOC was measured as Non Purgeable Organic Carbon (NPOC) using a TOC-VCPH 2.00 device with a detection limit of 0.25 mg L^{-1} (Shimadzu, Japan) involving a catalytic combustion process at 680°C.

Stable water isotopes ($\delta^{18}O$, δD)

Oxygen and hydrogen stable water isotopes were measured at the ISOLAB Facility at AWI, with a Finnigan MAT Delta-S mass-spectrometer following the equilibration method after Meyer et al. (2000). The isotope compositions of hydrogen and oxygen are represented using the δ-notation (δD and $\delta^{18}O$) in per mille (‰) versus Vienna Standard Mean Ocean Water (V-SMOW) as the standard. The standard deviation includes all measurements of three samples per lake, which remains better than the external error of long-term standard measurements of ±0.8‰ for δD and ±0.10‰ for $\delta^{18}O$ (Meyer et al., 2000). The second order parameter, deuterium excess (d) was calculated as $d = \delta D - 8 * \delta^{18}O$, using the mean δ-values, according to Dansgaard (1964). The global linear relationship between hydrogen and oxygen isotopes is represented by the global meteoric water line (GMWL; Craig, 1961). Local evaporation lines (LELs) were calculated by fitting a linear regression to the $\delta^{18}O$ and δD values of the lake water samples for all lowland lakes as $Yak21_{Lowland}$, and mountain lakes as $Yak21_{ML}$ and separately by lowland thermokarst lake types (connected alaas lakes ($Yak21_{CAL}$), old alaas lakes ($Yak21_{OAL}$), new thermokarst lakes ($Yak21_{NTL}$). As the stable isotopic composition ($\delta^{18}O$ and δD) in lakes may be also influenced by additional water sources from the surrounding we further included stable isotopic data from Yedoma ground ice from ice wedges and segregated ice in Central Yakutia (Popp et al. 2006; Windirsch et al., 2019, 2020; Ulrich et al., 2021; Pavlova et al., 2024; Torgovkin et al.,

2024). The slope values of the LELs were compared to the GMWL, the Local Meteoric Water Line (LMWL) for Yakutsk based on monthly mean precipitation data from Kloss (2008) and to an existing LEL of Central Yakutian lakes (Wetterich et al., 2008) to characterise the isotopic signature of the investigated lake waters and to assess the effects of secondary processes.

Sedimentary DNA from aquatic and terrestrial plants

SedDNA extraction to polymerase chain reaction (PCR) was conducted for the lake surface-sediment samples in the paleogenetic laboratories at AWI under a cleaned and UV-irradiated working hood (Biosan, Latvia). DNA extractions were performed using the Dneasy PowerSoil Max DNA Isolation Kit (Qiagen, Germany) with about 5–8 g sediment input, following Epp et al. (2019). Sediments were added into 15 mL PowerBeadPro tubes with 1.2 mL C1 buffer (VWR International, Germany), 0.4 mL Proteinase K (VWR International, Germany), 0.1 mL 5M dithiothreitol solution (VWR International, Germany) and vortexed for 30 s on the highest speed. Samples were homogenised using FastPrep-24 bead beating grinder (Biomedicals, USA) for 50 s and in an incubator with a rotating system at 56°C overnight. For each extraction batch, one extraction blank and No Template Controls for PCR preparation step were added to control for potential chemical contamination during the DNA extraction and PCR setup following Zimmermann et al. (2017). Extracted sedDNA was combined and concentrated with the GeneJet PCR purification kit (Thermo Scientific, USA). The concentrated DNA was quantified with a broad-range sedDNA Assay Qubit Fluorometer (Invitrogen, USA) with DNA diluted to 3 ng μL^{-1} for initial input into the PCR reactions. For PCR set-up we followed Baisheva et al. (2023) with standard primers targeting the chloroplast trnL P6 loop amplification of vascular plant DNA metabarcoding (Taberlet et al., 2007). The APMG-60 pool of PCR samples was prepared by Fasteris (Genesupport, Fasteris SA, Switzerland) into a PCR-free library using the metafast protocol and sequenced in paired-end mode on a NextSeq Illumina sequencing device with the NextSeq Mid kit (Illumina).

DNA amplicon sequencing and taxonomic assignment

After Illumina sequencing, datasets of the sequenced plants were processed using OBITools3 (https://git.metabarcoding.org/obitools/obitools3) following the bioinformatic pipeline after Boyer et al. (2016). Data were combined using the "*obi alignpairedend*" command to align forward and reverse reads and "*obi grep*" was used to remove unpaired reads. To allocate reads to the corresponding combinations of primer tags the command "*obi ngsfilter*" was used. Grouping and counting of identical sequences was performed using "*obi uniq*". Denoising data using "*obi annotate*" removed sequences with <10 counts and <10 length. The taxonomic assignment was conducted by using the customised database for Siberian plants "SibAla" (Courtin et al., 2025). Output data separation into terrestrial and aquatic plants followed Baisheva et al. (2024). One lake (EN21436) with no sedDNA counts amplified and EN21432, 440, 431 with zero to only two counts were discarded from the terrestrial plant dataset. The final data consists of 62 lake surface sediment samples containing more than 8,606,990 counts, of which 6,729,397 are aquatic plants (78 %) and 1,877,639 are terrestrial plants (22 %). We then divided macrophytes into four functional groups as floating, submerged, submerged-emergent, and emergent macrophyte types (following Stoof-Leichsenring et al., 2022; Baisheva et al., 2023, 2024; Różańska-Boczula and Sender, 2025). Emergent plants include all plants which typically occur in marshlands, wetlands, bogs, and wet, boggy soils. Terrestrial plants were divided into three main functional groups: trees, shrubs (including subshrubs), and graminoids and forbs comprising one group (following Baisheva et al., 2024) including bryophytes (following Herzschuh et al., 2025).

2.4 Lake type classification

Multiple Unoccupied Aerial Vehicle (UAV) transects were flown at the 2021 expedition using a Yellowscan Mapper LiDAR (Light detection and ranging) sensor employed on a DJI M300 RTK UAV scanning the morphology together with a consumer-grade DJI Phantom-4 quadcopter acquiring multispectral (Blue, Green, Red, Red-edge and Near-infrared (NIR)) images

specifically along lake shorelines. For small to medium lakes, we mapped the lakes along their full shorelines, for large lakes we mapped representative sections of the lake shores. The LiDAR point cloud data was processed using proprietary software (Yellowscan, France) to derive digital surface and elevation models of resolutions at 5-10 cm per pixel (Fig. 2) (Kruse et al., 2023a-c, 2026). The multispectral UAV overflights for each lake were mosaiced together from flight-corrected flight stripes in the lake-specific area-true Universal-Transverse-Mercator (UTM) projection using Agisoft Metashape Professional and are published as multispectral orthomosaics (Stieg et al., 2023a,b). Using QGIS Geographic Information System 3.22.3, we manually delineated the lake shorelines for each lake using the NIR orthoimage as it contains the highest contrast between water and the land surface.

For 13 out of 66 lakes, lakes could not be surveyed in the field due to bad weather or the lake shore was only partly mapped because of the large lake size. In this case, we then manually digitised the lake shores on an ESRI high-resolution background image. Transforming all digitised lake outlines in their respective area-true UTM zones (UTM N52,53,54), we calculated area-true lake morphology variables such as area, length, and width. We further assigned the lake form using [C=lake length/lake width] after Grigoriev (1959) resulting in four categories: ‘round’ (C>1.5), ‘close to round’ (C=1.5–3.0), ‘close to oval’ (C=3.0–5.0), and ‘oval-elongated’ (C=5.0–7.0) (Table A1).

At the first hierarchical level, we first separated the mountain lakes that include two large deep glacial lakes (Fig. A2.A) and 13 smaller lakes (Fig. A2.B), and the lowland lakes (Fig. A2.C–H). We then assigned the specific stage of thermokarst lake development to the lowland thermokarst lakes by classifying them into the three lake types ‘new thermokarst lake’, ‘old alaas lake’ and ‘connected alaas lake’ based on our field knowledge, visual inspection of field photos (Fig. A2), UAV multispectral orthoimages, UAV LiDAR digital surface models (Fig. 2) and in few cases also using bathymetric data. In our lake collection we did not sample the first lake development stage ‘byllar’. Distinct geomorphological features for the assignment as a new thermokarst lake of the dyede lake stage is the existence of highly degraded former ice-wedges (baydjarakhs, Fig. 2.A) and of the tyympy lake stage, steep lake shore morphologies, also with erosion and leaning trees (Fig 2.D), the steep lake slope being visible in the field as well as in bathymetric data, when available. We kept these assignments on the ‘dyede’ and the ‘tyympy’ thermokarst lake stage, however, for the further analyses, we aggregated all of these lakes into the lake development stage that we refer to as new thermokarst lake. The majority of new thermokarst lakes have the lake shape factor C showing close to oval and close to round, and round lake shapes. In some cases, new thermokarst lakes occur with a considerable large lake surface area as in the sandy lithology of the first Lena terrace Bestyakh. The distinction between old alaas lakes as well as connected alaas lakes versus new thermokarst lakes could be well made due to the very distinct alaas geomorphology in which old and connected alaas lakes are located. Several of the connected alaas lakes show no surface water discharge in the connecting channels during the drier summer months, but they are known to be temporally connected during high discharge events by local knowledge and show very distinct channel flow-through morphological features. Connected alaas lakes and old alaas lakes are frequently of a very irregular lake shape, therefore the derivation of factor C may be less reliable for these lake types, in contrast to new thermokarst lakes. The shape irregularities are caused by high degradational processes with subsequent lake shore erosion, specifically due to strong water discharge events.

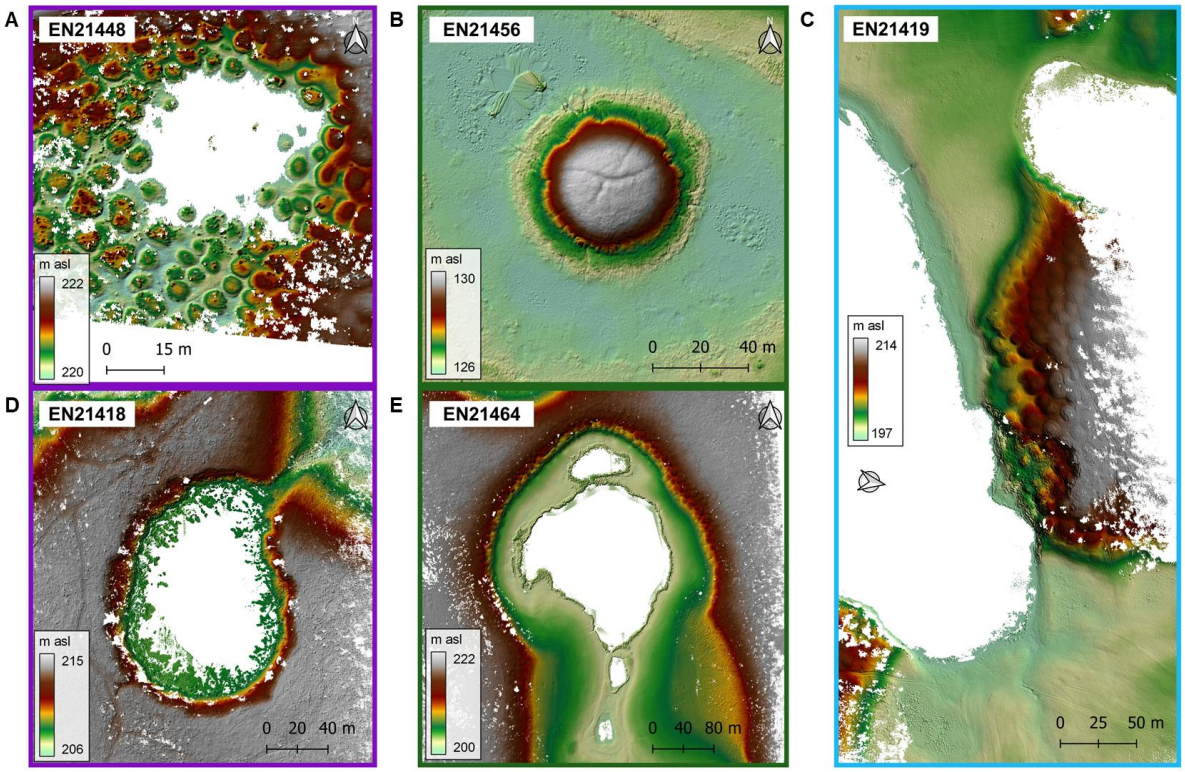


Figure 2: (A-E) Figurative examples from UAV-LiDAR derived surface models (with trees and understory vegetation removed and water surface masked in white with exception for lake EN21456) of the three thermokarst lake types (connected alaas lakes, new thermokarst lakes and old alaas lakes). In panels (A,D), two examples of new thermokarst lakes are EN21448 and EN21418 (purple outlines) . Lake EN21418 is located at a higher position in the alaas system and characterised by steep slopes with up to 6 m height difference to the top of the Yedoma plateau and EN21448 (A) showing the baydjarakhs (related to ice wedge degradation). (B,E) Two examples of old alaas lakes are EN21456 and EN21464 (green outlines). EN21456 (B) is one example with a nearly circular developed 'ice-hill' (pingo) of around 4 m height and 55 m diameter within an old alaas lake (in this case surface water not masked as white). (C) Lake EN21419 (blue outline) is of the connected alaas lake type showing a typical elongated shape.

Table A1, Figures 3 and A2 visualise our lake classification scheme into mountain lakes, old alaas lakes, new thermokarst lakes and connected alaas lakes.

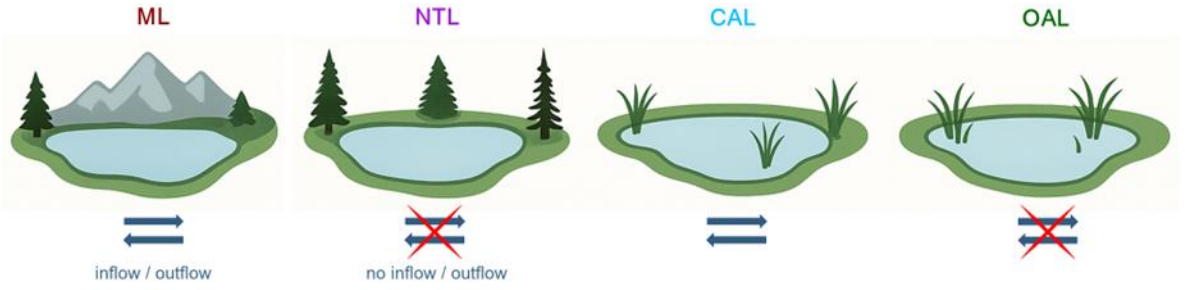


Figure 3: Scheme of the classified lake types in this study: new thermokarst lakes (NTL) and old alaas lakes (OAL) show no in- and outflows in contrast to mountain lakes (ML) and connected alaas lakes (CAL). The lake types in this figure were generated using Perplexity AI.

2.5 Environmental data processing

Satellite-derived land cover

We used the 10 m resolution European Space Agency (ESA) World Cover 2021 land cover product (derived from Sentinel-1 and Sentinel-2; Zanaga et al., 2022) to consistently extract dominant land cover around the lakes as the UAV coverage of the lake environments was not large enough, specifically around the large lakes. Owing to the flat, yet locally complex geomorphological relief in Central Yakutia which for example includes braided rivers, and a multitude of lakes close to each other, a robust lake catchment delineation for each of the lakes from Digital Elevation Model data could not be carried out.

Instead, we created 50-m buffer zones extending landward from the shoreline around each lake for a consistent extraction of the surrounding land cover. We also created a wider buffer zone of 360 m according to the relevant source area of pollen deposition areas in Central Yakutia as calculated in Geng et al. (2022).

ESA World Cover 2021 land cover in WGS84 geographic projection was reprojected to the respective UTM zones (N52,53, 54) using QGIS before extracting land cover for each buffer zone in area-true projection.

Up to seven ESA World Cover 2021 land cover classes occurred within the buffer zones of the mountain lakes: tree cover, shrubland, grassland, built-up, bare/sparse vegetation, permanent water bodies, moss/lichen. The land cover 'built up' seemed to be confused with 'bare/sparse vegetation'. Therefore, 'built-up' and 'bare/sparse vegetation' land cover classes were subsequently merged into a single 'barren' land cover class while the land cover class 'moss/lichen' was labelled 'tundra' for descriptive purposes. Buffer zones of the Central Yakutian lakes included up to nine land cover classes: tree cover, shrubland, grassland, cropland, built-up, bare/sparse vegetation, permanent water bodies, wetland, moss/lichen. For these buffer zones there was even more confusion for the land cover classes 'built up' and 'barren/sparse vegetation'. Similarly, also the land cover classes indicating the land use were not consistently correctly mapped according to our field knowledge and local knowledge. Therefore, the land cover classes 'grassland' and 'cropland' needed to be merged into a single land cover class 'grassland'. As 'moss/lichen' cannot occur in the boreal Central Yakutian lowland but truly represented sparsely vegetated areas in settlement and on agricultural land we further merged this class 'moss/lichen' into the 'barren' land cover class together with built-up and bare/sparse vegetation for the lowland region. As a result, we could not use the specific land cover classes 'built up' and 'cropland' to link to human land use. For the final analyses, we used five land cover classes for the mountain buffer zones: forest, grassland, tundra, wetland, barren and four land cover classes for the lowland buffer zones: forest, grassland, wetland, barren.

Climatology

We used contemporary climatologies at a spatial resolution of 1 km for the Earth's land surface (CHELSA) v.2.1 (Karger et al., 2017, 2023) to derive temperature and precipitation-related bioclimatic variables representing the mean conditions for the period 1981–2010 (Table A2). The bioclimatic variables corresponding to the CHELSA grid cell at each lake centre coordinate were extracted using the R platform (R Core Team, 2026) using the packages 'sf' (Pebesma and Bivand, 2023), 'raster' (Hijmans, 2025), 'devtools' (Wickham et al., 2022), and 'climatedata' (https://github.com/MirzaCengic/climatedata; last accessed on July, 2025). For the visualisation of the extracted data, we used the packages 'raster' (Hijmans, 2025) and 'maps' Becker et al. (2025).

Statistical processing and data visualisation

We used a range of complementary statistical analyses and data visualisations for processing the data using R (R Core Team, 2026) except for the Piper diagram. We applied the Piper diagram analyses (Piper, 1944) to delineate the hydrochemical facies of the sampled lakes from the concentrations of major cations and anions and to identify the chemical composition. The Piper calculations were done using macros developed in Microsoft Excel-2019 by the United States Geological Survey, USGS (https://halfordhydrology.com/piper-and-stiff; last accessed September, 2024), transforming concentrations in milligrams per litre (mg L^{-1}) and calculating total dissolved solids (TDS) and charge balances by the concentration of major ions. Two lake water samples were excluded from the Piper analyses because of one exceeding 50% major ion imbalance (EN21426-2) and one missing the measurement of HCO_3^- (EN21457).

To identify hydrochemical groups, clustering analysis was undertaken using the package 'stats' (R Core Team, 2026) on the lake data of major ions, DOC, TDS, and stable water isotopes (without deuterium excess). Data were first standardised and then scaled by the Euclidean method. The hierarchical clustering matrix was generated with the method 'ward.D2'. Figures of isotopes and land cover referenced against HCO_3^- are plotted as basic x, y plots (R Core Team, 2026). We used Principal

Component Analysis (PCA) to determine the main variations and dependencies in the datasets within lake types for all study lakes and lowland lakes only. We performed PCA for the hydrochemical and environmental variables using the package 'factoextra' (Kassambara et al. 2026) with the function 'prcomp'. Plot visualisations were done in R using 'ggfortify' (Tang et al. 2016), 'ggrepel' (Slowikowski, 2024), and 'ggplot2' (Wickham, 2025). Similarly to the Piper analyses, we excluded two lakes (EN21426-2, EN21457) from the PCA using the hydrochemistry as input, and an additional lake (EN21403) was missing sedDNA data for the multivariable PCA and multi-level statistics. To examine the lake area versus DOC and EC we created a scatterplot, using the ggplot library. To further understand the hydrochemical components of the lakes and potential sources of the dominating major ions, we applied the Gibbs diagram (Gibbs, 1970) in which the ratio of dominant cations $(Na^+)/(Na^+ + Ca^{2+})$ is referenced against TDS on a log-scale from 1 to 10000.

SedDNA data were visualised as Bubble charts, Chord diagrams, and a stratigram (R Core Team, 2026). Relative abundances of macrophytes and terrestrial plants were calculated for each lake using the package 'vegan' (Oksanen et al., 2022). Bubble charts were created using the package 'reshape2' (Wickham, 2007) to transform the data from wide format to long format by lake type with the function "melt", and with the 'ggplot2' package (Wickham, 2025) for visualisation. Data manipulation for Chord diagram filtering, grouping, and summarising was done using the package 'dplyr' (Wickham et al. 2023). To create circular plots of Chord diagrams, we used the package 'circlize' (Gu et al. 2014). Stratigraphic plots were visualised using the package 'rioja' (Juggins, 2024) with the function "strat.plot".

To examine relationships between environmental variables, we conducted a pairwise Pearson correlation analysis. The analysis was performed on the combined environmental dataset (n = 28), using the function "corr.test" from the package 'psych' (Revelle, 2025). Pairwise complete observations were used to handle missing data, and no adjustment for multiple testing was applied. The resulting correlation coefficients and corresponding p-values were visualised using the 'corrplot' package (Wei et al., 2024). A colour gradient was applied to reflect the strength and direction of correlations, and significance levels were overlaid using yellow labelled asterisks (*$p < 0.05$, **$p < 0.01$, ***$p < 0.001$). We applied multi-level pattern analyses (MPA) to see the associations and patterns between our environmental and hydrochemical data for the different lake types using the package 'indispecies' (De Cáceres et al., 2025) with the function 'multipatt'. To compare land cover distribution across lake types, we created boxplots using the function 'ggboxplot' from package 'ggpubr' (Kassambara, 2026), highlighting medians, interquartile ranges, whiskers and outliers without hypothesis testing. Scatterplots were created using the function 'ggscatter' from package 'ggpubr' (Kassambara, 2026).

3 Results

3.1 Summary of the morphological, physicochemical and stable water isotopic lake characteristics

Our collection of lake data forms a large dataset across a west to east gradient encompassing two contrasting groups of lakes: thermokarst lowland lakes (n = 51) and mountain lakes (n = 15). In terms of lake morphology, most of the sampled mountain lakes (n = 13) are characterised by a small surface water area with a median of 0.05 km² (0.003–0.31 km²) and a median water depth of 7.4 m (Table 1). However, a characteristic of the Verkhoyansk mountain range is also the existence of large glacial lakes. We were able to sample two deep glacial lakes, Lake Uluu (EN21401) and lake EN21405 with an area of 4.78 km² and 0.55 km² and maximum lake depth measured during our expedition of 43 m and 33.8 m, respectively. In contrast, for the sampled lowland lakes, the lake surface ranges between 0.0008 km² and 3.7 km² (Table 1). The group of connected alaas lakes (n = 8) show the largest lake surface area with a high variability with a median of 0.54 km², compared to old alaas lakes (n = 28) with a median of 0.05 km², and new thermokarst lakes (n = 15) with a median of 0.02 km².

Limnological variables and lake hydrochemical and hydrophysical properties (Tables 1, A1, A3) are published in Baisheva et al. (2022a,b) and Stieg et al. (2022). Mountain lakes are characterised by a median neutral pH of 7.6. Contrastingly, lowland lakes display neutral (~7) to strongly alkaline (~9) pH values with a median pH of 8.8. EC (median and range) shows large

differences being over an order of magnitude greater for lowland lakes than the very low conductivity values of the mountain lakes. In accordance, TDS of mountain lakes are low with a median of 61 mg L^{-1}, compared to lowland lakes with a median of 886 mg L^{-1} in connected alaas lakes, 870 mg L^{-1} in new thermokarst lakes and 1384 mg L^{-1} in old alaas lakes. Similarly, lowland lakes have high concentrations of DOC, which is highest in the new thermokarst lakes with a median of 106.1 mg L^{-1}, in contrast to the very low DOC in mountain lakes with a median of 13.3 mg L^{-1}.

The analyses of the lowland lake area versus the mineral content expressed as EC and the organic content expressed as DOC shows that their relationship is not strongly linked to the three different thermokarst lake types (Fig A3). The range of lake area is wide for new thermokarst lakes linking high DOC also to larger lakes, whereas lower EC values also occur in smaller new thermokarst lakes.

Table 1: Major hydrophysical and hydrochemical parameters of the different sampled lake types. Values are shown as median across all lakes per category. In this table, we did not incorporate the two large mountain lakes with outstanding properties (e.g., maximum water depth > 30 m). The parameter values of the two deep mountain lakes are shown in Table A3.
EC = electrical conductivity; TDS = total dissolved solids; DOC = dissolved organic carbon. Not Available (NA) and Not Determined (ND) refer to lakes per category with no data available, or not applicable, respectively; dl and bdl refer to detection limit and below detection limit, respectively.

Lake type	**Mountain Lakes (ML) (without 2 deep glacial lakes)**	**New thermokarst lakes (NTL)**	**Old alaas lakes (OAL)**	**Connected alaas lakes (CAL)**
Number	13 (of 15)	15	28	8
Variable	**median** min-max	**median** min-max	**median** min-max	**median** min-max
Elevation (m a.s.l.)	**1036** 789-1310	**202** 126-307	**173** 115-246	**150** 134-299.6
Lake area (km^2)	**0.05** 0.0025-0.31	**0.02** 0.0008-1.4	**0.05** 0.0008-1.6	**0.54** 0.07-3.7
Lake depth (m)	**7.4** 3-14.3	**3.2** 1-19.1	**2** 0.5-8.4	**2.4** 1.7-6.9
Secchi depth (m)	**2.56** 1.35-5.4	**1.3** 0.2-2	**0.5** 0.2-1.9	**0.4** 0.2-0.8
pH	**7.6** 6.6-8.6	**8.6** 7-9.2	**8.9** 8-9.4	**9** 8.1-9.4
EC (µS cm^{-1})	**83.2** 14-194	**999** 274-3140	**1619** 487-6010	**894** 379-1238
TDS (mg L^{-1}	**61** 8-115	**870** 238-3294	**1384** 228-5276	**886** 336-1248
DOC (mg L^{-1})	**13.3** 4.53-23.9	**106.1** 4.57-417	**763** 52-279	**69** 34-117
Ca^{2+} (mg L^{-1})	**10.6** 1.61-18.6	**32.7** 9.78-64.8	**18.9** 2.7-46.8	**28** 15.3-39.7
Mg^{2+} (mg L^{-1})	**4.21** 0.59-7.98	**111.6** 16.8-388	**118.5** 29.5-274	**92** 33.7-139
Na^{+} (mg L^{-1})	**0.94** 0.21-2.08	**78.1** 7.32-401	**209.4** 46.7-1222	**94** 13.5-122
K^{+} (mg L^{-1})	**0.66** 0.32-0.95	**4.9** 2.09-50	**12.1** 5.44-105	**8.6** 5.37-20.1
HCO_3^{-} (mg L^{-1})	**32.6** 5.2-82.5	**607.4** 179.9-2153.8	**835.9** (ND=1) 320.3-2791.4	**613** 250.92-924.2
Cl^{-} (mg L^{-1}) dl - 0.1 mg L^{-1}	**NA** (bdl=13)	**30.8** 0.9-258	**89.2** 5.7-697	**39.7** 2.5-58.2
SO_4^{2-}(mg L^{-1}) dl - 0.1 mg L^{-1}	**1.74** (bdl=2) 0.12-20.5	**7.7** (bdl=5) 1.38-507	**33.9** (bdl=4) 0.28-947	**1** (bdl=2) 0.15-15.9
F^{-} (µg L^{-1}) dl - 0.1 mg L^{-1}	**NA** (bdl=13) 0.13-0.15	**0.43** 0.14-1.3	**0.29** (bdl=2) 0.15-1.42	**0.38** 0.28-0.48
$\delta^{18}O$ (‰ V-SMOW)	**-17.67** -19.6 to -14.07	**-9.1** -14.7 to -7.3	**-7.7** (ND=1) -11.3 to -5.2	**-8.9** -10.1 to -6.3
δD (‰ V-SMOW)	**-148.9** -159.3 to -135.91	**-112.9** -142.1 to -96.5	**-99.8** (ND=1) -121.3 to -85.1	**-105.1** -111.6 to -84.9
d excess (‰)	**-10.1** -23.3 to 4.5	**-34.06** -41.2 to -24.9	**-39.8** (ND=1) -46.5 to -30.1	**-35.6** -40.8 to -30.5

The dominant hydrochemical facies of the majority of lakes of the $CaMgHCO_3$ type as shown by the Piper analyses (Fig. 4) is indicative of calcium and magnesium carbonate weathering. Weak acids exceed the strong acids ($CO_3^-+HCO_3^-$)>($SO_4^{2-}+Cl^-$), for the majority of the lakes (n = 60), corresponding to the bicarbonate type in the anion triangle. Lake cations most frequently correspond to the magnesium type (n = 32), while the calcium type is encountered in 13 mountain lakes (EN21401 to 409, EN21412 to 415) and one new thermokarst lake (EN21423). In Central Yakutia, eight brackish to saline lakes (EN21420, 426, 428, 430, 431, 436, 440, 444) are of the sodium type. One highly saline lake EN21426 is of the NaCl type, while two other high saline lakes (EN21430, 436) are of the $NaHCO_3$ alkali carbonate type. For brackish Central Yakutian lakes, alkalis often exceed alkaline earths (Na^++K^+)>($Ca^{2+}+Mg^{2+}$) (n = 25) and extreme hydrochemical facies characterise four of the sampled lakes (EN21426, 448, 456, 465) with strong acids exceeding weak acids ($SO_4^{2-}+Cl^-$)>($CO_3^-+HCO_3^-$).

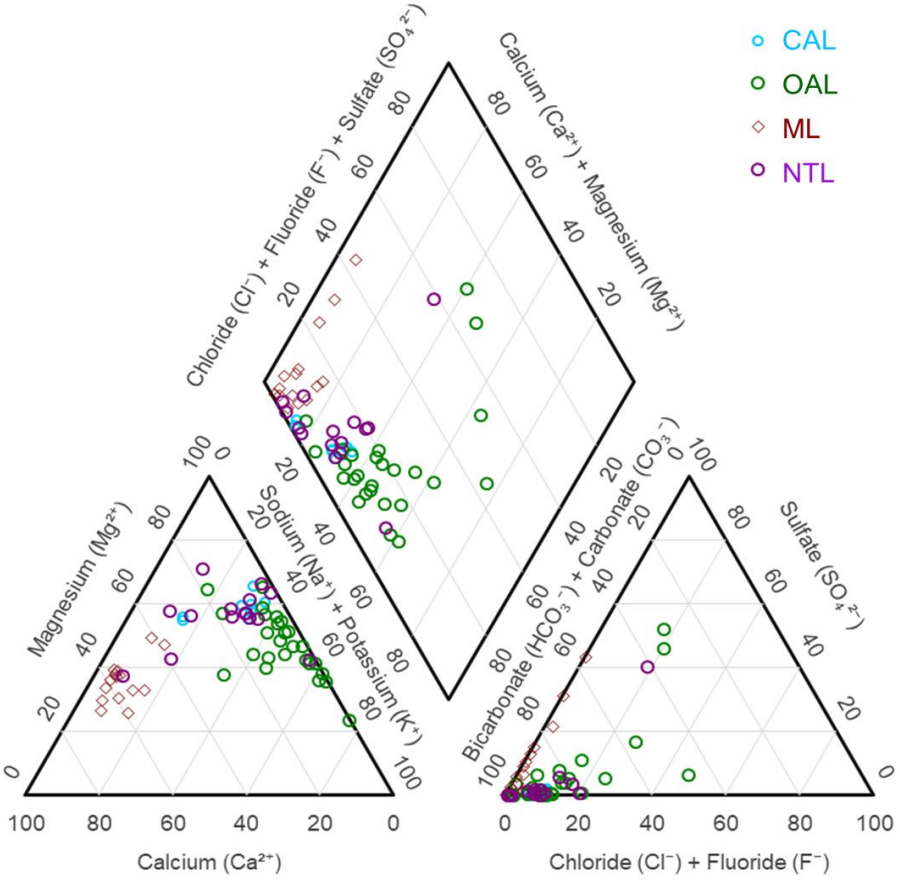


Figure 4: Piper diagram showing the hydrochemical facies of the different lake types: connected alaas lakes (CAL), old alaas lakes (OAL), mountain lakes (ML), new thermokarst lakes (NL).

The hierarchical clustering of the lakes (n = 64) according to the major ion hydrochemistry (Fig. A4) confirms the clustering in the Piper hydrochemical facies (Fig. 4), with the lakes grouping according to the concentration of salts into three main clusters

Brackish lowland lakes with high ion content (Clusters 1, 2; n = 26) are clearly separated from the freshwater lakes from mountain and lowland areas (Cluster 3, n = 38), with the exception of three brackish lakes (EN21418, 453, 462). Cluster 1 specifically envelops three old alaas lakes (EN21430, 436, 440) characterised by very high TDS at 4006 mg L^{-1}, 3324 mg L^{-1}, and 5276 mg L^{-1}, respectively. Cluster 2 includes 23 lowland lakes of different lake types with brackish waters. Similarly, the brackish lakes are also grouped by multilevel pattern analyses (Table 2). The freshwater lakes in Cluster 3 include 38 lakes of which 15 are mountain lakes, forming a separate subcluster together with one new thermokarst lake (EN21445) and 23 lowland freshwater lakes of different lake types. TDS for three of the freshwater lakes in this subcluster (EN21418, 453, 462) show moderately high concentrations at 1357, 1001, and 1192 mg L^{-1}, respectively.

The Gibbs diagram (Fig. A5) partitions the mountain lakes into precipitation and runoff dominated systems while the majority of lowland lakes, specifically of the old alaas lake type, are clustered in the sector assigned to evaporation as the dominating process, although several of the new thermokarst lakes and connected alaas lakes are also located in the sector that characterises more diluted waters commonly associated with runoff influenced systems.

We use linear regressions of dD and d18O of lake systems, in the following called Local Evaporation Lines (LELs), even though other effects like snow or ground ice melt might impact on the lake hydrology. The stable water isotopic composition of 65 sampled lakes is published in Stieg et al. (2022), clearly separating the lakes into two groups, lowland lakes and mountain lakes (Fig. 5). δD and $\delta^{18}O$ are strongly positively correlated within all lake types (Pearson's r = 0.94–0.98, p < 0.001), with linear models explaining 88–96% of the variation in δD. The correlation of δD and $\delta^{18}O$ shows a low slope of 6.14 (n = 50) for the lowland lakes ($Yak21_{Lowland}$) and an even lower slope of 3.71 (n = 15) for the mountain lakes ($Yak21_{ML}$). As surface waters evaporate during the lake-ice free season, they become enriched in heavy isotopes and deviate from the GMWL with their deuterium excess values decreasing due to kinetic fractionation. The range in the isotopic composition within the group of mountain lakes results also due to another secondary effect, the altitude effect. The stable isotopic composition of mountain lakes intercepts the LMWL at -20‰ $\delta^{18}O$ (V-SMOW) indicating summer precipitation as the dominant water source. This is in contrast to $Yak21_{Lowland}$ intersecting with the GMWL at -30‰ $\delta^{18}O$ (V-SMOW) suggesting an isotopically more depleted water source that we assume is still the signal of the snowmelt. In the case of the lowland lakes, there seems to be no relevant impact of isotopically-enriched summer precipitation. We see a temporal snapshot, representative for sampling lowland lakes and mountain lakes at a specific time in summer 2021. Only one local single and not strong rain event (Fig. 5) took place in August 2021 early during our sampling activities in the lowlands and there were no more rain events across Eastern Central Yakutia in August 2021.

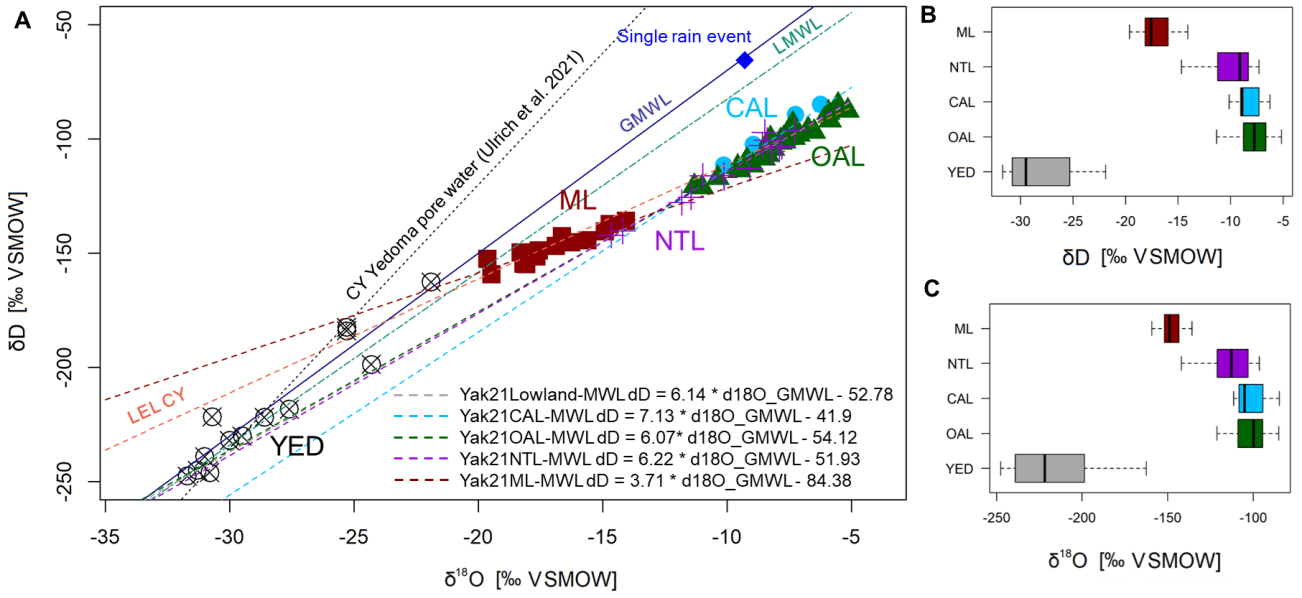
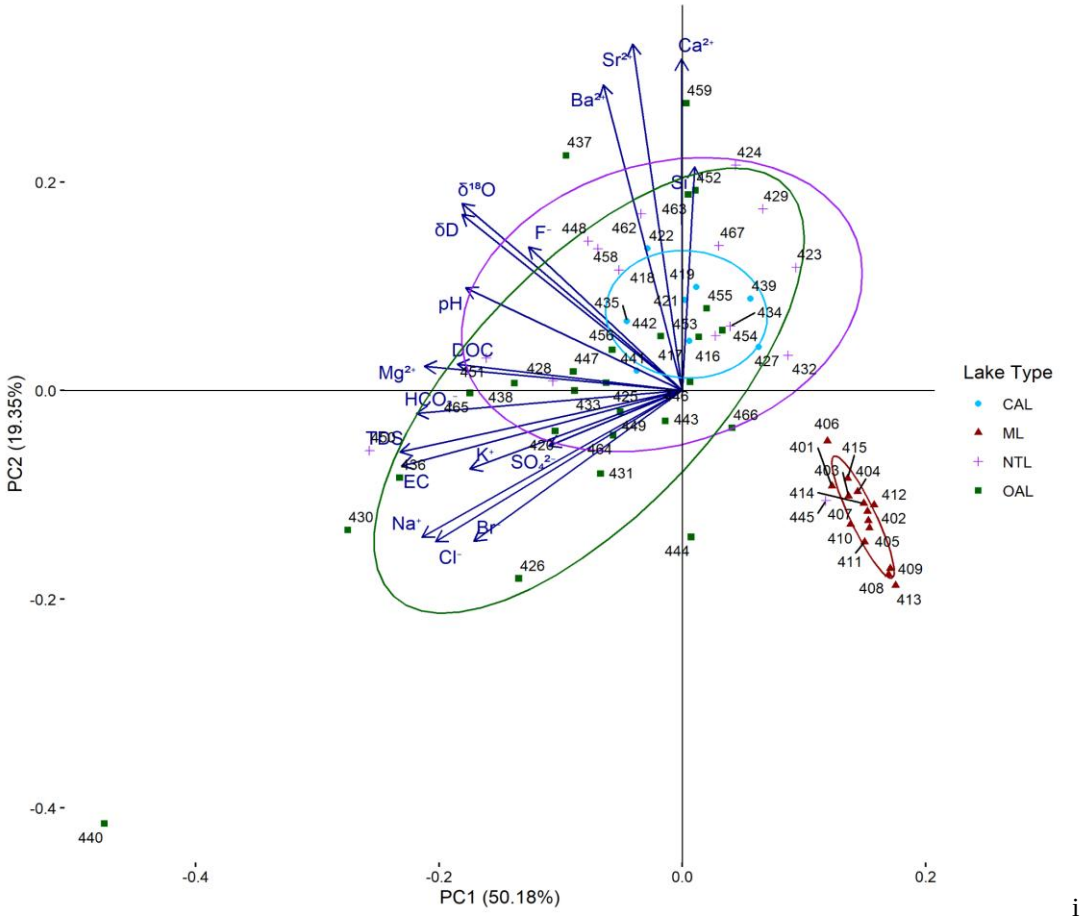


Figure 5: Co-isotope plot ($\delta^{18}O$ and δD) from lake surface water and from one summer precipitation sample (August 2021) along a 700 km west to east transect from Central Yakutia (old alaas lakes (OAL), connected alaas lakes (CAL), new thermokarst lakes (NTL)) to the Oymyakon High mountain plateau in the east (mountain lakes (ML)). YED values (crossed circles) include ice wedges and segregated ice in Yedoma from Pavlova et al. (2024) et al; Torgovkin et al. (2024); Popp et al. (2006); Windirsch et al. (2020); Ulrich et al. (2021). Displayed are the Global Meteoric Water Line (in solid blue), GMWL: $\delta D = 8*\delta^{18}O + 10$ (Craig 1961), the Local Meteoric Water Line (in dashed green) LMWL: $\delta D = 7.57*\delta^{18}O_GMWL - 6.86$ (Kloss, 2008), and a local evaporation line from Central Yakutia (in dashed orange), LEL CY: $\delta D = 4.99*\delta^{18}O_GMWL - 61.41$ (Wetterich et al. 2008), CY Yedoma pore water: $11.53*\delta^{18}O_GMWL - 110.56$ (Ulrich et al. 2021), and our local evaporation lines based on the different lake types ($Yak21_{Lowland}$, $Yak21_{CAL(Connected\ alaas\ lakes)}$, $Yak21_{OAL(Old\ alaas\ lakes)}$, $Yak21_{NTL(New\ thermokarst\ lakes)}$, and $Yak21_{ML(Mountain\ lakes)}$).

Due to the arid summer climate in Central Yakutia, we can assume that the contemporary evaporation processes govern the lowland lake stable water isotope geochemistry. Interestingly, the three different lowland lake types show different

characteristics of the LELs. A distinct characterisation for new thermokarst lakes is the lightest composition, i.e., a more depleted isotope signal compared to the older lowland lakes. This could be indicative for the contribution of isotopically light sources, through lateral erosion or direct ground ice melt if lakes expand to greater depths or erosion with blocks falling into the lake. Considering a potential ground ice signal, the isotopic composition of syngenetic ice wedges from Yedoma deposits shows in fact a very light isotope composition (–31 ‰ to –24.3 ‰ for $\delta^{18}O$ and –239 ‰ for δD (Pavlova et al. 2024; Torgovkin et al. 2024; Popp el al., 2006), also the isotopic composition of segregated and pore ice in Yedoma, varying more widely: –31.7 ‰ to –21.9 ‰ for $\delta^{18}O$; –247.5 to –162.6‰ for δD (Pavlova et al. 2024; Torgovkin et al. 2024; Ulrich et al. 2021; Windirsch et al. 2019; Popp et al. 2006) (see also Figure 5).

The results for the PC including all hydrophysical and hydrochemical variables (minor and major ions, hydrophysics, stable water isotope composition) shows that the first two PCs explain a high proportion (69.53 %) of the total variance showing a strong separation of the mountain and lowland lakes (Fig. 6). The PC1 score for a lake may be thought of as a composite measure of ionic strength as (Kokelj et al. 2009) formulated it for thermokarst lakes in the Mackenzie Delta region. While mountain lakes form a distinct cluster, lowland lakes are more scattered across PC1 and PC2 without a clear distinction between the different lake types. Relevant lake hydrochemistry variables, such as DOC, Mg^{2+}, HCO_3^-, TDS, EC, and K^+ show the strongest negative loadings along the PC1 axis for all lowland lakes. However, for a PCA considering the group of lowland lakes only (Fig. A6), HCO_3^-, TDS, EC, and Mg^{2+} show strong positive loadings on PC1, potentially separating the lake types, whereas DOC and SO_4^{2-} show less separability for the lowland lakes only. The major ions Ca^{2+} and Si^+ and the minor ions Sr^{2+} and Ba^{2+} are mainly expressed along the positive PC2 axis when analysing all lakes (Fig. 6), when analysing only the lowland lakes, the minor ions Ba^{2+} and Sr^{2+} align along the negative axis of PC2 (Fig. A6).



i

Figure 6: Principal component (PC) 1-2 biplot of hydrochemical variables (minor and major ions, hydrophysics, isotopes) from all lakes with ellipses outlining the lake types with mountain lakes (ML) forming a separate cluster, but overlapping for all lowland thermokarst lakes: new thermokarst lakes (NTL), old alaas lakes (OAL), and connected alaas lakes (CAL). The length of the vectors expresses the loadings of the hydrochemical variables in the PC1 to PC2 space.

3.2 Aquatic plants per lake type

Total macrophyte sedDNA richness for all lake types is represented by 87 amplicon sequence variants (ASVs), with the highest diversity in emergent (65 ASVs), followed by submerged (13 ASVs), floating (7 ASVs), and submerged-emergent (2 ASVs) macrophyte taxa (Fig. 7, A7). Most counts are from submerged macrophytes (74 %), with the three other functional groups accounting for only a quarter of the total counts with emergent 17 %, floating 5 %, and submerged-emergent macrophytes 4 %. Macrophyte composition varies by lake type, with certain taxa associated with specific lake types (Fig. A7, Table A4). However, submerged macrophytes consistently dominate across all lakes, comprising a median of 94 % in connected alaas lakes, 82 % in old alaas lakes, 63 % in mountain lakes, and 46 % in new thermokarst lakes.

Emergent macrophytes are well represented in old alaas lakes (median of 13 % of total share). Submerged-emergent macrophytes are the least diverse group (only two *Hippuris* ASVs), yet relatively frequent in ten mountain lakes, with a median of 40 % of the macrophyte total share per lake. The dominant submerged macrophytes are *Potamogeton*-1, (with a median of 32 %) across all lake types, and *Stuckenia pectinata* in connected alaas lakes (with a median of 31 %) and old alaas lakes (with a median of 13 %). Two submerged macrophytes *Myriophyllum* and *M. verticillatum* occur only in freshwater lakes, as does the submerged-emergent *Hippuris*, except for one brackish new thermokarst lake (EN21451).

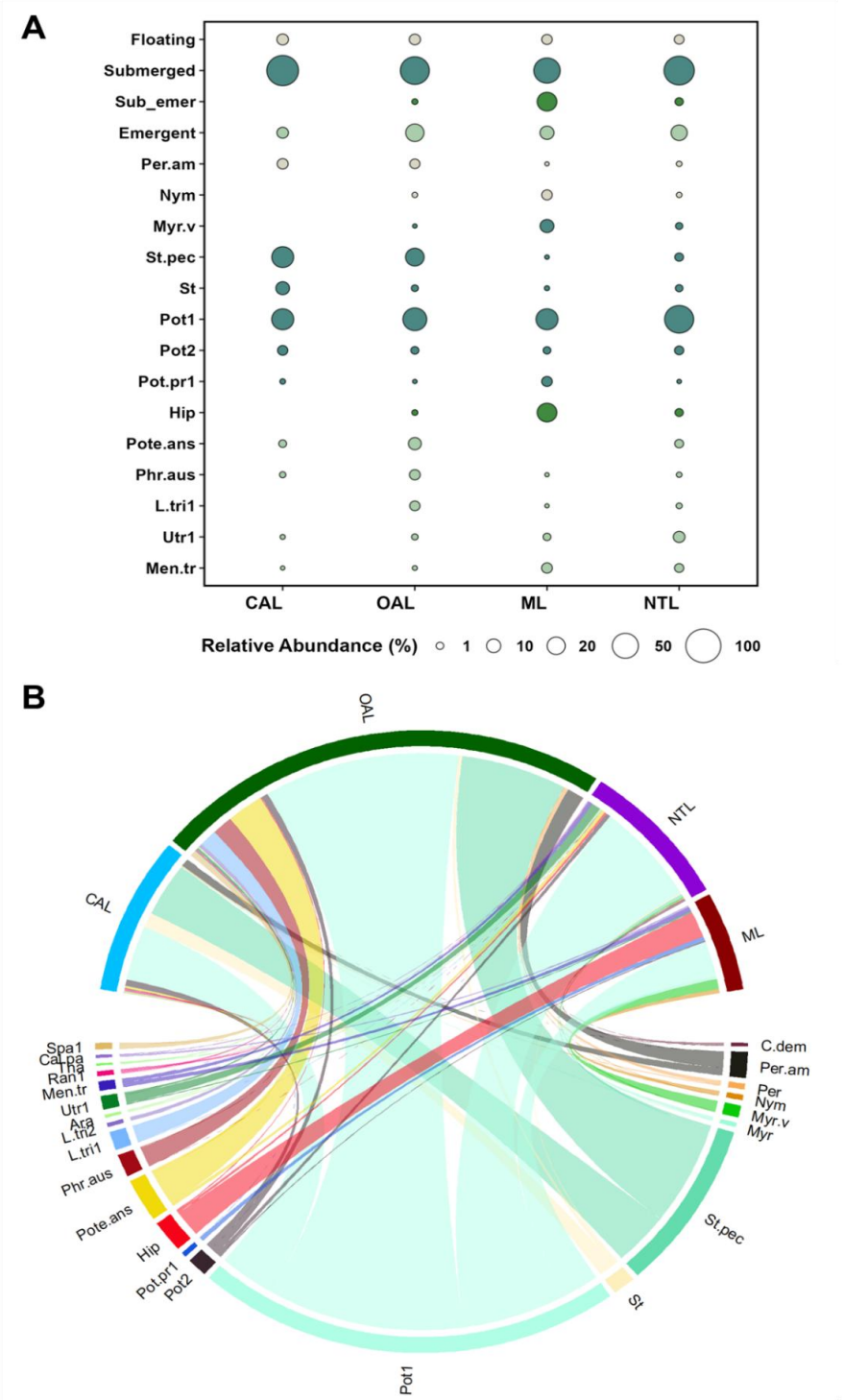


Figure 7: (A) Bubble-chart illustrating the relative abundance of macrophytes in four lake types: mountain lakes (ML), old alaas lakes (OAL), connected alaas lakes (CAL), and new thermokarst lakes (NTL). Relative abundance of plant types is displayed as the total share per lake type. A subset of plants with > 4 % occurrence is also shown. (B) Chord-diagram showing the most abundant taxa within the four lake types and their relationship to lake type. Short names of taxa refer as follows: Spa1-*Sparganium1*, Cal.pa-*Caltha palustris*, Tha-*Thalictrum*, Ran1-*Ranunculus1*, Men.tr-*Menyanthes trifoliata*, Utr1-*Utricularia1*, Ara-Aracaceae, L.tri1-*Lemna triscula1*, Phr.aus-*Phragmites australis*, Pote.ans-*Potentilla anserina*, Hip-*Hippuris*, Pot.pr1-*Potamogeton praelongus1*, Pot2-*Potamogeton2*, Pot1-*Potamogeton1*, St-*Stuckenia*, St.pec-*Stuckenia pectinata*, Myr-*Myriophyllum*, Myr.v-*Myriophyllum verticillatum*, Nym-Nymphaeaceae, Per-*Persicaria*, Per.am-*Persicaria amphibia*, C.dem-*Ceratophyllum demersum*.

3.3 Land cover and terrestrial vegetation

Terrestrial vegetation richness derived from sedDNA (total 116 ASVs) is highest for grasses and herbs (83 ASVs), with lower richness for shrubs (16 ASVs), trees (9 ASVs), and mosses (8 ASVs) (Fig. A8, A9). The most count-contributing terrestrial plants are trees (54 %) followed by grasses and herbs (39 %), shrubs (8 %), and mosses (only 0.1 %). Taxonomic richness and relative abundance vary with lake type (Fig. A8,A9; Table A5), with new thermokarst lakes exhibiting the highest richness of

terrestrial vegetation in lake surface sediments (17 taxa), followed by connected alaas lakes (14 taxa), old alaas lakes (12 taxa) and mountain lakes (11 taxa). Grasses and herbs are the most taxonomically diverse terrestrial vegetation group deposited in lowland lakes, with a median richness ranging from 9 to 9.5 taxa. These taxa are dominant in the surface sediments specifically in connected alaas lakes (75 %) and old alaas lakes (74 %), while contributing less in new thermokarst lakes (25 %). In contrast, trees and shrubs represent the dominant sedDNA-derived material in new thermokarst lakes (75 %) and mountain lakes (93 %), with the latter showing the highest tree richness (median of 4 taxa per lake), are around a quarter in old alaas lakes (24 %) and in connected alaas lakes (25 %). Prominent woody taxa include Salicaceae, *Larix*, and *Betula*, particularly in mountain lakes and new thermokarst lakes, while old alaas lakes and connected alaas lakes show a more evenly distributed taxonomic occurrence of grasses and herbs (Fig. A8).

Results of sedDNA-derived terrestrial plant assemblages agree with the satellite-derived land cover composition surrounding the lakes: The fraction of forest land cover has a significant ($p \leq 0.001$) positive correlation ($R = 0.40$) with the proportion of trees derived from sedDNA, while the fraction of grassland land cover correlates ($R = 0.43$) significantly ($p \leq 0.001$) with the proportions of sedDNA-derived grasses and forbs.

Satellite-derived land cover differs according to lake type within the 50 m and 360 m buffer zones (Fig. A10, A11). In the Central Yakutian lowlands, grasslands are the most abundant class within the 50 m buffer zone of old alaas lakes (60 %) and connected alaas lakes (55 %) (Fig. A10), also comprising the cultivated grasses for hay and grain production according to our local knowledge. In contrast, forest becomes the dominant land cover class when extending the buffer zone to 360 m for old alaas lakes (70 %) and connected alaas lakes (54 %) (Fig. A10). Old alaas lakes and connected alaas lakes also show the highest proportions of wetlands around them, compared to mountain and new thermokarst lakes, although the proportion is only up to 4 %. Most mountain lake environments are dominated by forest (83 %), while only two of the sampled mountain lakes (EN21412 and 413) are surrounded by tundra (64 %, 44 %). Similarly, forest is the dominant land cover around new thermokarst lakes (83 % median proportion). Land cover dominance and relative proportions remain mostly unchanged for both mountain lakes and new thermokarst lakes under both buffer widths (Fig. A10,A11). Seven lakes (EN21421, 427, 439, 440, 441, 458, 459) occur within settlement areas, one in the settlement Churapcha, one in the summer settlement Aryylaakh, three in the settlement Tungulu, and two in the settlement Maya, respectively.

3.4 Combined environmental analyses

The CHELSA-derived mean annual temperature spatial distribution is characterised by a west-to-east decreasing gradient ranging from a maximum value of -8.9 °C in the westernmost region around the settlement Maya to -10.3 °C eastwards in the Tattinsky district and a minimum of -13°C in the Verkhoyansky mountain region to the east (Fig. A12). Conversely, mean annual precipitation shows a west-to-east increasing gradient in the lowland with the lowest value of 291 mm in the west and higher values in the mountain areas, with the highest value of 365 mm reached in the Tomponsky district (Fig. A13).

Land cover related to DOC and HCO_3^- displays positive and negative relationships for forest (Fig. A10,A11,A14) with a strong negative relationship observed between tundra and HCO_3^- for mountain lakes in the 360 m buffer zone. A positive relationship is observed between wetlands and DOC for old alaas lakes. The highest percentage of forest land cover occurs together with relatively higher DOC concentrations than for other land cover types, for both mountain and lowland lake types. Specifically, new thermokarst lakes that are characterised by a high percentage of forest in the immediate 50 m buffer show highest DOC concentrations. The land cover assigned hydrochemistry in the Piper diagram visualisation (Fig. A15) shows that settlement and grassland-linked lakes are widespread along the chloride and fluoride and the potassium and sodium ranges in contrast to forest-linked lakes mostly located in the lower mineralised range. Freshwater lakes are associated with Sr^{2+} and Ca^{2+}.

The first two principal components performed on hydrochemical lake data (major and minor ions, stable water isotopes, TDS, EC, pH) with all environmental variables (lake type, elevation, hydrochemical clusters, climate variables, % land cover classes within 50 m buffer zone, terrestrial vegetation functional type and aquatic plants) explain 83 % of the variability in lake

hydrochemical facies (Fig. A16). Variables and vectors reveal that the strongest direction of hydrochemistry variability along PC1 occurs linked to forest and tundra land cover together with SedDNA-derived trees and shrubs associated with mountain lakes, while sedDNA-derived grasses and land cover grass are associated with lowland lakes. The clear distinction between lowland and mountain lakes seems specifically related to the highly soluble alkali Ca^{2+} versus HCO_3^-, TDS, EC, freshwater, and its associated Cluster 3, versus brackish and the associated major ions of Cluster 2. HCO_3^- also shows a strong negative loading on PC1, grouping brackish old alaas lakes into a separate cluster along with EC and TDS. Connected alaas lakes occur across the brackish to freshwater gradients shared between PC1 and PC2, whereas the old alaas lake type is specifically spread along the negative PC1, close to brackish waters.

The climate variables precipitation of the driest month, mean annual air temperature and mean maximum air temperature of the warmest month show strong negative PC1 loadings, separating lowland lakes from mountain lakes. In contrast, precipitation of the wettest month and lake elevation are linked to the distribution of mountain lakes along the positive PC1 axis. Clear distinction between sedDNA-derived macrophytes occurs in mountain lakes associating with sub-emergent macrophytes and connected alaas lakes with floating macrophytes.

Table 2: Results from the multi-level pattern analysis showing the list of statistically significant associations of environmental variables with the different lake types: connected alaas lakes (CAL), old alaas lakes (OAL), new thermokarst lakes (NTL), mountain lakes (ML). Significance level coding: * ≤ 0.001, ** ≤ 0.01, * ≤ 0.05.**

Lake type	Associated variables	Short names	*p*-value
OAL	Major ion Cluster 2	C2	0.0122 *
ML	Elevation of the lake	Elev	0.0001 ***
	Precipitation of the wettest month	Pwet	0.0001 ***
	SedDNA submerged-emergent macrophytes	subemergent	0.0002 ***
	Land cover Tundra	TUNDRA	0.0003 ***
	Minimum annual temperature of the coldest month	Tmin	0.0030 **
	SedDNA-derived shrubs	shrubs	0.0061 **
Group: CAL + OAL	Land cover Grass	GRASS	0.0001 ***
	SedDNA-derived grasses and forbs	grasses	0.0001 ***
	Land cover Wetland	WETLAND	0.0095 **
Group: CAL + ML	Freshwater	freshwater	0.0021 **
Group: NTL + OAL	Positively charged sodium ions	Na^+	0.0015 **
	Negatively charged chloride ions	Cl^-	0.0023 **
	Brackish water	brackish	0.0019 **
	SedDNA-derived emergent macrophytes	emergent	0.0422 *
	Negatively charged bromide ions	Br^-	0.0149 *
Group: ML + NTL	Land cover Forest	FOREST	0.0001 ***
	SedDNA-derived trees and shrubs	trees	0.0008 ***
Group: CAL + ML + NTL	Major ion Cluster 3	C3	0.0088 **
Group: CAL + OAL + NTL	Mean annual temperature	MAT	0.0001 ***
	Maximum annual temperature of the warmest month	Tmax	0.0001 ***
	Oxygen stable isotope	$\delta^{18}O$	0.0001 ***
	Hydrogen stable isotope	δD	0.0001 ***
	Precipitation of driest month	Pdry	0.0001 ***
	Power of hydrogen	pH	0.0001 ***
	Barium ion with two positive charges	Ba^{2+}	0.0001 ***
	Specific electrical conductivity	EC	0.0003 ***

Negatively charged bicarbonate ions	HCO_3^-	0.0001 ***
Total dissolved solids	TDS	0.0003 ***
Magnesium ions with two positive charges	Mg^{2+}	0.0005 ***
Strontium ions with two positive charges	Sr^{2+}	0.0001 ***
Negatively charged fluoride ions	F^-	0.0001 ***
Calcium ions with two positive charges	Ca^{2+}	0.0006 ***
Dissolved organic carbon	DOC	0.0032 **
Positively charged potassium ions	K^+	0.0168 *

Multi-level pattern analysis of 43 combined hydrochemical and environmental variables identified 35 variables with strong associations with specific lake types and groups of lake types (Table 2). Only two lake types (old alaas lakes and mountain lakes) could be distinctly separated. Old alaas lakes were primarily associated with the hydrochemical major ions of Cluster 2, while mountain lakes were associated with more physical variables, with the strongest driver of the minimum annual temperature of the coldest month and also associated with sedDNA-derived shrubs. Connected alaas lakes and mountain lakes as a group were connected with freshwater waters, and connected alaas lakes and old alaas lakes as a group with the land cover wetland. The group of new thermokarst lakes and old alaas lakes are strongly associated with the emergent macrophyte composition, followed by the occurrence of the minor anion of Bromid and brackish waters as well Na^+ and Cl^- enriched waters. Notably, potassium positively characterises the group of lowland lakes, followed by DOC.

4 Discussion

4.1 Environmental drivers of physico-chemical lake characteristics

In general, the fractional cover of forest and wetland and soil carbon density influence the chemical composition in lakes (Xenopoulos et al. 2003; Sobek et al. 2007). Specifically, high-latitude lake hydrochemistry is governed by surface runoff due to very limited ground filtrated water or ground water contributions due to the permafrost barrier (Fedorov and Konstantinov, 2003; Walvoord and Kurylyk, 2016). For the sampled lowland lakes, our results indicate that their specific lake hydrochemistry shows a strong linkage to the lake development stage within the thermokarst chronosequence that we defined for our sampled lakes into: new thermokarst lakes, old alaas lakes and connected alaas lakes. In particular, we detect linkages between the thermokarst lake type in the chronosequence and DOC, pH, hydrogen carbonate, and stable water isotopic composition, as well as the alkali and earth alkali hydrochemical facies types. In agreement with previous studies for Central Yakutia (Hughes-Allen et al. 2020; Jongejans et al. 2021), we find that new thermokarst lakes are characterised by the highest DOC concentrations, though with considerable variability. Most of the sampled new thermokarst lakes are surrounded by forest, therefore the high organic input into surface waters can be explained by the dominating forest land cover with high plant biomass, litter and organic rich forest soils as environmental drivers, whereby input from high-organic Yedoma porewater also seems to be prevalent as new studies show in Ollivier et al. (2026). The climatic drivers of temperature and precipitation are strongly differing between the Central Yakutian lowland and the Verkhoyansk mountain region, therefore, several land surface properties indirectly linked to the harsher climate in the mountains are climate-equivalent environmental divers. For example, the mountain region is characterised by a large fraction of barren land surface, where larch forest occurs with sparse forest biomass (e.g., Miesner et al. 2022) and also thin organic soils, considerably reducing the input of minerogenic-organic material into the lakes. In contrast, in the densely forested boreal landscape of Central Yakutia, forest-induced processes (more biomass and therefore more organic detritus, organic-rich deep forest soils) contribute to higher HCO_3^- and DOC input into the lakes relative to those in tundra and forest-tundra landscapes (Herzschuh et al., 2013). Accordingly, within the mountain lake group, lakes with higher forest cover are also characterised by higher DOC.

For the lowland thermokarst lakes, their geomorphological features governing the hydrological connectivity appear as a major external driver of terrigenous input into the lakes. Thermokarst lake types with no inlet and outlet such as the new thermokarst lakes and old alaas lakes show higher DOC, mineral content, and salinity in contrast to connected alaas lakes. According to local knowledge, connected alaas lakes are regularly flushed during strong precipitation events and the regularly occurring spring floods after snow melt, resulting in lower water retention times with higher dilution, successively leading to lower levels of minerals, major ions, and DOC. Similarly, the much lower DOC and mineral content observed in mountain lakes is related to their higher dilution capacities provided by frequent flushing events and the larger water volumes of the lakes.

Conversely, high-latitude tundra lakes with no inlets and outlets are characterised by low organic and mineral content (Williamson et al. 2009). However, on the modern floodplain terraces, tundra lakes may be connected during the spring flood to large river systems experiencing the opposite process of being flushed with much higher DOC and mineral concentrations by this resulting in high DOC and mineral concentrations for these connected tundra lakes also in summer (Abiznova et al. 2012; Dvornikov et al. 2018; Skorospekhova et al., 2018).

4.2 Saline lakes in Central Yakutia

Central Yakutia lies within an arid climate zone and has a considerably low annual precipitation of only 280 mm. The coefficient of precipitation-to-potential evaporation ratio with 0.7 to 0.85 (Gavrilova, 1973; Ershov, 1989) indicates a negative lake-water balance resulting in strong aridification or even desiccation (Czerniawska and Chlachula, 2020) and a generally high lake-water mineral content (Pestryakova et al., 2012; Herzschuh et al., 2013). Lopez et al. (2007) found elevated salt concentrations in the active layer of alaas and pingo sites, indicating that salts previously trapped within permafrost were released during thawing migrating upward and producing a salinisation in the active layer. Also Meyer et al. (2002, 2010) discussed elevated salt concentrations in permafrost cores and sequences in Northern Yakutia and Alaska. In Central Yakutia, terraces contain high salt content in their lithology and subsequently high epigenetic salinisation of the alaas soils, like specifically the Abalakh terrace, which is traditionally known for lakes with balneological effects.

The lake salinisation in the Central Yakutian lowland thermokarst lakes is also evident in our hydrochemical and isotopic analyses, with the Gibbs-derived assignment of a large majority of the lowland lakes into the evaporative sector and also showing enriched stable isotope signal indicating evaporation. Most of the sampled lowland lakes belong to the magnesium-type hydrochemical classification with weak acids predominating over strong acids and alkaline earths exceeding alkali metals. Some of the sampled lowland lakes in Central Yakutia have exceptionally high salinities with no consistent relationship to either a specific terrace or the surrounding vegetation or land use. Although Kumke et al. (2007) propose that very high salinity levels in Yakutian lakes could result from anthropogenic influences, their hypothesis was not substantiated by field data or data analyses.

On the contrary, our findings indicate that high salinity in the lakes we sampled cannot be explained by anthropogenic impacts as they are located far away from settlements and managed lands. In fact, chloride concentrations show high variability across different terraces, land cover, and lake types. For the group of lowland lakes, the relationship between chloride concentrations and $\delta^{18}O$ exhibits significant scatter (Fig. A6). Notably, although some of the highly saline lakes show enriched $\delta^{18}O$, at the same time they show low to moderate chloride concentrations but elevated fluoride. This suggests that contemporary evaporation processes are not the primary drivers of the observed $\delta^{18}O$ variability. These sampled highly saline lakes with enriched oxygen isotopic composition show low chloride concentrations and are all specifically characterised by elevated fluoride concentrations causing the high salinity. This interesting relationship suggests an influence of local lithology, potentially involving fluoride leaching from Holocene lacustrine sediments or older salt deposits as has been described for other subarid and arid regions (Olago et al., 2009; Wen et al., 2013).

Pavlova and Fedorova (2022) investigated the hydrochemistry in water sampled from wells below permafrost in Central Yakutia and identified high fluoride concentrations in the subpermafrost aquifers resulting from weathering of Jurassic source

rocks. Over the Jurassic bedrocks, the Aldan Basin contains several hundred metres of sediment successions of Neogene to late Pleistocene age (Alekseev et al., 1990). These Cenozoic and Late Pleistocene sediments are covered by Quaternary sediments, comprising fluvial, glacial and loess-like deposits (Soloviev, 1973). The permafrost table in the lowlands of Central Yakutia is 400 to 700 m thick, increasing in depth within the central Verkhoyansk Mountains up to 1000 m (Agriculture Atlas of the Republic Sakha (Yakutia), 1989). In locations of tectonical disturbances there might be pathways upwards for fluoride rich subpermafrost waters under pressure, however this is not described by Pavlova and Fedorova (2022). Therefore, in contrast to the conclusions of Kumke et al. (2007), who link elevated lake salinity to anthropogenic factors, our results suggest that high salinity in some of our sampled lakes could be a legacy of highly saline conditions for example, by leakage from older fluoride-bearing lacustrine sediments of evaporites or some other hydrological link to old or new local salt deposits.

4.3 Specificity of lakes and lake hydrochemistry

In our study, we investigated different lake types in the Central Yakutian lowland and mountain permafrost landscapes. The sampled mountain lakes in the Verkhoyansk mountain range include a wide range of lake sizes and differ in terms of lake genesis and lake depth and surface area. Mountain lakes are, on one hand, glacial lakes spanning from large deep lakes to small lakes representing bedrock-dammed and moraine-dammed glacial lakes. On the other hand, lakes in moraine settings and mountain river floodplains formed due to thermokarst. For the mountain lakes we could not proceed further to specific lake classification, as we would have to carry out more related field work and geomorphological analyses. In contrast, for the lowland thermokarst lakes, we could well classify the lakes into three different thermokarst lake types of different lake development stages, of those two: i) new thermokarst lakes encompassing both, the dyede and the tyympy stage and ii) the old alaas lakes represent the lake chronosequence for Central Yakutia according to Bosikov (1991; Soloviev (1959); Desyatkin and Desyatkin (2006) and Desyatkin, (2008). Related to our sampled lake selection, we added an additional lake stage: the connected alaas lake type (as also described in Hughes-Allen et al. 2021, 2023; Ollivier et al., 2026), that formed due to further degradation of the alaases related to more recent hydrological connections.

For comparison, for the Western Siberian permafrost peatland, Kirpotin et al., (2007, 2009) and Pokrovsky et al., (2011, 2014) describe a cyclic chronosequence for peatland thermokarst lakes, using lake diameter as a proxy for the lake age. Shirokova et al. (2009) and Manasypov et al. (2014) describe that a typical feature of western Siberian thermokarst peatland lakes, ponds and drained thermokarst lakes (khasyreys) is a linear relationship between DOC concentration and specific electrical conductivity, respectively versus the lake surface area. The authors describe how DOC together with the specific electrical conductivity decrease along with increasing lake size and lake age. High DOC and mineralisation characterise the youngest and smallest water bodies due to leaching and thawing of surface soil ice. In contrast, the larger West Siberian water bodies are characterised by low DOC and specific electrical conductivity, predominantly due to much long residence times and strong mineralisation of DOC. This Western Siberian peatland lake chronosequence however is different compared to the Central Yakutian thermokarst lake chronosequence described in this study. For the Central Yakutian thermokarst lakes, we cannot find a systematic relationship of lake surface area inverse to DOC or specific electrical conductivity. For example, new thermokarst lakes also occur as larger lakes, e.g. on the sandy Bestyakh terrace of Lena River showing high DOC due to the dominant forest land cover and a large lake area at the same time. In addition, the old alaas lake type in our study shows high scatter in the DOC and lake surface area relationship. The sampled old alaas lakes are often located in settlement areas or in alaases with intense herding of cattle, however to statistically study the influence of cattle herding and human land use was beyond the capacity of this study as not all relevant data could be robustly sampled during our field work and afterwards. This potentially important influence of cattle herding connected to the old alaas lakes in the alaases is another major difference to the Western Siberian peatland thermokarst lake sequence.

In Central Yakutia, the sampled new thermokarst lakes showing a depleted isotopic composition are the ones also located in Yedoma sedimentary deposits that are known for their high ice content, and by this high potential for permafrost degradation

due to ground-ice melt, as also Ollivier et al. (2026) could trace the ground ice thaw in Yedoma and the successive organic input by carbon isotopic analyses. We assume, this is in contrast to the old alaas lakes and connected alaas lakes that are located within the considerably reworked and ground-ice depleted Holocene alaas deposits (e.g., Windirsch et al., 2019, 2020) where no signals from ground ice melt are to be expected.

The limited role of groundwater for contributing dissolved and particulate input from the surrounding sediments and rocks is characteristic of lakes in permafrost landscapes (Pienitz et al. 1997; Pienitz and Smol, 1993), in contrast to groundwater as a dominating source in non-permafrost areas (Wetzel, 2001). Groundwater and intermediate flows in sediment and rocky sublayers are strongly limited due to permafrost acting as a barrier to downward and upward water movements, although flow is possible through the thawed active layer in summer and perennially unfrozen talik that forms beneath deeper surface water bodies due to the high heat capacity of water (Pienitz et al. 1997; Pavlova et al. 2016; Strauss et al. 2017). Thus, the thawed active layer in the late summer months and sub-lake and sub-river taliks can function as aquifers enabling isotope and ionic transports (Walvoord and Kurylyk, 2016) as we could also show in a study throughout the summer on Herschel Island in Canada (Coch et al. 2019).

In their review, Arsenault et al. (2019, 2022) summarise how thermokarst lakes combine the morphological and chemical characteristics of lakes as well as peatland ponds. The authors consider typical thermokarst lakes as lakes with a shallow lake-water level. The absence of thermal and chemical stratification is a key characteristic of thermokarst lakes and khasyreys in Western Siberia. Shallow lake water levels are also typical for the old alaas lakes in our thermokarst lake sequence. Deeper thermokarst lakes, such as the new thermokarst lakes, may stratify during the warm summer months, especially if they are located in forests that also restrict lake mixing by wind forcing. For most of the old alaas lakes, in contrast, wind-driven mixing of the shallow water bodies in summer leads to lake circulation with subsequent effects on enhanced alkalinity and organic matter recycling (Wetterich et al., 2008).

4.4 Aquatic and terrestrial plant diversity derived from sedimentary DNA

SedDNA provided rich information on aquatic plant diversity between the different lake types, as well on the terrestrial plant diversity surrounding the sampled lakes in mountain and lowland regions. Previous studies from lakes in northern and Central Yakutia show that summer temperature and lake-water mineral levels are the main drivers of aquatic plant diversity with highest species richness occurring when July temperatures are higher than 12°C and electrical conductivity ranges between 40 and 400 $\mu S\ cm^{-1}$ (Stoof-Leichsenring et al., 2022). Related to the harsher environment, such as cooler summers, mountain lake surface-sediments generally contain a lower richness compared to lowland lakes, following trends where macrophyte richness tends to decrease along latitudinal and elevational gradients due to decreasing temperature and nutrient availability (Squires and Lesack, 2003; Stoof-Leichsenring et al., 2022). Higher variability in macrophyte richness is shown within the lowland lake types, with the highest macrophyte median richness of 20 taxa occurring in connected alaas lakes with the connected alaas lakes also containing specifically floating macrophytes.

We can see that there are distinctions between a few aquatic plant taxa which have clear preferences, such as sub-emergent *Hippuris* genera occurring mainly in the freshwater mountain lakes, or the submerged macrophytes *Myriophyllum* and *Myriophyllum verticulatum* that are freshwater taxa and hence only occur in the freshwater lakes in the lowland and mountain regions. In contrast, the cosmopolitan submerged macrophytes *Stuckenia pectinata* and *Potamogeton* sp. can live in highly mineralised water, which explains their abundance across all lakes. The Potamogetonaceae are typical submerged macrophyte taxa of highly mineralised lake water, whereas *Stuckenia pectinata*, which can live in brackish waters, is the only macrophyte species occurring in the highly saline EN21440 lake. This generalist species has a high capability of acclimation and adaptation to environmental changes (Malea et al., 2021).

Submerged macrophytes can completely disappear with lake eutrophication (Bennion et al., 2000, 2018), specifically due to low water transparencies. Despite the observed low water transparencies in old alaas and connected alaas lakes, the submerged

macrophyte abundance in our study does not appear to be limited. Macrophytes actively can promote water clarity due to chemical exudates, by this creating suitable habitats for more aquatic organisms (Burks et al., 2006). As well, these lakes provide extensive areas of very shallow water, where light can still penetrate to the very shallow lake bottom despite poor water transparency. Therefore, these shallow lake zones still offer suitable habitats for submerged macrophytes, which often form dense surface mats and also for extensive emergent macrophyte belts. These extensive macrophyte vegetation belts provide important habitats for semi-terrestrial animals like the muskrat and Siberian weasel (Zakharov et al., 2022), which were introduced during the Soviet era for fur production (Zakharov et al., 2023), and for birds.

SedDNA-derived terrestrial vegetation groups match well with the satellite-derived dominant land cover in the 50-m buffer zone around our study lakes for forest and grassland, but less so for the sedDNA-derived emergent macrophyte abundance corresponding to the satellite-derived land cover fraction for wetland. Extensive wetland areas occur only around very few old alaas lakes and connected alaas lakes, specifically as several of them are located in alaases with settlements and human land use. We assume the discrepancy on one hand due to a spatial resolution mismatch between the coarser scale of the satellite-derived wetland classification compared to very localised abundance of wetland taxa, in addition to the more localised information provided by sedDNA, which can capture contributions from very localised submersed, floating, and emergent macrophytes from the lake shore environments. A study by Li et al. (2021) highlights that vegetation signals from sedDNA are extremely localised from a small catchment area for lowland lakes due to limited inflow and outflow. However, the alkaline lake water conditions that frequently occur in old alaas lakes may be unfavorable for the preservation of sedDNA (Jia et al., 2022). Because high mineral levels can result in low preservation of sedDNA, there is also the absence of terrestrial plant reads in two of our studied lakes, including the complete absence of any preserved sedDNA in one of the lowland lakes.

4.5 Yakutian lakes as resource

Lakes in the more densely populated region of Central Yakutia have served as primary sources of drinking water for humans, as well as for herded cattle and wild animals (Vladimirtseva and Germogenov, 2013; Zakharova et al., 2018) since the first settlements of the Sakha people in the 12th century (Alekseev et al., 2020). Traditionally, families resided in their winter settlement (called *kystyk* in the Sakha language) in their alaases, while in spring, they would relocate with their cattle to their summer settlements (called *saiylyk* in the Sakha language) closer to freshwater sources by the river banks (Alekseev et al., 2020). This seasonal migration could help prevent overgrazing and soil degradation in the alaases, as the vegetation diversity of meadows directly depends on grazing and trampling by cattle and horses (Danilova et al., 2013).

During the Soviet era half a century before, this traditional management system was largely replaced by a centralised hydro-territorial order enforced by a state-driven top-down management approach. This included the consolidation of large-scale subsidiary agricultural and livestock farms (referred to as collective farms, *kolkhozes*, in Russian) and the promotion of industrialisation, which led to the intensive use of surface waters (Crate et al., 2017). Settlements and villages were preferentially and strategically established near rivers or, when unavailable, in alaases with large lakes (Zakharova et al., 2018), predominantly of the connected alaas lake type. As a result, bigger settlements such as Churapcha, Tungulu, and Maya integrate several lakes of the connected alaas lake type. The surface waters experienced increased anthropogenic pressure due to higher population densities and intensified land use.

To this day, most of the communities continue to rely on these lakes, often sharing the same water bodies for both human and livestock consumption. In many cases, cattle have unrestricted access to the lakes, which raises concerns about water quality in the population. While monitoring programmes have been initiated, such as the inclusion of Tungulu Lake in the official water quality monitoring programme of the Republic of Sakha (Ministry of Nature Protection, 1994), not all lakes inhabited areas are subject to regular assessments. Many smaller lakes, which are actively used by local populations, lack more formal monitoring or protective management.

The exploration of drinking water extraction from ground water below the permafrost seems to be possible in areas, where aquifers are hydraulically connected with the Lena River through open taliks along this major river system (Pavlova & Fedorova, 2022). The authors could identify the spatial distribution patterns of fluoride in the subpermafrost aquifers from an impressive collection of analysed water samples from wells widely distributed over Central Yakutia that needs to be taken into account when planning to use subpermafrost water from wells for drinking water supply for the population.

In our study, most surface waters of alaas lakes are brackish, rendering them unsuitable for drinking water during the ice-free season due to high salinity and also due to algal blooms in these shallow water bodies. In response, the Sakha people developed an adaptive strategy that involves harvesting low-salinity ice from brackish lakes during winter time (Zakharova et al., 2018). This practice likely originated as a pragmatic way to store ice blocks outdoors through the long cold season. In spring, as temperatures begin to rise, the harvested lake ice is transferred to permafrost cellars, where it serves as a critical freshwater resource throughout the year (S.A. Fedorova, personal communication, Sakha, Aryylakh, Sakha Republic).

These sustainable water management practices are deeply rooted in centuries of traditional ecological traditional knowledge, and still in use today. However, climate change poses a growing threat to their viability. Ongoing permafrost degradation and warming temperatures increasingly hinder the use of ice cellars, prompting some communities to relocate them or abandon them altogether (Lytkin et al., 2021). Local communities are concerned about wetter and more degraded, softer soils (Popova, 2024).

The traditional, yet still dominant lifestyle of the Sakha people is closely linked to the seasonal use of natural resources (Isaev et al., 2024). Lakes are communal resources, used not only for sustenance but also for recreation and collective wellness. For instance, saline lakes are traditionally valued for their medicinal properties (Alekseev et al., 2020). The lakes also support fishing activities, both during the summer months and under ice in winter (Popova et al., 2020), although autumn to winter fishing is preferred because of easy cold storage during winter, as well as more fat supply to locals, in terms of high-calorie food products (Platonov et., 2020). Use of these resources is traditionally governed by sustainable practices, such as ceasing fishing when overexploitation of a lake is observed (A. Baishev and T. Struchkov, personal communication, Sakha, Tungulu, Sakha Republic).

We see in our study that the different chronological stages of thermokarst lake development offer various resource potentials. We find in our hydrochemical analyses that new thermokarst lakes, which formed in recent decades typically from human land use or fire disturbance exhibit good drinking water quality. These lakes could support traditional land uses such as fishing and drinking water resources for humans and forest wildlife. In contrast, it seems that in Central Yakutia, old alaas lakes have not expanded or deepened significantly in recent decades (Fedorov et al., 2014). However, alaas rims display evidence of thermokarst activity, including the development of thaw slumps (Séjourné et al. 2015), which may still increase turbidity and impact water quality in the future. Indigenous Peoples commonly view water not as a resource, but as a good to be respected (Martinez-Cruz et al., 2024). As nowadays there seem to exist fewer top-down social and political barriers in Yakutia, as the Soviet-era large-scale agriculture has been drastically reduced, traditional land use is returning, and local responsible governance of water resources should become common practice.

4.6 Potential future pathways

There is need for more data on lake hydrochemistry to improve predictions of future trajectories and the hydrochemical responses of lakes as they might differ even with a similar climate forcing. Future climate driven processes will have an influence on future lake hydrochemistry. Previous studies have demonstrated that thaw of Yedoma permafrost contains one of the largest amounts of frozen organic carbon (Strauss et al. 2017) and mobilizes both mineral solutes and organic carbon, while changes in hydrological flow paths promote their lateral transport into aquatic ecosystems (Vonk et al. 2015; Ulrich et al. 2021, Olivier et al., 2026). Thus, continued climate warming may increase vulnerability through permafrost degradation and therefore higher organic input into the lakes, altering the hydrochemical composition.

Here, we provide a conceptual framework for the trajectories of lake hydrochemistry of our studied lake types under future climate warming (Fig. 8). Specifically, old alaas lakes, as residual lakes in alaas depressions, represent the lowland thermokarst lake endmember of this continuum with highest salinities. Mountain lakes with low mineralization and low DOC represent the opposite endmember. Under future climate warming, old alaas lakes will be endangered as their trajectory will encompass enhanced evaporation with the lake hydrochemistry becoming further enriched in salinity. However, connected alaas lakes, which are characterised by lower organic and mineral content, will represent a more diluted lake hydrochemistry. A key question for future research is whether intensified thermokarst processes will lead to the formation of more complex fluvial landscapes with an increasing number of interconnected water bodies. Recent studies suggest a potential shift in hydrological dynamics, for example, Shpakova et al. (2021) who documented a rise in river discharge in Central Yakutia coinciding with the significant temperature increases observed at the majority of meteorological stations. Enhanced river discharges and enhanced connectivity in lake systems may mitigate some of the adverse effects of climate change by improving surface water connectivity, reducing concentrations of nutrients, pollutants, and salts, and potentially compensating for increased evaporation rates under a warming climate. Therefore, future permafrost degradation might increase the hydrological conductivity leading to the formation of more connected alaas lakes, and might form new thermokarst lakes with lower salinities. Future permafrost degradation processes could increase in future the relative share of surface water bodies with lower mineralisation, potentially enriching their usability as resources in Yakutia (Fig. 8).

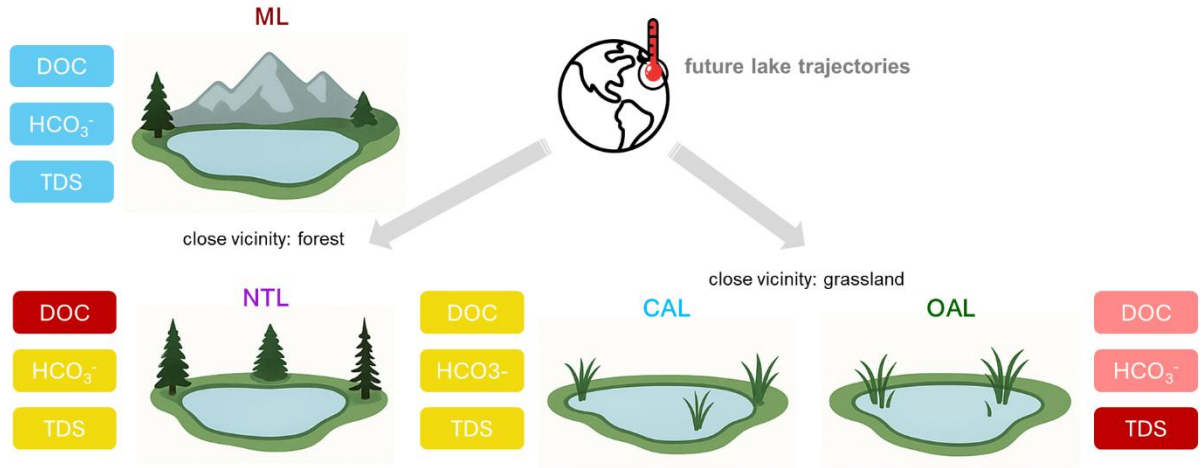


Figure 8: Schematic diagram displaying the main summer-season hydrochemical characteristics of thermokarst lowland lakes in the thermokarst lake chronosequence and of mountain lakes, highlighting the direction of future lake-type development. In the upper row, mountain lakes (ML) are characterised by least dissolved organic carbon (DOC), HCO_3^-, and total dissolved solids (TDS) (blue) in contrast to the thermokarst lakes in the lower row (yellow to red colours, yellow indicating medium concentrations, orange high concentrations up to red, highest concentrations). Connected alaas lakes (CAL) are most diluted with the lowest DOC, HCO_3^-, and TDS (yellow) in the thermokarst lake sequence. New thermokarst lakes (NTL), typically located in the forests, have moderate DOC and HCO_3^- (orange) but also lower TDS (yellow). In contrast, old alaas lakes (OAL) are characterised by highest TDS (red) and by moderate DOC and HCO_3^- (pink). We predict that future lake trajectories will result in the formation and higher abundance of CAL and NTL lake types. The lake types in this figure were generated using Perplexity AI.

5. Conclusions

Our study provides a new comprehensive assessment of the limnological state of lakes in the Central Yakutian permafrost lowland alaas landscapes and the data-deficient Oymyakon high mountain plateau in the Verkhoyansk mountain range. We classified the lakes in the Central Yakutian lowland according to the thermokarst lake development sequence into new thermokarst lakes, old alaas lakes and connected alaas lakes. Our analyses suggest that specific lake-type properties within the thermokarst lake sequence seem to drive hydrophysics and inorganic, organic, and stable water isotopic lake water composition. New thermokarst lakes are mainly located in forests and characterised by high DOC and relatively low mineral content. Whereas old alaas lakes located in alaases, typically with a high fraction of grassland land cover show medium DOC

and are mostly brackish to saline. Connected alaas lakes, where settlements are typically located, show lower DOC and mineral content due to higher dilution due to their hydrological connectivity. Based on their hydrochemical characteristics, the connected alaas lakes together with mountain lakes, represent a major group of freshwater lakes.

Specifically, the highly saline lowland lakes that we sampled were characterised by high fluoride and low chloride levels together with stable water isotopic enrichment. For highly saline lowland lakes, there seems to be no connection to specific land cover or land use. Low chloride concentration implies that contemporary evaporation processes in these lakes are not predominantly responsible for the observed high salinities and maximum stable water isotopic enrichment. Instead, there could exist a legacy of lacustrine sediments or leakage from fluoride-bearing salt deposits.

Future warming and prolonged exposure to evaporation may lead to more extreme conditions, and therefore, less diversification within lake macrophyte assemblages in old alaas lakes. On the other hand, enhanced permafrost degradation and rising surface water discharge as it is already observed in Eastern Siberia may also lead to higher hydrological connectivity and an increase of connected alaas lakes, in this case providing more freshwater to the region. New thermokarst lakes also provide good water quality supporting traditional land uses such as fishing and drinking water resources for humans and forest wildlife.

6 Acknowledgements

All data were collected and processed by scientists from the Alfred Wegener Institute, Helmholtz Centre for Polar and Marine Research (AWI), Germany, the University of Potsdam, Germany, and the North-Eastern Federal University of Yakutsk (NEFU), Russia. Our sincere gratitude goes to Iris Eder, Boris K. Biskaborn, Philip Meister, Jan Kahl, Igor Syrovatsky and Aleksey N. Pestryakov for supporting the field work and handling of the expedition samples. We acknowledge the help of Sarah Olischläger and Holly Blevins with sedDNA extractions, Mikaela Weiner for assistance in the ISOLAB, and Bennet Juhls for the support in the Hydrochemistry Laboratory and optical measurements. We also thank Thomas Böhmer for helpful discussion of geodata processing.

7 Funding

The author(s) declare financial support was received for the research, authorship, and/or publication of this article. This study was supported through the ERC consolidator grant no. 772852 to UH (PI) and partially by FSRG-2023-0027. IB was supported by the DAAD Scholarship No.91775743, the AWI Graduate School (POLMAR), and a PhD Completion Scholarship provided by University of Potsdam, Germany.

8 Data availability

The hydrochemical data, the isotopic composition of the lakes and the drone-derived lake data presented in this study are published in the PANGAEA repository (Baisheva et al. 2022a,b) and (Stieg et al. 2023a,b, 2022), respectively. SedDNA data are available in the European Nucleotide Archive (ENA) at EMBL-EBI under accession number PRJEB89990.

9 Author contributions

IB, BH, UH and LAP designed this study. IB and BH led the data collection and synthesis. LAP, UH, PVD, SNL, RMG and LAP organized the Yakutia 2021 expedition in Central Yakutia. IB, BH, AS, RG, ESZ, AVE, PVD, LAU, RJ, SK, LAP and UH participated in fieldwork. IB and KRS conducted the sedDNA analyses. AS, HM and NT conducted isotopic analyses and supported the interpretation. AE and PPO processed the hydrochemical samples and provided guidance. AS, SK and RJ

provided and processed the drone image data, IB, BH, AH and JGM undertook the satellite-derived land cover analyses. IB and AS created the data publications. IB performed statistical analyses and created figures with input from BH, JGM and UH. IB and BH led the writing of the first draft of manuscript, supported by JGM and UH. All coauthors contributed to the revision of the draft.

10 Disclaimer

This study presents results previously included as a chapter in a doctoral thesis (Baisheva, 2025).

11 References

Abnizova, A., Siemens, J., Langer, M., and Boike J.: Small ponds with major impact: The relevance of ponds and lakes in permafrost landscapes to carbon dioxide emissions, Global Biogeochem. Cy., 26, GB2041, https://doi.org/10.1029/2011GB004237, 2012.

Agricultural Atlas of the Republic Sakha (Yakutia), 1989: Matveev, I.A. (ed.), Nauk, Moscow, 115 pp. (in Russian)

Alekseev, M.N., Grinenko, O.V., Kamaletdinov, V.A. and, Mochanov, Y.A.: Neogene and Quaternary Sediments of the Lower Aldan Depression and the Middle Lena (Central Yakutia). Guidebook of Geologic Excursions (Yakutsk, July 12–21, 1990). Yakutsk, Yakutsk Sci. Center Publ., 42 p. (in Russian), 1990.

Arsenault, J., Talbot, J., Moore, T.R., Beauvais, M.-P., Franssen, J., and Roulet, N.T.: The Spatial Heterogeneity of Vegetation, Hydrology and Water Chemistry in a Peatland with Open-Water Pools, Ecosystems, 22, 1352–1367, https://doi.org/10.1007/s10021-019-00342-4, 2019.

Arsenault, J., Talbot, J., Brown, L.E., Holden, J., Martinez-Cruz, K., Sepulveda-Jauregui, A., Swindles, G. T., Wauthy, M., and Lapierre, J.-F.: Biogeochemical Distinctiveness of Peatland Ponds, Thermokarst Waterbodies, and Lakes, Geophysical Research Letters, 49, e2021GL097492, https://doi.org/10.1029/2021GL097492, 2022.

Baisheva, I.: Past and present environmental conditions in Yakutia - a (palaeo)ecological study using lake sediments, Universität Potsdam, https://doi.org/10.25932/publishup-67056, 2025.

Baisheva, I., Biskaborn, B.K., Stoof-Leichsenring, K.R., Andreev, A., Heim, B., Meucci, S., Ushnitskaya, L.A., Zakharov, E.S., Dietze, E., Glückler, R., Pestryakova, L.A., and Herzschuh, U.: Late Glacial and Holocene vegetation and lake changes in SW Yakutia, Siberia, inferred from sedaDNA, pollen, and XRF data, Front. Earth Sci., 12, https://doi.org/10.3389/feart.2024.1354284, 2024.

Baisheva, I., Pestryakova, L.A., Levina, S., Glückler, R., Biskaborn, B.K., Vyse, S.A., Heim, B., Herzschuh, U., and Stoof-Leichsenring, K.R.: Permafrost-thaw lake development in Central Yakutia: sedimentary ancient DNA and element analyses from a Holocene sediment record, J Paleolimnol, 70, 95–112, https://doi.org/10.1007/s10933-023-00285-w, 2023.

Baisheva, I., Pestryakova, L.A., Ushnitskaya, L., Davydova, P., Levina, S., Egorov, A., Zakharov, E.S., Gorodnichev, R., Glückler, R., Stieg, A., Eder, I., Kahl, J., Meister, P., Wieczorek, M., Overduin, P., Eulenburg, A., Stoof-Leichsenring, K., Biskaborn, B., Herzschuh, U. and Heim, B.: Summer anorganic hydrochemistry (cations and anions) of thermokarst lakes in the Central Yakutian Lowland and mountain lakes in the Verkhoyansk Mountain Range in Eastern Yakutia [dataset]. PANGAEA, https://doi.org/10.1594/PANGAEA.959459, 2022a.

Baisheva, I., Pestryakova, L.A., Ushnitskaya, L., Davydova, P., Levina, S., Egorov, A., Zakharov, E.S., Gorodnichev, R., Glückler, R., Stieg, A., Eder, I., Kahl, J., Meister, P., Wieczorek, M., Overduin, P., Eulenburg, A., Stoof-Leichsenring, K., Biskaborn, B., Herzschuh, U. and Heim, B.: Summer hydrophysical properties of thermokarst lakes in the Central Yakutian Lowland and mountain lakes in the Verkhoyansk Mountain Range in Eastern Yakutia [dataset]. PANGAEA, https://doi.org/10.1594/PANGAEA.952355, 2022b.

Becker, R.A., Wilks, A. R., Brownrigg, R., Minka, T.P., and Deckmyn, A.: maps: Draw Geographical Maps, https://doi.org/10.32614/CRAN.package.maps, 2025.
Bekryaev, R.V., Polyakov, I.V., and Alexeev, V.A.: Role of Polar Amplification in Long-Term Surface Air Temperature Variations and Modern Arctic Warming, Journal of Climate, 23, 3888–3906, https://doi.org/10.1175/2010JCLI3297.1, 2010.
Bennion, H., Appleby, P.G., Boyle, J.J., Carvalho, L., Luckes, S.J., and Henderson, A.C.G.: Water quality investigation of Loweswater, Cumbria, (ECRC Research Report 68). Environmental Change Research Centre: London, Environmental Change Research Centre, London, 80 pp., https://discovery.ucl.ac.uk/id/eprint/10112405, 2000.
Bennion, H., Sayer, C.D., Clarke, S.J., Davidson, T.A., Rose, N.L., Goldsmith, B., Rawcliffe, R., Burgess, A., Clarke, G., Turner, S., and Wiik, E.: Sedimentary macrofossil records reveal ecological change in English lakes: implications for conservation, J Paleolimnol, 60, 329–348, https://doi.org/10.1007/s10933-017-9941-7, 2018.
Biskaborn, B.K., Smith, S.L., Noetzli,J., Matthes, H., Vieira, G., Streletskiy, D.A., Schoeneich, P., Romanovsky, V.E., Lewkowicz, A.G., Abramov, A., Allard, M., Boike, J., Cable, W.L., Christiansen, H.H., Delaloye, R., Diekmann, B., Drozdov, D., Etzelmüller, B., Grosse, G., Guglielmin, M., Ingeman-Nielsen, T., Isaksen, K., Ishikawa, M., Johansson, M., Johannsson, H., Joo, A., Kaverin, D., Kholodov, A., Konstantinov, P., Kröger, T., Lambiel, C., Lanckman, J.-P., Luo, D., Malkova, G., Meiklejohn, I., Moskalenko, N., Oliva, M., Phillips, M., Ramos, M., Sannel, A.B.K., Sergeev, D., Seybold, C., Skryabin, P., Vasiliev, A., Wu, Q., Yoshikawa, K., Zheleznyak, M., and Lantuit, H.: Permafrost is warming at a global scale, Nat Commun, 10, 264, https://doi.org/10.1038/s41467-018-08240-4, 2019.
Biskaborn, B.K., Subetto, D.A., Savelieva, L.A., Vakhrameeva, P.S., Hansche, A., Herzschuh, U., Klemm, J., Heinecke, L., Pestryakova, L.A., Meyer, H., Kuhn, G. and Diekmann, B.: Late Quaternary vegetation and lake system dynamics in north-eastern Siberia: Implications for seasonal climate variability, Quaternary Science Reviews, 147, 406-421, https://doi.org/10.1016/j.quascirev.2015.08.014, 2016.
Biskaborn, B.K., Herzschuh, U., Bolshiyanov, D., Savelieva, L., and Diekmann, B.: Environmental variability in northeastern Siberia during the last ~13,300 yr inferred from lake diatoms and sediment–geochemical parameters, Palaeogeography, Palaeoclimatology, Palaeoecology, 329–330, 22–36, https://doi.org/10.1016/j.palaeo.2012.02.003, 2012.
Bosikov, N.P.: Evolution of alas of Central Yakutia (in russian), USSR Academy of Sciences, Siberian Branch, Institute of Permafrost Science, Yakutsk, 136 pp., 1991.
Bouchard, F., MacDonald, L.A., Turner, K.W., Thienpont, J.R., Medeiros, A.S., Biskaborn, B.K., Korosi, J., Hall, R.I., Pienitz, R., and Wolfe, B.B.: Paleolimnology of thermokarst lakes: a window into permafrost landscape evolution, Arctic Science, 3(2), 91-117, https://doi.org/10.1139/as-2016-0022, 2017.
Boyer, F., Mercier, C., Bonin, A., Le Bras, Y., Taberlet, P., and Coissac, E.: obitools: a unix-inspired software package for DNA metabarcoding, Molecular Ecology Resources, 16, 176–182, https://doi.org/10.1111/1755-0998.12428, 2016.
Brouchkov, A., Fukuda, M., Fedorov, A., Konstantinov, P., and Iwahana, G.: Thermokarst as a short-term permafrost disturbance, Central Yakutia, Permafr. Periglac. Process., 15, 81-87, https://doi.org/10.1002/ppp.473, 2004.
Burks, R.L., Mulderij, G., Gross, E., Jones, I., Jacobsen, L., Jeppesen, E., and Van Donk, E.: Center Stage: The Crucial Role of Macrophytes in Regulating Trophic Interactions in Shallow Lake Wetlands, in: Wetlands: Functioning, Biodiversity Conservation, and Restoration, vol. 191, edited by: Bobbink, R., Beltman, B., Verhoeven, J. T. A., and Whigham, D. F., Springer Berlin Heidelberg, Berlin, Heidelberg, 37–59, https://doi.org/10.1007/978-3-540-33189-6_3, 2006.
Coch, C., Juhls, B., Lamoureux, S.F., Lafreniere, M.J., Fritz, M., Heim, B., and Lantuit, H.: Comparisons of dissolved organic matter and its optical characteristics in small low and high Arctic catchments, Biogeosciences, 16(23), 4535-4553, https://doi.org/10.5194/bg-16-4535-2019, 2019.
Craig, H.: Isotopic Variations in Meteoric Waters, Science, 133, 1702–1703, https://doi.org/10.1126/science.133.3465.1702, 1961.

Crate, S., Ulrich, M., Habeck, J.O., Desyatkin, A.R., Desyatkin, R.V., Fedorov, A.N., Hiyama, T., Iijima, Y., Ksenofontov, S., Mészáros, C., and Takakura, H.: Permafrost livelihoods: a transdisciplinary review and analysis of thermokarst-based systems of indigenous land use, Anthropocene, 18, https://doi.org/10.1016/j.ancene.2017.06.001, 2017.

Czerniawska, J., and Chlachula, J.: Climate-Change Induced Permafrost Degradation in Yakutia, East Siberia, ARCTIC, 73, 509–528, https://doi.org/10.14430/arctic71674, 2020.

Danilov, N.S. (Ed.), Diversity of the Flora of Yakutia. Novosibirsk, Izd. Sib. Otd. Ross. Akad. Nauk, 326 p. (in Russian), https://kpabg.ru/cyanopro/index.html%3Fq=toolbar%252Ftoggle&destination=taxonomy%252Fterm%252F570.html, 2005.

Danilova, A.A., Danilov, P.P., Savvinov, G.N., Gavrilyeva, L.D., Petrov, A.A., and Alekseev, G.A.: Changes in properties of alas soils in Central Yakutia caused by pasture degradation, Arid Ecosyst, 3, 205–211, https://doi.org/10.1134/S2079096113040057, 2013.

Dansgaard, W.: Stable isotopes in precipitation, 16, 436, https://doi.org/10.1111/j.2153-3490.1964.tb00181.x, 1964.

De Cáceres Miquel: Indicator species analysis, https://emf-creaf.github.io/indicspecies, 2025.

Desyatkin, R., Filippov, N., Desyatkin, A., Konyushkov, D., and Goryachkin, S.: Degradation of Arable Soils in Central Yakutia: Negative Consequences of Global Warming for Yedoma Landscapes, Front. Earth Sci., 9, 683730, https://doi.org/10.3389/feart.2021.683730, 2021.

Desyatkin, A.R., Takakai, F., Fedorov, P.P., Nikolaeva, M.C., Desyatkin, R.V., and Hatano, R.: CH4 emission from different stages of thermokarst formation in Central Yakutia, East Siberia, Soil Science and Plant Nutrition, 55, 558–570, https://doi.org/10.1111/j.1747-0765.2009.00389.x, 2009.

Desyatkin, R.V.: Soil Formation in Thermokarst Depressions - Alases of Cryolithozone (in Russian), Nauka, Novosibirsk, 324 p. pp., ISBN 978-5-02-023245-7, 2008.

Desyatkin, R. and Desyatkin, A.: Thermokarst transformation of soil cover on cryolithozone flat territories, Symp. Environ. Chang. Sib. Permafr. Reg., 213–224. 2006.
http://lab.agr.hokudai.ac.jp/env/ctc_siberia/abstract_pdf_2005/22Desyatkin_abstract.pdf

Directive 2000/60/EC of the European Parliament and of the Council of 23 October 2000 establishing a framework for Community action in the field of water policy, EUR-Lex: https://eur-lex.europa.eu/eli/dir/2000/60/oj/eng, last access: 29 July 2025.

Du, Y., Chen, F., Zhang, Y., He, H., Wen, S., Huang, X., Song, C., Li, K., Wang, J., Keellings, D., and Lu, Y.: Human Activity Coupled With Climate Change Strengthens the Role of Lakes as an Active Pipe of Dissolved Organic Matter, Earth's Future, 11, e2022EF003412, https://doi.org/10.1029/2022EF003412, 2023.

Dudarev, A.A.: Public Health Practice Report: water supply and sanitation in Chukotka and Yakutia, Russian Arctic, International Journal of Circumpolar Health, 77, 1423826, https://doi.org/10.1080/22423982.2018.1423826, 2018.

Dvornikov, Y., Leibman, M., Heim, B., Bartsch, A., Herzschuh, U., Skorospekhova, T., Fedorova, I., Khomutov, A., Widhalm, B., Gubarkov, A. and Rößler, S.: Terrestrial CDOM in Lakes of Yamal Peninsula: Connection to Lake and Lake Catchment Properties, Remote Sensing, 10(2), 167. https://doi.org/10.3390/rs10020167, 2018.

Enguehard L., Kruse, S., Heim, B., Nitze, I., Falco, N., Demir, B. and Herzschuh, U.: Unraveling boreal forest composition and drivers across scales in eastern Siberia, Environmental Research Letters, 19(7), https://doi.org/10.1088/1748-9326/ad5742, 2024.

Epp, L.S., Zimmermann, H.H., and Stoof-Leichsenring, K.R.: Sampling and Extraction of Ancient DNA from Sediments, in: Ancient DNA, vol. 1963, edited by: Shapiro, B., Barlow, A., Heintzman, P.D., Hofreiter, M., Paijmans, J.L.A., and Soares, A.E.R., Springer New York, New York, NY, 31–44, https://doi.org/10.1007/978-1-4939-9176-1_5, 2019.

Fedorov, A. and Konstantinov, P.: Observations of surface dynamics with thermokarst initiation, Yukechi site, Central Yakutia, Proceedings of the 8th International Permafrost Conference, Zurich, Switzerland, pp. 239–243, ISBN 978-5-02-023245-7, 2003.

Fedorov, A.N., Ivanova, R.N., Park, H., Hiyama, T., and Iijima, Y.: Recent air temperature changes in the permafrost landscapes of northeastern Eurasia, Polar Science, 8, 114–128, https://doi.org/10.1016/j.polar.2014.02.001, 2014.

Gavrilova, M.K.: Climate of Central Yakutia (in Russian), Yakutsk Publishing House, Yakutsk, 63 p. pp., 1962.

Geng, R., Andreev, A., Kruse, S., Heim, B., van Geffen, F., Pestryakova, L., Zakharov, E., Troeva, E., Shevtsova, I., Li, F., Zhao, Y., and Herzschuh, U.: Modern Pollen Assemblages From Lake Sediments and Soil in East Siberia and Relative Pollen Productivity Estimates for Major Taxa, Front. Ecol. Evol., 10, 837857, https://doi.org/10.3389/fevo.2022.837857, 2022.

Gross, G., Jones, B., Arp, C.: Thermokarst lakes, drainage, and drained basins, in: Treatise on Geomorphology, edited by: Shroder, J. (Editor in Chief), Giardino, R., and Harbor, J., Academic Press, San Diego, CA, Glacial and Periglacial Geomorphology, 8, 325–353, https://doi.org/10.1016/B978-0-12-374739-6.00216-5, 2013.

Gu, Z., Gu, L., Eils, R., Schlesner, M., and Brors, B.: circlize implements and enhances circular visualization in R, Bioinformatics, 30, 2811–2812, https://doi.org/10.1093/bioinformatics/btu393, 2014.

Piper and Stiff–A workbook for creating Piper plots and Stiff diagrams, version 9: https://halfordhydrology.com/piper-and-stiff/, last access: 9 July 2024.

Herzschuh, U., Pestryakova, L.A., Savelieva, L.A., Heinecke, L., Böhmer, T., Biskaborn, B.K., Andreev, A., Ramisch, A., Shinneman, A.L.C., and Birks, H.J.B.: Siberian larch forests and the ion content of thaw lakes form a geochemically functional entity, Nat Commun, 4, 2408, https://doi.org/10.1038/ncomms3408, 2013.

Herzschuh, U., Liu, Y., Liu, S., Stoof-Leichsenring, K.R., Porada, P., Courtin, J., Farkas, L.Z., Böhmer, T., Biskaborn, B.K., Diekmann, B., Huang, Y., Kaufman, D., Melles, M., Meyer, H., Pestryakova, L.A., Russell, J. M., and Wagner, B.: Arctic-Boreal Bryophyte Dynamics Since the Last Glacial Inferred From Ancient DNA Metabarcoding, Journal of Biogeography, n/a, e70015, https://doi.org/10.1111/jbi.70015, 2025.

Hijmans, R.J., Etten, J. van, Sumner, M., Cheng, J., Baston, D., Bevan, A., Bivand, R., Busetto, L., Canty, M., Fasoli, B., Forrest, D., Ghosh, A., Golicher, D., Gray, J., Greenberg, J. A., Hiemstra, P., Hingee, K., Ilich, A., Geosciences, I. for M. A., Karney, C., Mattiuzzi, M., Mosher, S., Naimi, B., Nowosad, J., Pebesma, E., Lamigueiro, O. P., Racine, E. B., Rowlingson, B., Shortridge, A., Venables, B., and Wueest, R.: raster: Geographic Data Analysis and Modeling, https://doi.org/10.32614/CRAN.package.raster, 2025.

Holden, J., Moody, C.S., Edward Turner, T., McKenzie, R., Baird, A. J., Billett, M.F., Chapman, P.J., Dinsmore, K.J., Grayson, R.P., Andersen, R., Gee, C., and Dooling, G.: Water-level dynamics in natural and artificial pools in blanket peatlands, Hydrological Processes, 32, 550–561, https://doi.org/10.1002/hyp.11438, 2018.

Hu, J., Long, Y., Zhou, W., Zhu, C., Yang, Q., Zhou, S., and Wu, P.: Influence of different land use types on hydrochemistry and heavy metals in surface water in the lakeshore zone of the Caohai wetland, China, Environmental Pollution, 267, 115454, https://doi.org/10.1016/j.envpol.2020.115454, 2020.

Hughes-Allen, L., Bouchard, F., Laurion, I., Séjourné, A., Marlin, C., Hatté, C., Costard, F., Fedorov, A., and Desyatkin, A.: Seasonal patterns in greenhouse gas emissions from thermokarst lakes in Central Yakutia (Eastern Siberia), Limnology and Oceanography, 66, S98–S116, https://doi.org/10.1002/lno.11665, 2021.

Hughes-Allen, L., Bouchard, F., Séjourné, A., Fougeron, G., and Léger, E.: Automated Identification of Thermokarst Lakes Using Machine Learning in the Ice-Rich Permafrost Landscape of Central Yakutia (Eastern Siberia), Remote Sensing, 15, 1226, https://doi.org/10.3390/rs15051226, 2023.

Huser, B.J., Futter, M.N., Bogan, D., Brittain, J.E., Culp, J.M., Goedkoop, W., Gribovskaya, I., Karlsson, J., Lau, D.C.P., Rühland, K.M., Schartau, A.K., Shaftel, R., Smol, J.P., Vrede, T., and Lento, J.: Spatial and temporal variation in Arctic freshwater chemistry—Reflecting climate-induced landscape alterations and a changing template for biodiversity, Freshwater Biology, 67, 14–29, https://doi.org/10.1111/fwb.13645, 2022.

IPCC: Climate Change 2022 – Impacts, Adaptation and Vulnerability: Working Group II Contribution to the Sixth Assessment Report of the Intergovernmental Panel on Climate Change, 1st ed., Cambridge University Press, https://doi.org/10.1017/9781009325844, 2022.

Isaev, A.P., Gavrilyeva, T.N., Mikhaleva, L.G., and Chikidov, I.I.: Forest food resources in the Sakha Republic (Yakutia), Siberian Journal of Life Sciences and Agriculture, 16, 474–503, https://doi.org/10.12731/2658-6649-2024-16-3-847, 2024.

Jia, W., Liu, X., Stoof-Leichsenring, K. R., Liu, S., Li, K., and Herzschuh, U.: Preservation of sedimentary plant DNA is related to lake water chemistry, Environmental DNA, 4, 425–439, https://doi.org/10.1002/edn3.259, 2022.

Jones B.M., Grosse G., Arp C.D., Jones M.C., Anthony K.M.W., and Romanovsky V.E:. Modern thermokarst lake dynamics in the continuous permafrost zone, northern Seward Peninsula, Alaska, Journ. Geophys. Research Biogeosciences, 116, https://doi.org/10.1029/2011JG001666, 2011.

Jorgenson M.T. and Shur Y.: Evolution of lakes and basins in northern Alaska and discussion of the thaw lake cycle, Journ. Geophys. Research, Earth Surfaces, 112, F02S17, https://doi.org/10.1029/2006JF000531, 2007.

Juggins, S.: rioja: Analysis of Quaternary Science Data, https://doi.org/10.32614/CRAN.package.rioja, 2024.

Karger, D.N., Conrad, O., Böhner, J., Kawohl, T., Kreft, H., Soria-Auza, R. W., Zimmermann, N.E., Linder, H.P., and Kessler, M.: Climatologies at high resolution for the earth's land surface areas, Sci Data, 4, 170122, https://doi.org/10.1038/sdata.2017.122, 2017.

Karger, D.N., Nobis, M.P., Normand, S., Graham, C.H., and Zimmermann, N.E.: CHELSA-TraCE21k – high-resolution (1 km) downscaled transient temperature and precipitation data since the Last Glacial Maximum, Climate of the Past, 19, 439–456, https://doi.org/10.5194/cp-19-439-2023, 2023.

Kassambara, A.: ggpubr: "ggplot2" Based Publication Ready Plots, https://doi.org/10.32614/CRAN.package.ggpubr, 2026.

Kassambara, A., Mundt, F., Erdey, L.: factoextra: Extract and Visualize the Results of Multivariate Data Analyses, https://doi.org/10.32614/CRAN.package.factoextra, 2026.

Katamura, F., Fukuda, M., Bosikov, N.P., Desyatkin, R.V., Nakamura, T., and Moriizumi, J.: Thermokarst Formation and Vegetation Dynamics Inferred from A Palynological Study in Central Yakutia, Eastern Siberia, Russia, Arctic, Antarctic, and Alpine Research, 38, 561–570, https://doi.org/10.1657/1523-0430(2006)38[561:TFAVDI]2.0.CO;2, 2006.

Khudoley, A. and Prokopiev, A.: Defining the eastern boundary of the North Asian craton from structural and subsidence history studies of the Verkhoyansk fold-and-thrust belt, Special Paper of the Geological Society of America, 433, 391–410, https://doi.org/10.1130/2007.2433(19), 2007.

Kirpotin, S.N., Naumov, A.V., Vorobiov, S.N., Mironycheva-Tokareva, N.P., Kosykh, N.P., Lapshina, E.D., Marquand, J., Kulizhski, S.P. and Bleuten, W.: Western-Siberian Peatlands: Indicators of Climate Change and Their Role in Global Carbon Balance, in: Climate Change and Terrestrial Carbon Sequestration in Central Asia, edited by: Lal, R., Suleimenov, M., Stewart, B.A, Hansen, D.O. and Doraiswamy, P., Taylor and Francis, Amsterdam, 453–472, https://doi.org/10.1201/9780203932698, 2007.

Kirpotin, S.N., Polishchuk, Y.M., Zakharova, E., Shirokova, L., Pokrovsky, O., Kolmakova, M. and Dupré, B.: One of possible mechanisms of thermokarst lakes drainage in West-Siberian North, Int. J. Environ. Stud., 65, 631–635, https://doi.org/10.1080/00207230802525208, 2008.

Klein Tank, A.M.G. and Coauthors, 2002. Daily dataset of 20th-century surface air temperature and precipitation series for the European Climate Assessment. Int. J. of Climatol., 22, 1441-1453. Data and metadata available at https://www.ecad.eu/dailydata/predefinedseries.php (last accessed on August 2026)

Kloss, A.L.: Water isotope geochemistry of recent precipitation in Central and North Siberia as a proxy for the local and regional climate system, Diplom, Leibniz Universität Hannover, 95 pp., https://epic.awi.de/id/eprint/25524/, 2008.

Kokelj, S.V. and Jorgenson, M. T.: Advances in Thermokarst Research: Recent Advances in Research Investigating Thermokarst Processes, Permafrost and Periglacial Processes, 24, 108–119, https://doi.org/10.1002/ppp.1779, 2013.

Kokelj, S.V.; Zajdlik, B.; Thompson, M.S. The impacts of thawing permafrost on the chemistry of lakes across the subarctic boreal-tundra transition, Mackenzie Delta region, Canada. Permafr. Periglac., 20, 185–199. https://doi.org/10.1002/ppp.641, 2009

Ksenofontov, S.S., Kuklina, V., Kholodov, A., and Petrov, A.: On good terms: pathways to decolonizing science-appropriated Indigenous terminologies in Arctic research, Arctic Science, 11, 1–9, https://doi.org/10.1139/as-2025-0025, 2025.

Kruse, S., Jackisch, R., Gloy, J., Farkas, L., Schladebach, J., Hao, K., Heim, B., Kolmogorov, A., Zakharov, E.S., Pestryakova, L.A., Förster, M., Kleinschmit, B., and Herzschuh, U.: Point clouds with ground point classification and individual tree segmentation of 89 northern boreal forest and tundra sites from UAV-based lidar surveys in Yakutia, Russia in 2021 [dataset], PANGAEA, https://doi.org/10.1594/PANGAEA.980735, 2025.

Kruse, S., Jackisch, R., Heim, B., Gloy, J., Herzschuh, U., Kolmogorov, A., Zakharov, E.S., Pestryakova, L.A., Förster, M. and Kleinschmit, B.: Structure-from-motion (SfM) based point clouds of 21 Forest successional plots from UAV-based high-resolution photogrammetric survey in Central and Eastern Yakutia, Siberia [dataset], PANGAEA, https://doi.org/10.1594/PANGAEA.958184, 2023a.

Kruse, S., Jackisch, R., Heim, B., Gloy, J., Herzschuh, U., Kolmogorov, A., Zakharov, E.S., Pestryakova, L.A., Förster, M. and Kleinschmit, B.: Point clouds and high-level data products of 21 Forest successional plots from UAV-based Lidar survey in Central and Eastern Yakutia, [dataset]. PANGAEA, https://doi.org/10.1594/PANGAEA.957253, 2023b.

Kruse, S., Jackisch, R., Heim, B., Gloy, J., Herzschuh, U., Kolmogorov, A., Zakharov, E.S., Pestryakova, L.A., Förster, M. and Kleinschmit, B.: Lidar and multispectral footprint data of 21 forest successional plots from UAV-based survey in Central and Eastern Yakutia, Siberia [dataset]. PANGAEA, https://doi.org/10.1594/PANGAEA.958188, 2023c.

Kruse, S., Herzschuh, U., Schulte, L., Stuenzi, S.M., Brieger, F., Zakharov, E.S., and Pestryakova, L.A.: Forest inventories on circular plots on the expedition Chukotka 2018, NE Russia [dataset] PANGAEA, https://doi.org/10.1594/PANGAEA.923638, 2020.

Kruse, S., Bolshiyanov, D., Grigoriev, M., Morgenstern, A., Pestryakova, L., Tsibizov, L., and Udke, A.: Russian-German Cooperation: Expeditions to Siberia in 2018, Berichte zur Polar- und Meeresforschung, 734, 136–153, https://doi.org/10.2312/BzPM_0734_2019, 2019.

Kumke, T., Ksenofontova, M., Pestryakova, L., Nazarova, L., and Hubberten, H.-W.: Limnological characteristics of lakes in the lowlands of Central Yakutia, Russia, J Limnol, 66, 40, https://doi.org/10.4081/jlimnol.2007.40, 2007.

Lento, J., Culp, J.M., Levenstein, B., Aroviita, J., Baturina, M.A., Bogan, D., Brittain, J.E., Chin, K., Christoffersen, K.S., Docherty, C., Friberg, N., Ingimarsson, F., Jacobsen, D., Lau, D.C.P., Loskutova, O.A., Milner, A., Mykrä, H., Novichkova, A.A., Ólafsson, J.S., Schartau, A.K., Shaftel, R., and Goedkoop, W.: Temperature and spatial connectivity drive patterns in freshwater macroinvertebrate diversity across the Arctic, Freshwater Biology, 67, 159–175, https://doi.org/10.1111/fwb.13805, 2022.

Li, K., Stoof-Leichsenring, K.R., Liu, S., Jia, W., Liao, M., Liu, X., Ni, J., and Herzschuh, U.: Plant sedimentary DNA as a proxy for vegetation reconstruction in eastern and northern Asia, Ecological Indicators, 132, 108303, https://doi.org/10.1016/j.ecolind.2021.108303, 2021.

Li, W., Cao, X., Stoof-Leichsenring, K., Hou, X., Yu, S.-Y., Tian, F., and Herzschuh, U.: Holocene lake response to glacier and catchment changes on the eastern Tibetan Plateau from quantitative conductivity reconstructions based on sedaDNA-derived macrophyte records, Quaternary Science Reviews, 338, 108806, https://doi.org/10.1016/j.quascirev.2024.108806, 2024.

Lopez, C.M.L., Brouchkov, A., Nakayama, H., Takakai, F., Fedorov, A.N., and Fukuda, M.: Epigenetic salt accumulation and water movement in the active layer of central Yakutia in eastern Siberia, Hydrological Processes, 21, 103–109, https://doi.org/10.1002/hyp.6224, 2007.

Lytkin, V., Suleymanov, A., Vinokurova, L., Grigorev, S., Golomareva, V., Fedorov, S., Kuzmina, A., and Syromyatnikov, I.: Influence of Permafrost Landscapes Degradation on Livelihoods of Sakha Republic (Yakutia) Rural Communities, Land, 10(2), 101; https://doi.org/10.3390/land10020101, 2021.

Marsh, P., Russell, M., Pohl, S., Haywood, H., and Onclin, C.: Changes in thaw lake drainage in the Western Canadian Arctic from 1950 to 2000, Hydrol. Process., 23, 145-158, https://doi.org/10.1002/hyp.7179, 2009.

Malea, L., Nakou, K., Papadimitriou, A., Exadactylos, A., and Orfanidis, S.: Physiological Responses of the Submerged Macrophyte Stuckenia pectinata to High Salinity and Irradiance Stress to Assess Eutrophication Management and Climatic Effects: An Integrative Approach, Water, 13, 1706, https://doi.org/10.3390/w13121706, 2021.

Manasypov, R.M., Pokrovsky, O.S., Kirpotin, S.N., and Shirokova, L.S.: Thermokarst lake waters across the permafrost zones of western Siberia, The Cryosphere, 8, 1177–1193, https://doi.org/10.5194/tc-8-1177-2014, 2014.

Mc Cartney, A.M., Anderson, J., Liggins, L., Hudson, M.L., Anderson, M.Z., TeAika, B., Geary, J., Cook-Deegan, R., Patel, H.R., and Phillippy, A.M.: Balancing openness with Indigenous data sovereignty: An opportunity to leave no one behind in the journey to sequence all of life, Proceedings of the National Academy of Sciences, 119, e2115860119, https://doi.org/10.1073/pnas.2115860119, 2022.

Meyer, H., Schirrmeister, L., Andreev, A., Wagner, D., Hubberten, H.-W., Yoshikawa, K., Bobrov, A., Wetterich, S., Opel, T., Kandiano, E., Brown, J.: Lateglacial and Holocene isotopic and environmental history of northern coastal Alaska - Results from a buried ice-wedge system at Barrow, Quaternary Science Reviews, 29(27), 3720-3735, https://doi.org/10.1016/j.quascirev.2010.08.005, 2010.

Meyer, H., Dereviagin, A., Siegert, C., Schirrmeister, L., and Hubberten, H.-W.: Palaeoclimate Reconstruction on Big Lyakhovsky Island, North Siberia—Hydrogen and Oxygen Isotopes in Ice Wedges, Permafrost and Periglacial Processes, 13: 91–105, https://doi.org/10.1002/ppp.416, 2002.

Meyer, H., Schönicke, L., Wand, U., Hubberten, H.W., and Friedrichsen, H.: Isotope Studies of Hydrogen and Oxygen in Ground Ice - Experiences with the Equilibration Technique, Isotopes in Environmental and Health Studies, 36, 133–149, https://doi.org/10.1080/10256010008032939, 2000.

Miesner, T., Herzschuh, U., Pestryakova, L.A., Wieczorek, M., Zakharov, E.S., Kolmogorov, A.I., Davydova, P.V., and Kruse, S.: Forest structure and individual tree inventories of northeastern Siberia along climatic gradients, Earth Syst. Science Data, 14, 5695–5716, https://doi.org/10.5194/essd-14-5695-2022, 2022.

Miner, K.R., Turetsky, M.R., Malina, E., Bartsch, A., Tamminen, J., McGuire, A.D., Fix, A., Sweeney, C., Elder, C.D., and Miller, C.E.: Permafrost carbon emissions in a changing Arctic, Nat Rev Earth Environ, 3, 55–67, https://doi.org/10.1038/s43017-021-00230-3, 2022.

Morgenstern, A., Heim, B., Pestryakova, L., Bolshiyanov, D., Grigoriev, M., Ayunov, D., and Dill, A.: Russian-German Cooperation: Expeditions to Siberia in 2021, https://doi.org/10.57738/BzPM_0772_2023, 2023.

Naumov, A., Akimova, V., Sidorova, D., and Topnikov, M.: Agriculture and land use in the North of Russia: Case study of Karelia and Yakutia, Open Geosciences, 12, 1497–1511, https://doi.org/10.1515/geo-2020-0210, 2020.

Nitzbon, J., Westermann, S., Langer, M., Martin, L.C.P., Strauss, J., Laboor, S., and Boike, J.: Fast response of cold ice-rich permafrost in northeast Siberia to a warming climate, Nat Commun, 11, 2201, https://doi.org/10.1038/s41467-020-15725-8, 2020.

Nitze, I., Grosse, G., Jones, B.M., Romanovsky, V.E., and Boike, J.: Remote sensing quantifies widespread abundance of permafrost region disturbances across the Arctic and Subarctic, Nat Commun, 9, 5423, https://doi.org/10.1038/s41467-018-07663-3, 2018.

Olago, D., Opere, A., and Barongo, J.: Holocene palaeohydrology, groundwater and climate change in the lake basins of the Central Kenya Rift, Hydrological Sciences Journal, 54, 765–780, https://doi.org/10.1623/hysj.54.4.765, 2009.

Ollivier, S., Séjourné, A., Hatté, C., Bouchard, F., Noret, A., Highes-Allen, L., Costard, F., Gandois, L.: Massive concentrations of old dissolved organic carbon from Yedoma thaw in lakes in Siberia, Commun Earth Environ, 7, 200, https://doi.org/10.1038/s43247-026-03229-0, 2026.

Pavlova, M.R., Galanin, A.A., Lytkin, V.M. and Torgovkin, N.V.: Structure and formation conditions of the ice complex in the lower reaches of the Vilyui River, Central Yakutia, Earth's Cryosphere, 28(6), 3–16, https://doi.org/10.15372/KZ20240601, 2024.

Pavlova, N.A. and Fedorova, S.V.: Fluoride Distribution in Subpermafrost Groundwater in Central Yakutia, Earth's Cryosphere, 2022, 26(2), 34–41, https://earthcryosphere.ru/arch/eng2022-2/pavlova_2022-2_eng, 2022.

Pavlova, N.A., Kolesnikov, A.B., Efremov, V.S., and Shepelev, V.V.: Groundwater chemistry in intrapermafrost taliks in Central Yakutia, Water Resour, 43, 353–363, https://doi.org/10.1134/S0097807816020135, 2016.

Pestryakova, L.A., Herzschuh, U., Wetterich, S., and Ulrich, M.: Present-day variability and Holocene dynamics of permafrost-affected lakes in central Yakutia (Eastern Siberia) inferred from diatom records, Quaternary Science Reviews, 51, 56–70, https://doi.org/10.1016/j.quascirev.2012.06.020, 2012.

Pienitz, R. and Smol, J.P.: Diatom assemblages and their relationship to environmental variables in lakes from the boreal forest-tundra ecotone near Yellowknife, Northwest Territories, Canada, Hydrobiol, 269, https://link.springer.com/article/10.1007/BF00028037, 1993.

Pienitz, R., Smol, J.P., and Lean, D.R.: Physical and chemical limnology of 59 lakes located between the southern Yukon and the Tuktoyaktuk Peninsula, Northwest Territories (Canada), Can. J. Fish. Aquat. Sci., 54, 330–346, https://doi.org/10.1139/f96-274, 1997.

Piper, A.M.: a graphic procedure in the geochemical interpretation of water-analyses: https://agupubs.onlinelibrary.wiley.com/doi/10.1029/TR025i006p00914, 1944, last access: 9 July 2024.

Platonov, T., Stepanov, K., Nyukkanov, A., Kuzmina, N., and Gorokhova, A.: Food value and basic parasitosis of fish used in food by indigenous populations of Yakutia, BIO Web Conf., 17, 00242, https://doi.org/10.1051/bioconf/20201700242, 2020.

Pokrovsky, O.S., Shirokova, L.S. and Kirpotin, S.N.: Biogeochemistry of Thermokarst Lakes of Western Siberia, Nova Science Publ. Inc., NY, 163 pp., ISBN 978-1-62948-799-1, 2014

Pokrovsky, O.S., Shirokova, L.S., Kirpotin, S.N., Audry, S., Viers, J. and Dupré, B.: Effect of permafrost thawing on organic carbon and trace element colloidal speciation in the thermokarst lakes of western Siberia, Biogeosciences, 8, 565–583, https://doi.org/10.5194/bg-8-565-2011, 2011

Popova, L.: Indigenous Subsistence Practices of the Sakha Horse Herders under Changing Climate in the Arctic, Climate, 12, 134, https://doi.org/10.3390/cli12090134, 2024.

Popova, N.V., Abramov, A.F., and Markova, L.N.: Fishing as an important source of food in the Arctic and subarctic zones of Yakutia, Open Agriculture, 5, 213–218, https://doi.org/10.1515/opag-2020-0022, 2020.

Popp, S., Diekmann, B., Meyer, H., Siegert, C., Syromyatnikov, I., and Hubberten, H.-W.: Palaeoclimate signals as inferred from stable-isotope composition of ground ice in the Verkhoyansk foreland, Central Yakutia, Permafrost and Periglacial Processes, 17, 119–132, https://doi.org/10.1002/ppp.556, 2006.

Rantanen, M., Karpechko, A.Y., Lipponen, A., Nordling, K., Hyvärinen, O., Ruosteenoja, K., Vihma, T., and Laaksonen, A.: The Arctic has warmed nearly four times faster than the globe since 1979, Commun Earth Environ, 3, 1–10, https://doi.org/10.1038/s43247-022-00498-3, 2022.

R Core Team. (2026) R: A Language and Environment for Statistical Computing. R Foundation for Statistical Computing. Scientific Research Publishing: https://cran.r-project.org/doc/manuals/r-release/fullrefman.pdf, last access: 20 September 2026.

Revéret, A., Alsos, I., and Heintzman, P.: Aquatic Vegetation DNA from Lake Sediments, 235–253, https://doi.org/10.1007/978-3-031-43799-1_8, 2023a.
Revéret, A., Rijal, D.P., Heintzman, P.D., Brown, A.G., Stoof-Leichsenring, K.R., and Alsos, I.G.: Environmental DNA of aquatic macrophytes: The potential for reconstructing past and present vegetation and environments, Freshwater Biology, 68, 1929–1950, https://doi.org/10.1111/fwb.14158, 2023b.
Rockström, J., Kotzé, L., Milutinović, S., Biermann, F., Brovkin, V., Donges, J., Ebbesson, J., French, D., Gupta, J., Kim, R., Lenton, T., Lenzi, D., Nakicenovic, N., Neumann, B., Schuppert, F., Winkelmann, R., Bosselmann, K., Folke, C., Lucht, W., Schlosberg, D., Richardson, K., and Steffen, W.: The planetary commons: A new paradigm for safeguarding Earth-regulating systems in the Anthropocene, Proceedings of the National Academy of Sciences, 121, e2301531121, https://doi.org/10.1073/pnas.2301531121, 2024.
Romanovsky, V.E., Drozdov, D.S., Oberman, N.G., Malkova, G.V., Kholodov, A.L., Marchenko, S.S., Moskalenko, N.G., Sergeev, D.O., Ukraintseva, N.G., Abramov, A.A., Gilichinsky, D.A., and Vasiliev, A.A.: Thermal state of permafrost in Russia, Permafrost and Periglacial Processes, 21, 136–155, https://doi.org/10.1002/ppp.683, 2010.
Romanovsky, N.N.: Basics of Cryogenesis of the Lithosphere. Moscow, Izd. Mosk. Gos. Univ., 366 p. (in Russian), https://www.geokniga.org/sites/geokniga/files/books/kriogeneza-litosfery-nnromanovskiy-1993.pdf, 1993.
Różańska-Boczula, M., and Sender, J.: Exploring the relationships between macrophyte groups and environmental conditions in lake ecosystems, Sci Rep, 15, 11162, https://doi.org/10.1038/s41598-024-80553-5, 2025.
Rumyantsev, V.A., Kondratyev, S.A., and Izmaylova, A.V.: Russian Lakes, Geographical Classification, in: Encyclopedia of Lakes and Reservoirs, edited by: Bengtsson, L., Herschy, R.W., and Fairbridge, R.W., Springer Netherlands, Dordrecht, 679–691, https://doi.org/10.1007/978-1-4020-4410-6_242, 2012.
Serreze, M.C. and Barry, R.G.: Processes and impacts of Arctic amplification: A research synthesis, Global and Planetary Change, 77, 85–96, https://doi.org/10.1016/j.gloplacha.2011.03.004, 2011.
Shahgedanova, M.: The Physical Geography of Northern Eurasia, Oxford University Press, 597 pp., 2003.
Shirokova, L.S., Pokrovsky, O.S., Kirpotin, S.N., Desmukh, C., Pokrovsky, B.G., Audry, S. and Viers, J.: Biogeochemistry of organic carbon, CO2, CH4, and trace elements in thermokarst water bodies in discontinuous permafrost zones of Western Siberia, Biogeochemistry, 113, 573–593, https://doi.org/10.1007/s10533-012-9790-4, 2013.
Shpakova, R.N.: Changes in the Behavior of Long-Term Waterflow Variations in the Middle Part of Yakutia under the Global Warming Conditions, IOP Conf. Ser.: Earth Environ. Sci., 666, 042010, https://doi.org/10.1088/1755-1315/666/4/042010, 2021.
Skorospekhova, T., Hei, B., Chetverova, A., Fedorova, I., Alekseeva, N., Bobrova, O., Dvornikov, Y., Eulenburg, A., Rössler, S., and Morgenstern, A.: Coloured Dissolved Organic Matter Variability in Tundra Lakes of the Central Lena River Delta (N-Siberia), Polarforschung 87(2), 125 – 133, 10.2312/polarforschung.87.2.125, 2018.
Slowikowski, K., Schep, A., Hughes, S., Dang, T.K., Lukauskas, S., Irisson, J.-O., Kamvar, Z.N., Ryan, T., Christophe, D., Hiroaki, Y., Gramme, P., Abdol, A.M., Barrett, M., Cannoodt, R., Krassowski, M., Chirico, M., Aphalo, P., and Barton, F.: ggrepel: Automatically Position Non-Overlapping Text Labels with “ggplot2,” https://slowkow.com/projects/ggrepel/, 2024.
Smith, S.L., O’Neill, H.B., Isaksen, K., Noetzli, J., and Romanovsky, V.E.: The changing thermal state of permafrost, Nat Rev Earth Environ, 3, 10–23, https://doi.org/10.1038/s43017-021-00240-1, 2022.
Spatial Data Science: https://r-spatial.org/book/, last access: 31 May 2024.
Sobek, S., Tranvik, L.J., Prairie, Y.T., Kortelainen, P., and Cole, J. J.: Patterns and regulation of dissolved organic carbon: An analysis of 7,500 widely distributed lakes, Limnology and Oceanography, 52, 1208–1219, https://doi.org/10.4319/lo.2007.52.3.1208, 2007.
Soloviev, P.A.: The permafrost zone of the northern part of the Lena-Amga interfluve (in Russian), Academy of Sciences of the USSR, V. A. Obruchev Institute of Permafrost Studies, Northeastern Branch, Moscow, 143 pp., 1959.

Squires, M., and Lesack, L.: The relation between sediment nutrient content and macrophyte biomass and community structure along a water transparency gradient among lakes of the Mackenzie Delta, Canadian Journal of Fisheries and Aquatic Sciences, 60, 333–343, https://doi.org/10.1139/f03-027, 2003.

Stieg, A., Kruse, S., Jackisch, R., Farkas, L., Büchner, J., Baisheva, I., Glückler, R., Zakharov, E.S., Heim, B., Wieczorek, M., Pestryakova, L.A., and Herzschuh, U.: 53 orthomosaics processed from Unoccupied Aerial Vehicle (UAV) image data of lake shorelines sampled during a field campaign in Central and Eastern Yakutia, Siberia in 2021 (RU-Land_2021_Yakutia) [dataset]. PANGAEA, https://doi.org/10.1594/PANGAEA.956223, 2023a.

Stieg, A., Kruse, S., Jackisch, R., Farkas, L., Büchner, J., Baisheva, I., Glückler, R., Zakharov, E.S., Heim, B., Wieczorek, M., Pestryakova, L.A., and Herzschuh, U.: Lake information on orthomosaics created from lake image data sampled during a field campaign in Central and Eastern Yakutia, Siberia in 2021 (RU-Land_2021_Yakutia) [dataset]. PANGAEA, https://doi.org/10.1594/PANGAEA.955723, 2023b.

Stieg, A., Herzschuh, U., Baisheva, I., Glückler, R., Eder, I., Zakharov, E.S., Biskaborn, B.K., Meister, P., Davydova, P.V.; Kahl, J., Weiner, M., Marent, A., Heim, B., Wieczorek, M. and Meyer, H.: Stable water isotope data of 66 lakes from a summer field campaign in Central and Eastern Yakutia, Siberia in 2021 (RU-Land_2021_Yakutia) [dataset]. PANGAEA, https://doi.org/10.1594/PANGAEA.950688, 2022.

Stoof-Leichsenring, K.R., Huang, S., Liu, S., Jia, W., Li, K., Liu, X., Pestryakova, L.A., and Herzschuh, U.: Sedimentary DNA identifies modern and past macrophyte diversity and its environmental drivers in high-latitude and high-elevation lakes in Siberia and China, Limnology and Oceanography, 67, 1126–1141, https://doi.org/10.1002/lno.12061, 2022.

Strauss, J., Schirrmeister, L., Grosse, G., Fortier, D., Hugelius, G., Knoblauch, C., Romanovsky, V., Schädel, C., Schneider Von Deimling, T., Schuur, E.A.G., Shmelev, D., Ulrich, M., and Veremeeva, A.: Deep Yedoma permafrost: A synthesis of depositional characteristics and carbon vulnerability, Earth-Science Reviews, 172, 75–86, https://doi.org/10.1016/j.earscirev.2017.07.007, 2017.

Sukneva, S.A.: Migration processes in the Sakha Republic (Yakutia), Espace populations sociétés. Space populations societies, https://doi.org/10.4000/eps.10352, 2021.

Suleymanov, A.A., Lytkin, V.M., Vinokurova, L.I., Grigoryev, S.A., Fedorov, S. I., Golomareva, V.Yu., Basharin, N.I., and Aprosimov, D.A.: Rural Communities of Yakutia in Conditions of Permafrost Degradation: Key Risks, Social Consequences, and Adaptation Mechanisms, AaN, 199–231, https://doi.org/10.37482/issn2221-2698.2023.52.199, 2023.

Taberlet, P., Coissac, E., Pompanon, F., Gielly, L., Miquel, C., Valentini, A., Vermat, T., Corthier, G., Brochmann, C., and Willerslev, E.: Power and limitations of the chloroplast trnL (UAA) intron for plant DNA barcoding, Nucleic Acids Research, 35, e14–e14, https://doi.org/10.1093/nar/gkl938, 2007.

Torgovkin, N.V., Sivtsev, D.E., Gavrilova, A.A., Platonov, I.A., Kizyakov, A.I., Schirrmeister, L., Opel, T., Wetterich, S., Breitenbach, S.F.M., and Meyer, H.: New Data on the Geochronology of Quaternary Sediments and Stable Oxygen and Hydrogen Isotopes in Ground Ice of the Mamontova Gora, Earth's Cryosphere, 28(5), 3–11, https://epic.awi.de/id/eprint/60768, 2024.

Troeva, E. I. (Ed.): The far North: plant biodiversity and ecology of Yakutia, Springer, Dordrecht; New York, 390 pp., 2010.

Ulrich M., Jongejans L.L., Grosse G., Schneider B., Opel T., Wetterich S., Fedorov A.N., Schirrmeister L., Windirsch T., Wiedmann J. and Strauss J.: Geochemistry and Weathering Indices of Yedoma and Alas Deposits beneath Thermokarst Lakes in Central Yakutia, Front. Earth Sci., 9, 704141, https://doi.org/10.3389/feart.2021.704141, 2021.

Ulrich, M.: Holocene thermokarst dynamics in Central Yakutia - A multi-core and robust grain-size endmember modeling approach, Quaternary Science Reviews, 18,10-33, https://doi.org/10.1016/j.quascirev.2019.06.010, 2019.

Ulrich, M., Wetterich, S., Rudaya, N., Frolova, L., Schmidt, J., Siegert, C., Fedorov, A.N., and Zielhofer, C.: Rapid thermokarst evolution during the mid-Holocene in Central Yakutia, Russia, The Holocene, 27, 1899–1913, https://doi.org/10.1177/0959683617708454, 2017a.

Ulrich, M., Matthes, H., Schirrmeister, L., Schütze, J., Park, H., Iijima, Y., and Fedorov, A.N.: Differences in behavior and distribution of permafrost-related lakes in Central Yakutia and their response to climatic drivers, Water Resources Research, 53, 1167–1188, https://doi.org/10.1002/2016WR019267, 2017b.

Ulrich M., Jongejans L.L., Grosse G., Schneider B., Opel T., Wetterich S., Fedorov A.N., Schirrmeister L., Windirsch T., Wiedmann J. and Strauss J.: Geochemistry and Weathering Indices of Yedoma and Alas Deposits beneath Thermokarst Lakes in Central Yakutia, Front. Earth Sci. 9:704141. https://doi.org/10.3389/feart.2021.704141, 2021.

van Geffen, F., Hänsch, R., Demir, B., Kruse, S., Herzschuh, U., and Heim, B.: A Benchmark Dataset for Sentinel-2 Based Forest Type Classification in the Siberian Summergreen-Evergreen Forest Transition Zone, IEEE Journal of Selected Topics in Applied Earth Observations and Remote Sensing, 18, 18509-18527, https://doi.org/10.1109/JSTARS.2025.3562912, 2025.

van Geffen, F., Heim, B., Brieger, F., Geng, R., Shevtsova, I. A., Schulte, L., Stuenzi, S. M., Bernhardt, N., Troeva, E. I., Pestryakova, L. A., Zakharov, E. S., Pflug, B., Herzschuh, U., and Kruse, S.: SiDroForest: a comprehensive forest inventory of Siberian boreal forest investigations including drone-based point clouds, individually labeled trees, synthetically generated tree crowns, and Sentinel-2 labeled image patches, Earth Syst. Science Data, 14, 4967–4994, https://doi.org/10.5194/essd-14-4967-2022, 2022.

Vladimirtseva, M.V. and Germogenov, N.I.: Birds of Yakutia: Fauna Diversity, Ecology, Role in Ecosystems and Human Life, J Biodivers Endanger Species, 01, https://doi.org/10.4172/2332-2543.1000114, 2013.

Vonk, J.E., Tank, S.E., Bowden, W.B., Laurion, I., Vincent, W.F., Alekseychik, P., Amyot, M., Billet, M.F., Canário, J., Cory, R.M., Deshpande, B.N., Helbig, M., Jammet, M., Karlsson, J., Larouche, J., MacMillan, G., Rautio, M., Walter Anthony, K.M., and Wickland, K.P.: Reviews and syntheses: Effects of permafrost thaw on Arctic aquatic ecosystems, Biogeosciences, 12, 7129–7167, https://doi.org/10.5194/bg-12-7129-2015, 2015.

Walsh, J.E.: Intensified warming of the Arctic: Causes and impacts on middle latitudes, Global and Planetary Change, 117, 52–63, https://doi.org/10.1016/j.gloplacha.2014.03.003, 2014.

Walvoord, M.A. and Kurylyk, B.L.: Hydrologic Impacts of Thawing Permafrost—A Review, Vadose Zone Journal, 15, vzj2016.01.0010, https://doi.org/10.2136/vzj2016.01.0010, 2016.

Wang, W., Jin, H., Zhang, Z., Zhelezniak, M.N., Spektor, V.V., Șerban, R.-D., Li, A., Tumskoy, V., Jin, X., Yang, S., Zhang, S., Li, X., Șerban, M., Wu, Q., and Wen, Y.: Monitoring Ground Surface Deformation of Ice-Wedge Polygon Areas in Saskylakh, NW Yakutia, Using Interferometric Synthetic Aperture Radar (InSAR) and Google Earth Engine (GEE), Remote Sensing, 15, 1335, https://doi.org/10.3390/rs15051335, 2023.

Wei, T., Simko, V., Levy, M., Xie, Y., Jin, Y., Zemla, J., Freidank, M., Cai, J., and Protivinsky, T.: corrplot: Visualization of a Correlation Matrix, https://doi.org/10.32614/CRAN.package.corrplot, 2024.

Wen, D., Zhang, F., Zhang, E., Wang, C., Han, S., and Zheng, Y.: Arsenic, fluoride and iodine in groundwater of China, Journal of Geochemical Exploration, 135, 1–21, https://doi.org/10.1016/j.gexplo.2013.10.012, 2013.

Wetterich, S., Herzschuh, U., Meyer, H., Pestryakova, L., Plessen, B., Lopez, C.M.L., and Schirrmeister, L.: Evaporation effects as reflected in freshwaters and ostracod calcite from modern environments in Central and Northeast Yakutia (East Siberia, Russia), Hydrobiologia, 614, 171–195, https://doi.org/10.1007/s10750-008-9505-y, 2008.

Wetzel, R.G.: Limnology: Lake and River Ecosystems, Gulf Professional Publishing, 1023 pp., 2001.

Wickham, H., Hester, J., Chang, W., Bryan, J., and RStudio: devtools: Tools to Make Developing R Packages Easier, https://doi.org/10.32614/CRAN.package.devtools, 2022.

Wickham, H., François, R., Henry, L., Müller, K., Vaughan, D., Software, P., and PBC: dplyr: A Grammar of Data Manipulation, https://doi.org/10.32614/CRAN.package.dplyr, 2023.

Wickham, H., Chang, W., Henry, L., Pedersen, T.L., Takahashi, K., Wilke, C., Woo, K., Yutani, H., Dunnington, D., Brand, T. van den, Posit, and PBC: ggplot2: Create Elegant Data Visualisations Using the Grammar of Graphics, https://ggplot2.tidyverse.org/reference/ggplot2-package.html, 2025.

Windirsch, T., Grosse, G., Ulrich, M., Schirrmeister, L., Fedorov, A.N., Konstantinov, P., Fuchs, M., Strauss, J.: Carbon characteristics of permafrost core PG-YUK15-YED1 from Yukechi Alas, Central Yakutia [dataset], PANGAEA, https://doi.org/10.1594/PANGAEA.898742, 2019.

Windirsch, T., Grosse, G., Ulrich, M., Schirrmeister, L., Fedorov, A. N., Konstantinov, P. Ya., Fuchs, M., Jongejans, L. L., Wolter, J., and Strauss, J.: Organic Carbon Characteristics in Ice-rich Permafrost in Alas and Yedoma Deposits, Central Yakutia, Siberia, Biogeosciences, 17, 3797–3814, https://doi.org/10.5194/bg-2019-470, 2020.

Williamson C.E., Saros J.E., Vincent W.F., and Smol J.P.: Lakes and reservoirs as sentinels, integrators, and regulators of climate change, Limnology and Oceanography, 54, https://doi.org/10.4319/lo.2009.54.6_part_2.2273, 2009.

Xenopoulos, M., Lodge, D., Frentress, J., Kreps, T., Bridgham, S., Grossman, E., and Jackson, C.: Regional Comparisons of Watershed Determinants of Dissolved Organic Carbon in Temperate Lakes from the Upper Great Lakes Region and Selected Regions Globally, Limnology and oceanography, 48, 2321–2334, https://doi.org/10.4319/lo.2003.48.6.2321, 2003.

Yao, X., Liu, S., Han, L., Sun, M., Zhao, L.: Definition and classification system of glacial lake for inventory and hazards study, Journal of Geographical Sciences, 28(2), 193–205, https://doi:10.1007/s11442-018-1467-z, 2018.

Zakharova, E.A., Kouraev, A.V., Stephane, G., Franck, G., Desyatkin, R.V., Desyatkin, A.R.: Recent dynamics of hydro-ecosystems in thermokarst depressions in Central Siberia from satellite and in situ observations: Importance for agriculture and human life, Science of The Total Environment, 615, 1290-1304, https://doi.org/10.1016/j.scitotenv.2017.09.059, 2018.

Zakharov, E., Smetanin, N., Sidorov, I., Zakharova, O., Filippova, V., and Zakharova, N.: Distribution of the Muskrat (Ondatra zibethicus L.) and the American Mink (Neovison vison Schreber) in Yakutia (Northeast Asia, Russia), Russian Journal of Biological Invasions, 14, 329–337, https://doi.org/10.1134/S2075111723030219, 2023.

Zakharov, E.S., Safronov, V.M., Zakharova, N.N., Petrov, R.E., Filippova, V.V., Koryakina, L.P., and Kruse, S.: Abundance dynamics of the Siberian weasel (Mustela sibirica) and their determinants on the northeastern periphery of its geographic range (Yakutia, Russia), Rus. J. Theriol., 21, 153–161, https://doi.org/10.15298/rusjtheriol.21.2.06, 2022.

Zanaga, D., Van De Kerchove, R., Daems, D., De Keersmaecker, W., Brockmann, C., Kirches, G., Wevers, J., Cartus, O., Santoro, M., Fritz, S., Lesiv, M., Herold, M., Tsendbazar, N.-E., Xu, P., Ramoino, F., and Arino, O.: ESA WorldCover 10 m 2021 v200 (v200) [dataset], ZENODO, https://doi.org/10.5281/zenodo.7254221, 2022.

Zhirkov, A., Sivtsev, M., Lytkin, V., Kirillin, A., Séjourné, A., and Wen, Z.: An Assessment of the Possibility of Restoration and Protection of Territories Disturbed by Thermokarst in Central Yakutia, Eastern Siberia, Land, 12, 197, https://doi.org/10.3390/land12010197, 2023.

Zimmermann, H.H., Raschke, E., Epp, L.S., Stoof-Leichsenring, K.R., Schwamborn, G., Schirrmeister, L., Overduin, P.P., and Herzschuh, U.: Sedimentary ancient DNA and pollen reveal the composition of plant organic matter in Late Quaternary permafrost sediments of the Buor Khaya Peninsula (north-eastern Siberia), Biogeosciences, 14, 575–596, https://doi.org/10.5194/bg-14-575-2017, 2017.

12 Appendix

Table A1: Overview of lake location and the administrative and topographic settings of the 66 sampled lakes sorted according to the lake type (mountain lakes, connected alaas lakes, old alaas lakes, new thermokarst lakes). In addition, we code the group of new thermokarst lakes related to their stage of thermokarst lake development (*dyede, §tyympy, #shallowing, see chapter introduction for details on the lake genesis). Lake shape (CTO close to oval, OE oval elongated, CTR close to round, R round)

Lake code EN21	District	Latitude N	Longitude E	Topographic setting	Area (ha)	Length (km)	Width (km)	Max depth (m)	Lake shape
Mountain lakes (ML)									
401	Verkhoyansky	63.33302	141.06282	Verkhoyansk mountains	478.01	4.01	1.86	43	CTO
402	Verkhoyansky	63.32696	141.0843	Verkhoyansk mountains	31.88	0.82	0.54	12.6	CTR
403	Verkhoyansky	63.32012	141.07993	Verkhoyansk mountains	2.83	0.3	0.18	14.1	CTO
404	Verkhoyansky	63.32943	141.1181	Verkhoyansk mountains	4.96	0.36	0.25	11.3	CTR
405	Verkhoyansky	63.43886	140.3983	Verkhoyansk mountains	55.36	1.04	0.84	33.8	CTR
406	Verkhoyansky	63.30998	141.072	Verkhoyansk mountains	1.78	0.23	0.09	6.7	CTR
407	Verkhoyansky	63.31018	141.0634	Verkhoyansk mountains	13.48	0.84	0.25	14.3	OE
408	Verkhoyansky	63.38775	140.5752	Verkhoyansk mountains	11.24	0.57	0.34	8.9	CTR
409	Verkhoyansky	63.39182	140.5811	Verkhoyansk mountains	0.34	0.13	0.06	5.5	CTO
410	Verkhoyansky	63.23035	142.9573	Verkhoyansk mountains	5.73	0.46	0.21	7.4	CTO
411	Verkhoyansky	63.22168	142.8945	Verkhoyansk mountains	16.11	0.71	0.41	7.8	CTO
412	Tomponsky	63.21885	139.5503	Verkhoyansk mountains	4.75	0.34	0.16	3.2	CTR
413	Tomponsky	63.22801	139.5759	Verkhoyansk mountains	0.25	0.12	0.09	4.1	OE
414	Verkhoyansky	63.32861	141.1654	Verkhoyansk mountains	1.39	0.25	0.08	5.2	CTO
415	Verkhoyansky	63.33238	141.1591	Verkhoyansk mountains	0.82	0.13	0.09	5.2	CTR
Connected alaas lake (CAL)									
417	Churapchinsky	62.07997	132.3637	Abalakh terrace	6.59	0.39	0.24	1.7	CTR
419	Churapchinsky	62.08767	132.3534	Abalakh terrace	14.78	0.57	0.42	3.4	CTR
421	Churapchinsky	62.01409	132.4127	Abalakh terrace	24.27	0.8	0.48	1.7	CTR
422	Churapchinsky	62.035	132.3634	Abalakh terrace	20.83	0.68	0.41	2.1	CTR
427	Megino-Kangalassky	62.14336	130.93548	Magan terrace	303.63	3.76	1.39	2.4	CTO
435	Megino-Kangalassky	62.35747	130.61391	Tyungyulu terrace	83.81	2.08	0.83	3.1	OE
439	Megino-Kangalassky	62.16978	130.67147	Tyungyulu terrace	354.34	3.19	2.3	6.9	CTR
441	Megino-Kangalassky	62.20703	130.71456	Tyungyulu terrace	368.51	2.06	2.02	2.4	R
Old alaas lake (OAL)									
420	Churapchinsky	62.03883	132.3943	Abalakh terrace	3.93	0.38	0.19	1.6	CTO
425	Megino-Kangalassky	62.16929	130.9102	Magan terrace	25.62	1.15	0.32	1.5	OE
426	Megino-Kangalassky	62.18077	130.8822	Magan terrace	7.70	0.68	0.18	8.4	OE
426-2	Megino-Kangalassky	62.17728	130.87956	Magan terrace	1.69	0.26	0.1		CTO

430	Megino-Kangalassky	62.31045	130.33331	Bestyakh terrace	25.25	0.63	0.42		CTR
431	Megino-Kangalassky	62.12932	130.86965	Magan terrace	8.24	0.41	0.39	2.1	CTR
433	Megino-Kangalassky	62.13806	130.87054	Magan terrace	6.24	0.46	0.22	7	CTO
436	Megino-Kangalassky	62.35076	130.35281	Bestyakh terrace	27.32	0.93	0.46	2.4	CTO
437	Megino-Kangalassky	62.3447	130.37543	Tyungyulu terrace	3.42	0.27	0.21	0.5	CTR
438	Megino-Kangalassky	62.15538	130.63903	Tyungyulu terrace	2.83	0.14	0.08	1.8	R
440	Megino-Kangalassky	62.20035	130.65014	Tyungyulu terrace	22.67	0.69	0.58	1	CTR
442	Megino-Kangalassky	61.78578	130.50197	Abalakh terrace	5.09	0.31	0.18	2	CTR
443	Megino-Kangalassky	61.78637	130.48923	Abalakh terrace	4.56	0.35	0.26	1.5	CTR
444	Megino-Kangalassky	61.7799	130.49321	Abalakh terrace	1.88	0.16	0.12	1.9	R
446	Megino-Kangalassky	61.76476	130.45989	Abalakh terrace	2.50	0.22	0.12	2	CTR
447	Megino-Kangalassky	61.7655	130.46841	Abalakh terrace	2.53	0.26	0.12	2.8	CTR
449	Megino-Kangalassky	61.7471	130.5389	Abalakh terrace	0.73	0.13	0.08	1.6	CTR
452	Megino-Kangalassky	61.76038	130.55066	Abalakh terrace	5.36	0.36	0.21	2.8	CTR
453	Megino-Kangalassky	61.89956	130.49017	Tyungyulu terrace	13.76	0.65	0.37	2.8	CTR
454	Megino-Kangalassky	61.89654	130.42726	Tyungyulu terrace	5.38	0.36	0.17	1.2	CTR
455	Megino-Kangalassky	61.90249	130.41174	Tyungyulu terrace	27.87	0.99	0.35	1	CTO
456	Megino-Kangalassky	61.88556	130.44829	Tyungyulu terrace	4.54	0.19	0.13		R
457	Megino-Kangalassky	61.73336	130.2533	Tyungyulu terrace	160.06	3.06	0.97	0.7	OE
459	Megino-Kangalassky	61.77814	130.37526	Abalakh terrace	52.73	0.99	0.54		CTR
463	Megino-Kangalassky	61.74491	130.50345	Abalakh terrace	7.67	0.5	0.22	2.8	CTO
464	Megino-Kangalassky	61.7558	130.49233	Abalakh terrace	2.76	0.22	0.2	5.6	CTR
465	Megino-Kangalassky	61.75424	130.4924	Abalakh terrace	0.08	0.05	0.03		CTR
466	Megino-Kangalassky	61.75357	130.49204	Abalakh terrace	0.08	0.04	0.03		CTR
New thermokarst lake (NTL)									
416*	Churapchinsky	62.08455	132.3706	Abalakh terrace	1.25	0.15	0.11	1.3	CTR
418§	Churapchinsky	62.08219	132.3473	Abalakh terrace	1.04	0.14	0.09	4.8	CTR
423*	Tattinsky	62.38716	133.7447	Abalakh terrace	1.59	0.24	0.08	3.1	CTO
424*	Tattinsky	62.3299	133.6651	Abalakh terrace	1.67	0.19	0.15	4.9	CTR
428*	Megino-Kangalassky	62.28146	130.3724	Bestyakh terrace	145.52	1.97	1	19.3	CTR
429*	Megino-Kangalassky	62.26311	130.33965	Bestyakh terrace	50.60	1.1	0.62	5.6	CTR
432*	Megino-Kangalassky	62.13574	130.88602	Magan terrace	2.64	0.25	0.14	2.1	CTR
434§	Megino-Kangalassky	62.14543	130.8669	Magan terrace	0.08	0.06	0.06	2.1	CTO
445*	Megino-Kangalassky	61.7676	130.49493	Abalakh terrace	0.14	0.06	0.03	1	CTR
448#	Megino-Kangalassky	61.74609	130.53302	Abalakh terrace	0.14	0.04	0.04	2	R

450§	Megino-Kangalassky	61.73757	130.52488	Abalakh terrace	3.12	0.31	0.11	3.9	CTO
451§	Megino-Kangalassky	61.73978	130.52555	Abalakh terrace	1.23	0.15	0.11		CTR
458#	Megino-Kangalassky	61.73217	130.26011	Tyungyulu terrace	2.05	0.14	0.14	4.1	R
462*	Megino-Kangalassky	61.71745	130.48135	Tyungyulu terrace	20.22	0.63	0.38	1.7	CTR
467§	Megino-Kangalassky	61.76225	130.48483	Abalakh terrace	0.34	0.08	0.05	3.2	CTR

1456

Table A2: Overview of temperature- and precipitation-related CHELSA bioclimatic variables (CHELSA V2.1, Karger et al. 2017) used in this study.

Abbreviation	CHELSA short name	Description	Unit
Temperature-related variables			
MAT	bio_1	Mean annual air temperature	°C
Tmax	bio_5	Mean maximum daily air temperature of the warmest month	°C
Tmin	bio_6	Mean minimum daily air temperature of the coldest month	°C
Precipitation-related variables			
TAP	bio_12	Total annual precipitation	kg m^{-2} $year^{-1}$
Pwet	bio_13	Precipitation amount of the wettest month	kg m^{-2} $month^{-1}$
Pdry	bio_14	Precipitation amount of the driest month	kg m^{-2} $month^{-1}$

Table A3: Hydrophysical and hydrochemical properties of surface water samples collected from the central part of the lakes (n = number of lakes, SD = standard deviation (±) and CV = coefficient of variation (%)). Below detection limit shows the number of samples under this category and elements with their detection limit.

Variable	n	Mean	Median	SD	Skew	n	Mean	Median	SD	Skew	n	401	405
	Lowland lakes					Mountain lakes					Deep mountain lakes		
Lake depth (m)	**44**	3.1	2.1	3.05	3.8	**13**	8.2	7.4	3.8	0.5	**2**	43	33.8
Secchi depth (m)	**33**	0.8	0.6	0.55	0.7	**13**	2.8	2.6	1.2	0.9	**2**	7.91	5.16
Elevation (m asl)	**51**	190	173	51	0.6	**13**	1069	1036	175	-0.1	**2**	946	1260
Lake area (km^2)	**51**	0.4	0.05	0.8	3.1	**13**	0.07	0.05	0.09	1.9	**2**	4.8	0.6
pH	**51**	8.7	8.8	0.55	-1	**13**	7.6	7.6	0.5	0.1	**2**	7.91	7.69
EC (µS cm^{-1})	**51**	1520.4	1228	1048.1	1.9	**13**	93.7	83.2	55.4	0.4	**2**	70.9	66.1
DOC (mg L^{-1})	**51**	97.8	75.9	73.8	2.5	**13**	14.8	14.0	5.2	0.1	**2**	7.29	5.15
TDS	**51**	1318	1161	1006.4	1.8	**13**	55.5	61.0	30.3	0.1	**2**	49	46
Ca^{2+} (mg L^{-1})	**51**	25	26	13.9	0.5	**13**	9.4	10.6	5.1	0.0	**2**	7.6	8.8
Mg^{2+} (mg L^{-1})	**51**	120	112	74.6	1.3	**13**	3.8	4.2	2.0	0.3	**2**	3	2.1
Na^{+} (mg L^{-1})	**51**	191	124	211.8	2.8	**13**	1.0	0.9	0.5	0.2	**2**	2.4	0.8
K^{+} (mg L^{-1})	**51**	17	10	21.4	2.9	**13**	0.6	0.7	0.2	0.0	**2**	0.6	0.5
Si (mg L^{-1})	**46***	3	2	2.7	1.6	**12**[a]	0.7	0.6	0.3	0.2	**2**	0.4	0.5
PO_4^{3-} (mg L^{-1})	**19**[§]	2	1	1.9	1.8	**0**[b]	-	-	-	-	**0**[n]	-	-
HCO_3^{-} (mg L^{-1})	**50**	904.4	709.3	606.9	1.4	**13**	36.6	32.6	21.9	0.5	**2**	31.3	30.4
Cl^{-} (mg L^{-1})	**51**	86.7	42.3	113.1	3.4	**0**[c]	-	-	-	-	**0**[o]	-	-
SO_4^{2-} (mg L^{-1})	**40**[+]	82.7	8.1	194.1	3.3	**11**[d]	4.6	1.7	6.2	2.1	**2**	4.4	2.8
F^{-} (µg L^{-1})	**49**[^]	0.4	0.4	0.3	2.1	**3**[e]	0.12	0.13	0.02	-0.8	**0**[p]	-	-
NO_3^{-} (mg L^{-1})	**2**[°]	0.4	0.4	-	-	**1**[f]	0.2	0.2	-	-	**1**[q]	0.3	-
Fe (µg L^{-1})	**9**[&]	373.5	238.8	318.4	1.32	**6**[g]	323.6	239.6	237.7	1.7	**0**[r]	-	-
Al (µg L^{-1})	**3**[#]	165.6	177.4	107.4	-0.5	**2**[h]	101.4	101.4	61.6	-	**0**[s]	-	-
Sr^{2+} (µg L^{-1})	**51**	217.2	207.9	99.3	0.33	**12**[i]	97.3	108.1	43.5	-0.3	**2**	79	81
Ba^{2+} (µg L^{-1})	**39**[$]	39.2	37.3	12.8	1.3	**1**[j]	21.9	21.9	-	-	**0**[t]	-	-
Mn (µg L^{-1})	**17**[@]	116.5	42.6	138.2	1.9	**4**[k]	42.7	33.2	26.4	1.5	**0**[u]	-	-
Br^{-} (µg L^{-1})	**47**[<]	2.8	1.5	4.7	4.7	**0**[l]	-	-	-	-	**0**[v]	-	-
P (mg L^{-1})	**24**[~]	0.6	0.5	0.6	1.7	**0**[m]	-	-	-	-	**0**[w]	-	-
Below detection limit	**(n=5, **Si** < 0.10 mg L^{-1})* *§ (n=32, **PO_4^{3-}** < 0.10 mg L^{-1})* *+ (n=11, **SO_4^{2-}** < 0.10 mg L^{-1})* *^ (n=2, **F^{-}** < 0.10 mg L^{-1})* *° (n=49, **NO_3^{-}** < 0.10 mg L^{-1})* *& (n=42, **Fe** < 100 µg L^{-1})* *# (n=48, **Al** < 50 µg L^{-1})* *$ (n=12, **Ba^{2+}** < 20 µg L^{-1})* *@ (n=34, **Mn** < 20 µg L^{-1})* *< (n=4, **Br^{-}** < 0.10 µg L^{-1})* *~ (n=27, **P** < 0.10 mg L^{-1})*					*[a] (n=1, **Si** < 0.10 mg L^{-1})* *[b] (n=13, **PO_4^{3-}** < 0.10 mg L^{-1})* *[c] (n=13, **Cl^{-}** < 0.10 mg L^{-1})* *[d] (n=2, **SO_4^{2-}** < 0.10 mg L^{-1})* *[e] (n=10, **F^{-}** < 0.10 µg L^{-1})* *[f] (n=12, **NO_3^{-}** < 0.10 mg L^{-1})* *[g] (n=7, **Fe** < 100 µg L^{-1})* *[h] (n=11, **Al** < 50 µg L^{-1})* *[i] (n=1, **Sr^{2+}** < 20 µg L^{-1})* *[j] (n=12, **Ba^{2+}** < 20 µg L^{-1})* *[k] (n=9, **Mn** < 20 µg L^{-1})* *[l] (n=13, **Br^{-}** < 0.10 µg L^{-1})* *[m] (n=13, **P** < 0.10 mg L^{-1})*					*[n] (n=2, **PO_4^{3-}** < 0.10 mg L^{-1})* *[o](n=2, **Cl^{-}** < 0.10 mg L^{-1})* *[p] (n=2, **F^{-}** < 0.10 µg L^{-1})* *[q] (n=1, **NO_3^{-}** < 0.10 mg L^{-1})* *[r] (n=2, **Fe** < 100 µg L^{-1})* *[s] (n=2, **Al** < 50 µg L^{-1})* *[t] (n=2, **Ba^{2+}** < 20 µg L^{-1})* *[u] (n=2, **Mn** < 20 µg L^{-1})* *[v] (n=2, **Br^{-}** < 0.10 µg L^{-1})* *[w] (n=2, **P** < 0.10 mg L^{-1})*		

Table A4: **Taxonomic richness of macrophyte amplicon sequence variants (median in bold, range, and counts (in brackets)) from sedDNA functional groups for the four lake types: connected alaas lakes (CAL), old alaas lakes (OAL), mountain lakes (ML), and new thermokarst lakes (NTL).**

Functional groups	CAL **median** min-max (counts)	OAL **median** min-max (counts)	ML **median** min-max) (counts)	NTL **median** min-max (counts)	Total richness (Total counts)
Floating	**3** 0-5 (75,679)	**2** 0-6 (192,048)	**0** 0-3 (34,847)	**1** 0-6 (39,177)	7 (341,751)
Submerged	**8** 4-10 (1,090,540)	**6.5** 2-11 (2,506,335)	**6** 1-10 (456,279)	**6** 1-9 (927,318)	13 (4,980,472)
Sub-emergent	-	**0** 0-1 (10,183)	**1** 0-1 (219,152)	**0** 0-1 (20,476)	2 (249,811)
Emergent	**8.5** 1-16 (75,058)	**8** 0-18 (801,663)	**5.5** 1-17 (85,692)	**7** 1-22 (194,950)	65 (1,157,363)
Total richness **median** min-max (total counts)	42 **20** 6-28 (1,241,277)	66 **17** 3-31 (3,510,229)	49 **9** 2-40 (795,970)	61 **17** 8-35 (1,181,921)	87 (6,729,397)

Table A5: Counts and taxonomic richness* of terrestrial plant amplicon sequence variants (ASVs) derived from sedDNA grouped by vegetation type for the four lake types: connected alaas lakes (CAL), old alaas lakes (OAL), mountain lakes (ML), and new thermokarst lakes (NTL).

Functional groups	CAL **median** min-max (counts)	OAL **median** min-max (counts)	ML **median** min-max) (counts)	NTL **median** min-max (counts)	Total richness (Total counts)
Trees	**2** 1-4 (39,077)	**2** 0-6 (152,642)	**4** 1-4 (564,065)	**3.5** 1-6 (243,701)	9 (999,485)
Shrubs	**0** 1-3 (75)	**0** 0-9 (10,622)	**3** 1-12 (123,766)	**0.5** 0-12 (15,827)	16 (150,290)
Grasses and herbs	**9** 3-25 (115,480)	**9.5** 1-29 (463,231)	**3.5** 0-30 (58,558)	**9.5** 0-23 (88,695)	83 (725,964)
Bryophyta	**0** 0-1 (11)	**0** 0-1 (861)	**0** 0-3 (323)	**0** 0-2 (705)	8 (1,900)
Total richness **median** min-max (total counts)	43 **14** 4-26 (154,643)	69 **12** 3-33 (627,356)	68 **11** 2-40 (746,712)	81 **17** 2-29 (348,928)	116 (1,877,639)

Table A6: Overview of abbreviations and details of variables in this study.

Group	Short name	Detailed description
Lake Types	ML	mountain lakes
	CAL	connected alaas lakes
	NTL	new thermokarst lakes
	OAL	old alaas lakes
Lake salinity	freshwater	freshwater lakes TDS < 1000 mg L^{-1} (mg L^{-1})
	brackish	brackish lakes TDS > 1000 mg L^{-1} (mg L^{-1})
Lake clusters	C1	Cluster 1 (*Fig. A4*)
	C2	Cluster 2 (*Fig. A4*)
	C3	Cluster 3 (*Fig. A4*)
SedDNA-derived macrophyte functional groups	DNA_fm	prop. of sedDNA-derived floating macrophyte functional group (%)
	DNA_sm	prop. of sedDNA-derived submerged macrophyte functional group (%)
	DNA_sem	prop. of sedDNA-derived submerged-emergent macrophyte functional group (%)
	DNA_em	prop. of sedDNA-derived emergent macrophyte functional group (%)
SedDNA-derived terrestrial plants functional groups	trees	prop. of sedDNA-derived tree terrestrial plant functional groups (%)
	shrubs	prop. of sedDNA-derived shrubs terrestrial plant functional groups (%)
	grasses	prop. of sedDNA-derived grasses and forbs terrestrial plant functional groups (%)
	bryophyta	prop. of sedDNA-derived bryophyte terrestrial plant functional groups (%)
Satellite-derived land cover*	FOREST	prop. of satellite-derived forest land cover (%)
	GRASS	prop. of satellite-derived grassland land cover (%)
	WETLAND	prop. of satellite-derived wetland land cover (%)
	BARE	prop. of satellite-derived barren land cover (%)
	TUNDRA	prop. of satellite-derived tundra land cover (%)
Topography**	Elev	elevation (m a.s.l)
Climate data***	MAT	mean annual air temperature (C°)
	Tmax	mean maximum daily air temperature of the warmest month (C°)
	Tmin	mean minimum daily air temperature of the coldest month (C°)
	TAP	total annual precipitation (kg m^{-2} $year^{-1}$)
	Pwet	precipitation amount of the wettest month (kg m^{-2} $month^{-1}$)
	Pdry	precipitation amount of the driest month (kg m^{-2} $month^{-1}$)

* Land cover was obtained from ESA World Cover 2021 (© ESA WorldCover project / Contains modified Copernicus Sentinel data (2021) processed by ESA WorldCover consortium; Zanaga et al. 2022. ESA WorldCover 10 m 2021 v200. https://doi.org/10.5281/zenodo.7254221, last accesses on May 2024)
** source for elevation was obtained during fieldwork
*** Climate data is derived from CHELSA V2.1 (Karger et al. 2017, last accessed on May 2024)

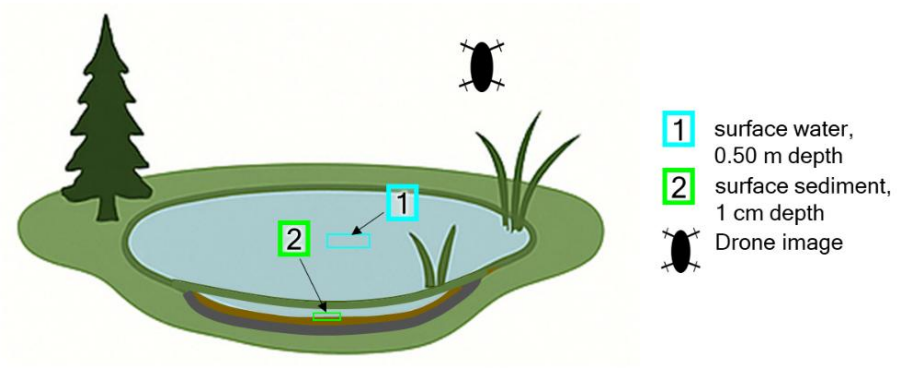


Figure A1: Scheme for the lake sampling during the 2021 Yakutia expedition. The sampling categories included surface water sampling [1] for in situ physico-chemical measurements and taking water samples, and [2] lake surface-sediment sampling for sedDNA. In addition, we mapped the lake shore area with multispectral drone-based imaging. The figure was generated using Perplexity AI.

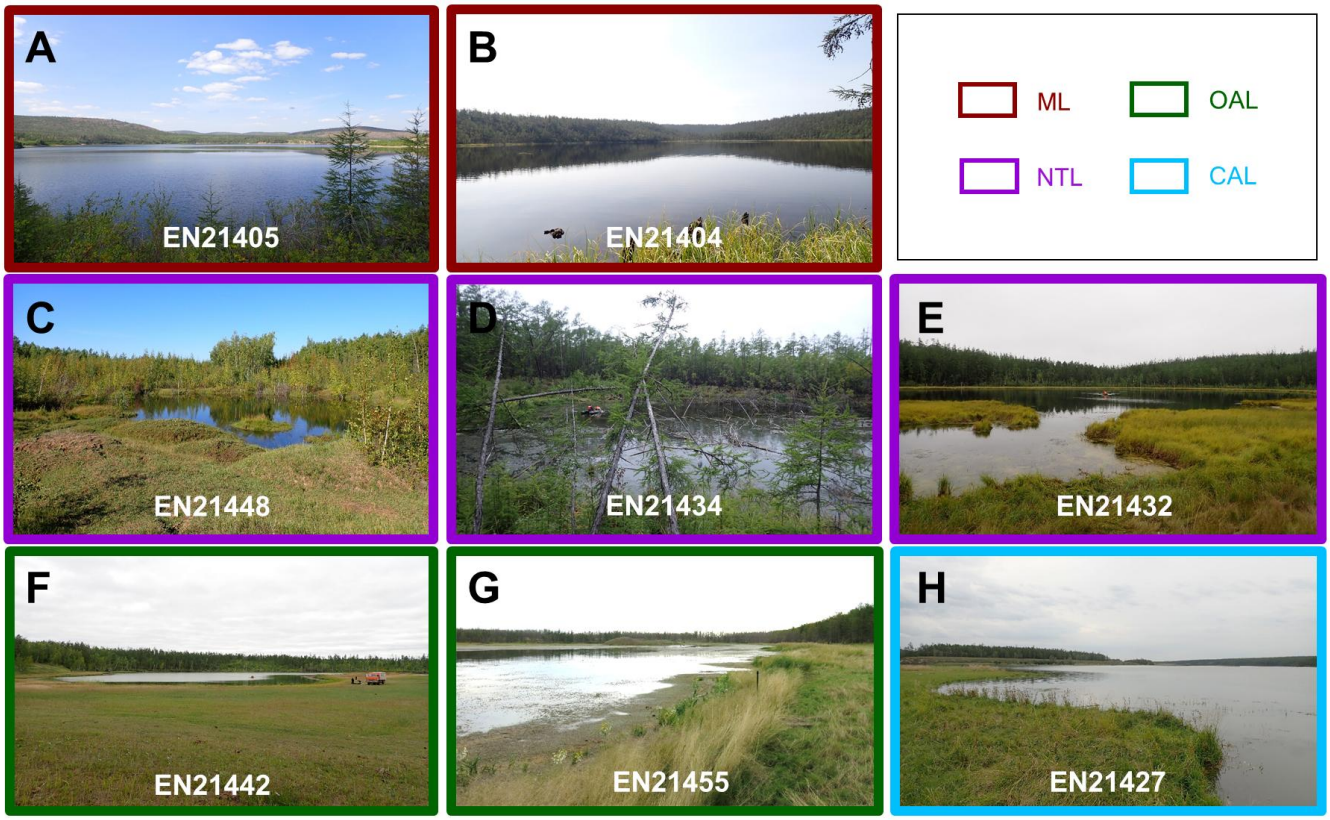


Figure A2: (A-H) Photos of examples of the different lake types sampled: A and B show mountain lakes (ML) in the Verkhoyansk Mountains (A-deep lake, B-shallow lake) and C–H show lowland thermokarst lakes in Central Yakutia (NTL-new thermokarst lakes, OAL-old alaas lakes, and CAL-connected alaas lakes). The lowland thermokarst lakes are sorted according to the thermokarst lake sequence (C-dyede lake stage, D-tyympy lake stage, E-shallowing lake stage, F-old alaas lake, G-old alaas lake with pingo, H-connected alaas lake).

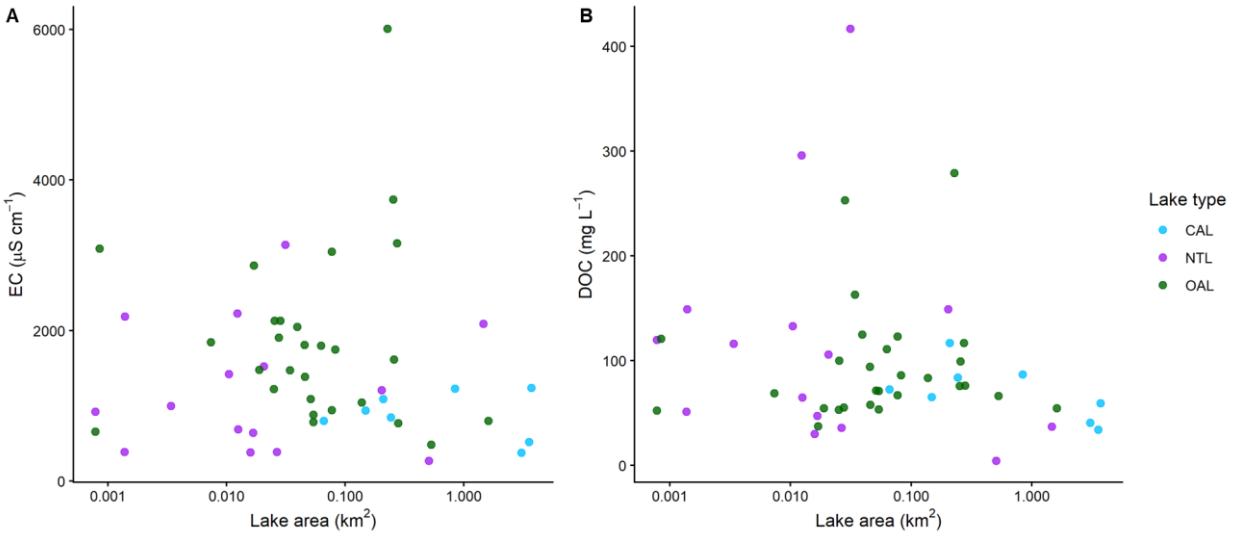


Figure A3 Linear-log graph of (A) specific electrical conductivity (EC) and (B) dissolved organic carbon (DOC) concentration versus lake area for Central Yakutian lowland lakes. Points are colour coded according to lake type: old alaas lakes (OAL, green), connected alaas lakes (CAL, blue), and new thermokarst lakes (NTL, purple). Note that lake area (km^2) in panels A, B is shown on a logarithmic scale.

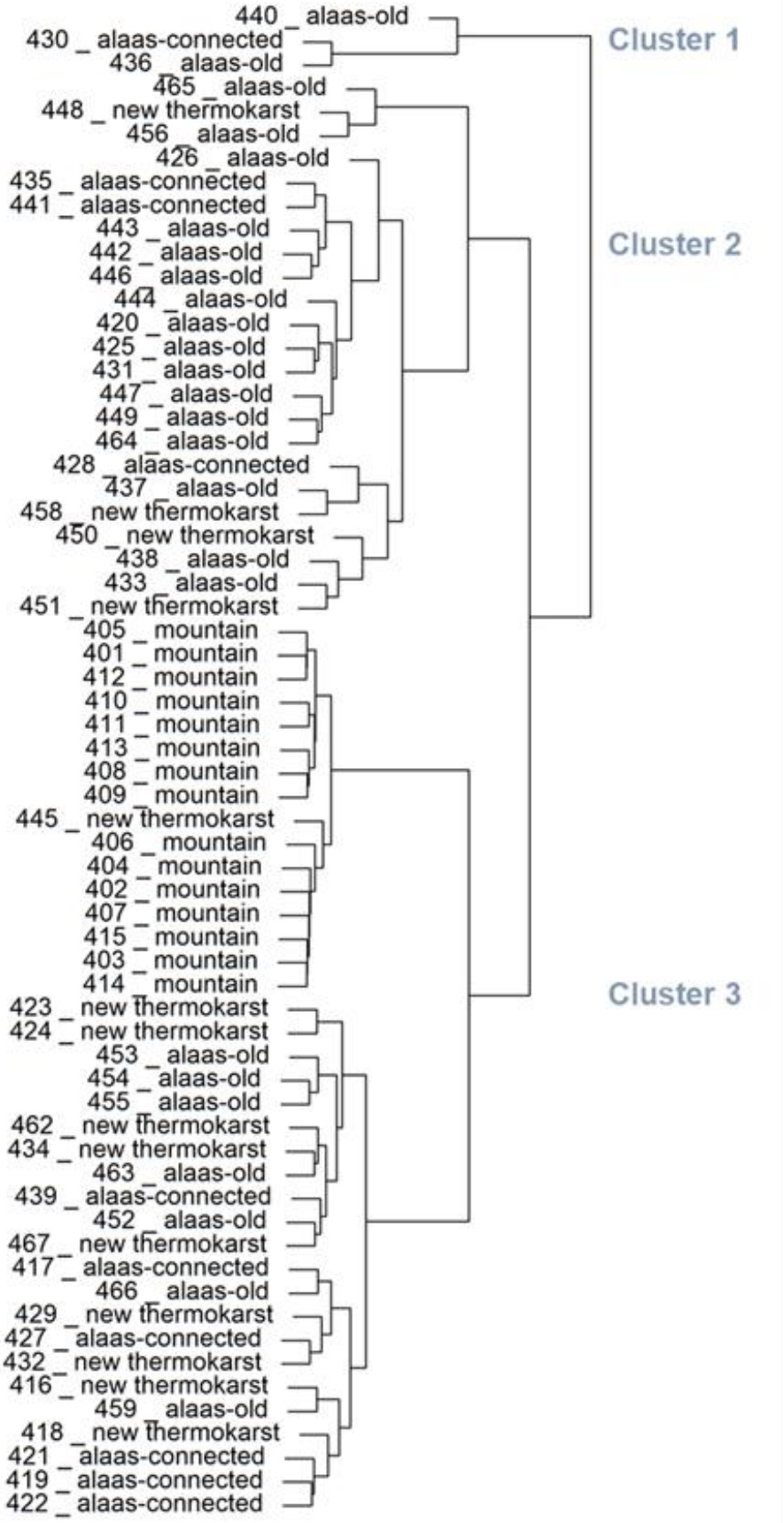


Figure A4: Hierarchical clustering of the sampled lakes by major ion hydrochemistry.

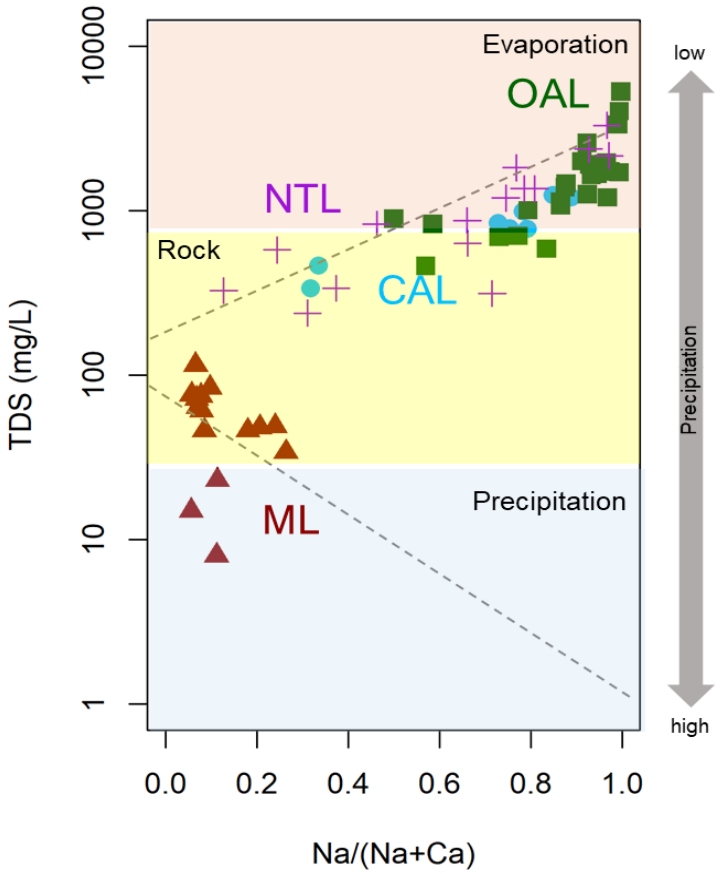


Figure A5: Gibbs diagram of Na^+ / (Na^+ + Ca^{2+}) versus log-normalised total dissolved solids (TDS: mg L^{-1}) in the sampled lakes. Mountain lakes (ML) are displayed as brown triangles, connected alaas lakes (CAL) as blue circles, old alaas lakes (OAL) as green squares, new thermokarst lakes (NTL) as purple crosses.

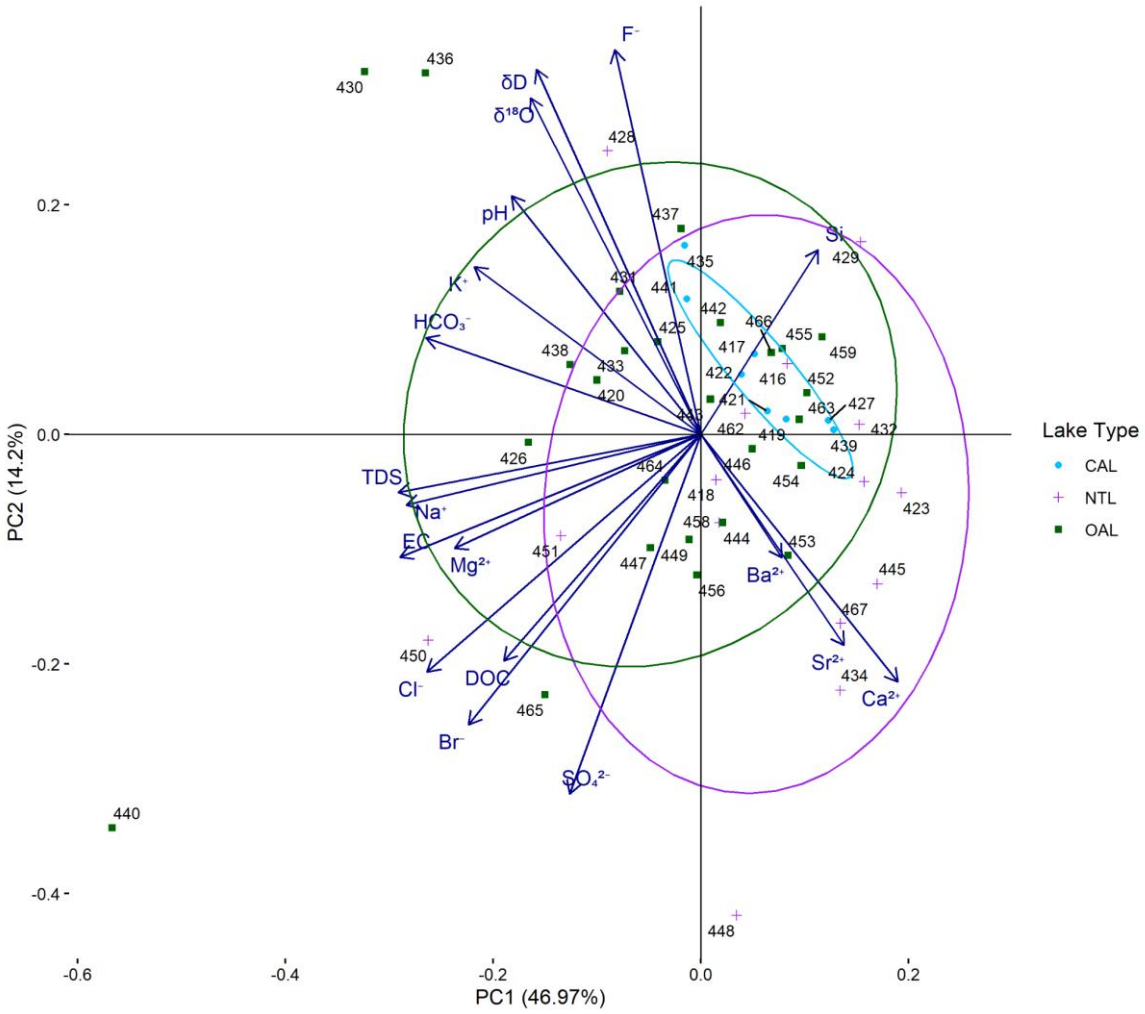


Figure A6: PC1-PC2 biplot of hydrophysical and hydrochemical variables (minor and major ions, hydrophysics, isotopes) from the group of lowland lakes only, with ellipses outlining the lake types: new thermokarst lakes (NTL; purple crosses), old alaas lakes (OAL; green squares), and connected alaas lakes (CAL; blue circles). The length of the vectors expresses the loadings of the hydrochemical variables in the PC1-PC2 space (abbreviations see Table A6).

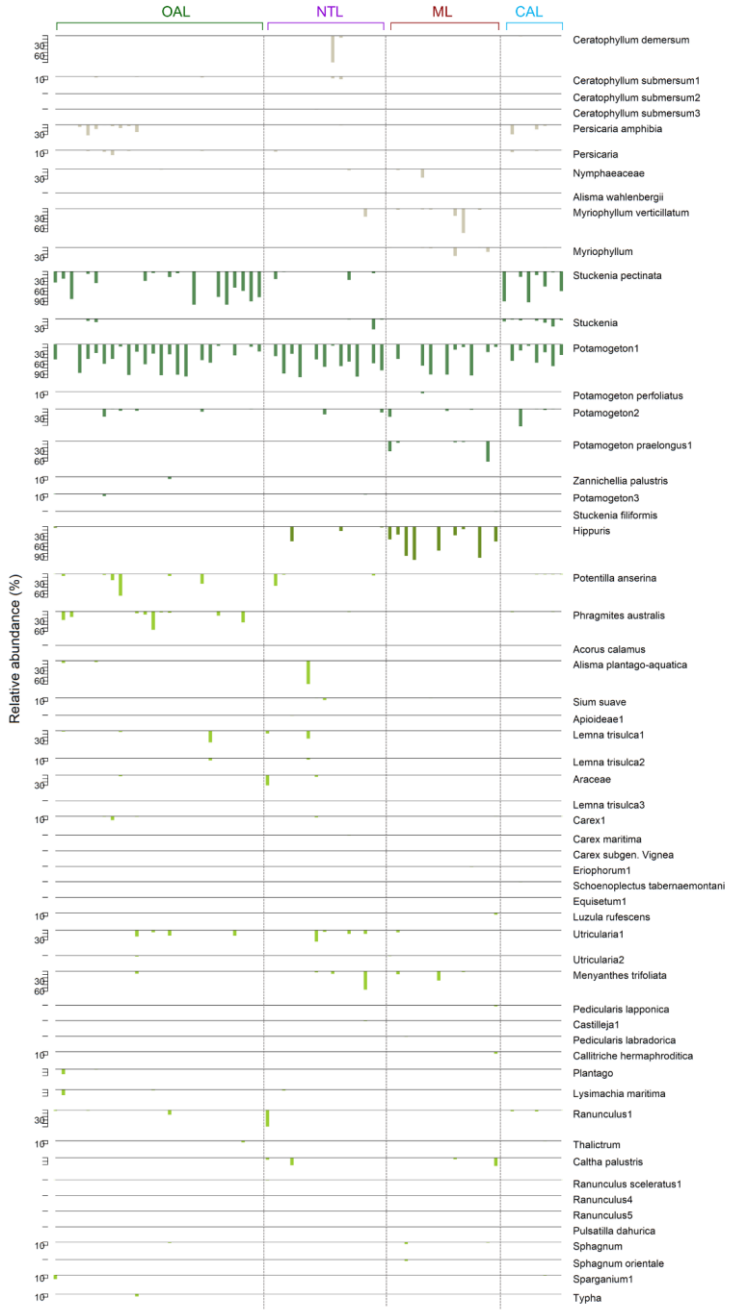


Figure A7: Relative abundance of sedDNA-derived macrophytes. Relative proportion is shown with a subset higher than 5%. Lake types are connected alaas lakes (CAL), old alaas lakes (OAL), mountain lakes (ML), new thermokarst lakes (NTL).

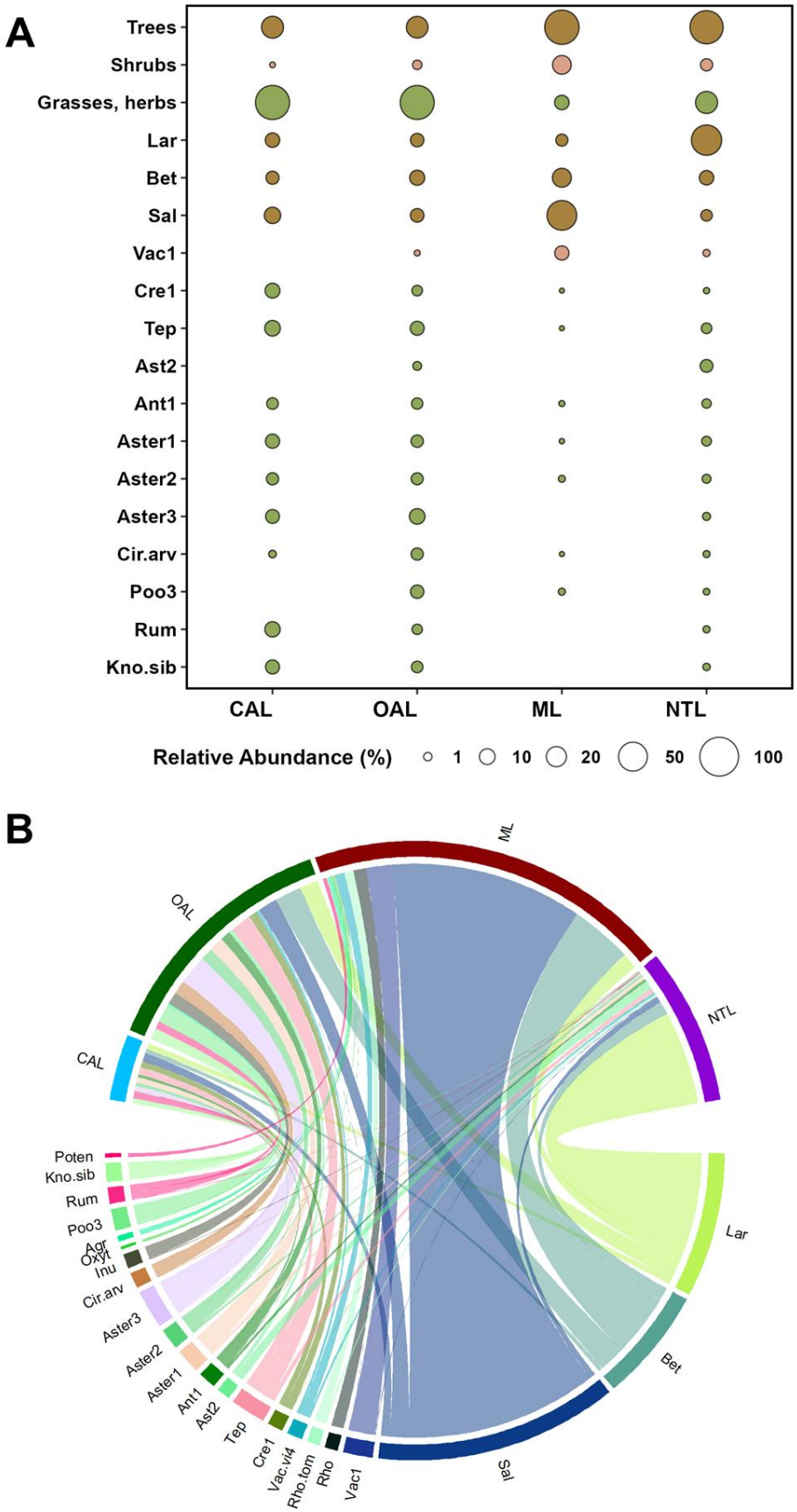


Figure A8: (A) Bubble-chart illustrating the relative abundance of terrestrial vegetation by lake type: mountain lakes (ML), old alaas lakes (OAL), connected alaas lakes (CAL), and new thermokarst lakes (NTL). Relative abundance of plant types is displayed as total share by lake type, and a subset of plants with >5% occurrence is also shown. (B) Chord-diagram showing the most abundant taxa within the four lake types and their relationship to lake type. Short names of taxa refer as follows: Poten-Potentilleae, Kno.sib-*Knorringia sibirica*, Rum-*Rumex*, Poo3-Pooideae3, Inu-*Inulinae*, Cir.arv-*Cirsium arvense*, Aster3-Asteraceae3, Aster2-Asteraceae2, Aster1-Asteraceae1, Ant1-Anthemideae1, Ast2-Asteroideae2, Tep-*Tephroseris*, Cre2-Crepidinae2, Vac.vi4-*Vaccinium vitis-idaea4*, Rho.tom-*Rhodondendron tomentosum*, Rho-*Rhodondendron*, Vac1-*Vaccinium1*, Sal-Salicaceae, Bet-*Betula*, Lar-*Larix*.

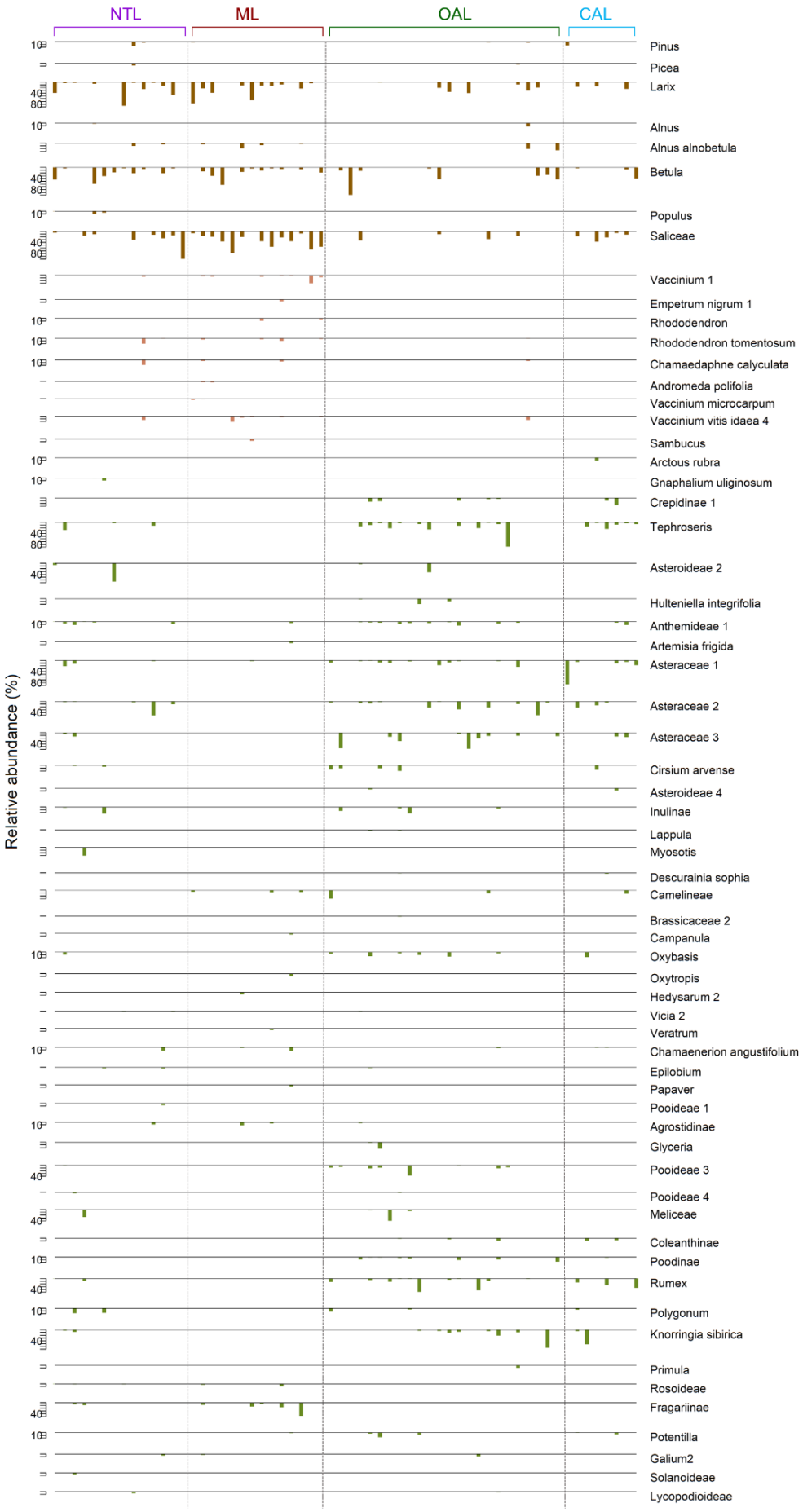


Figure A9: Relative abundance of sedDNA-derived terrestrial plants. Relative proportion is shown with a subset higher than 5%. Lake types are connected alaas lakes (CAL), old alaas lakes (OAL), mountain lakes (ML), new thermokarst lakes (NTL).

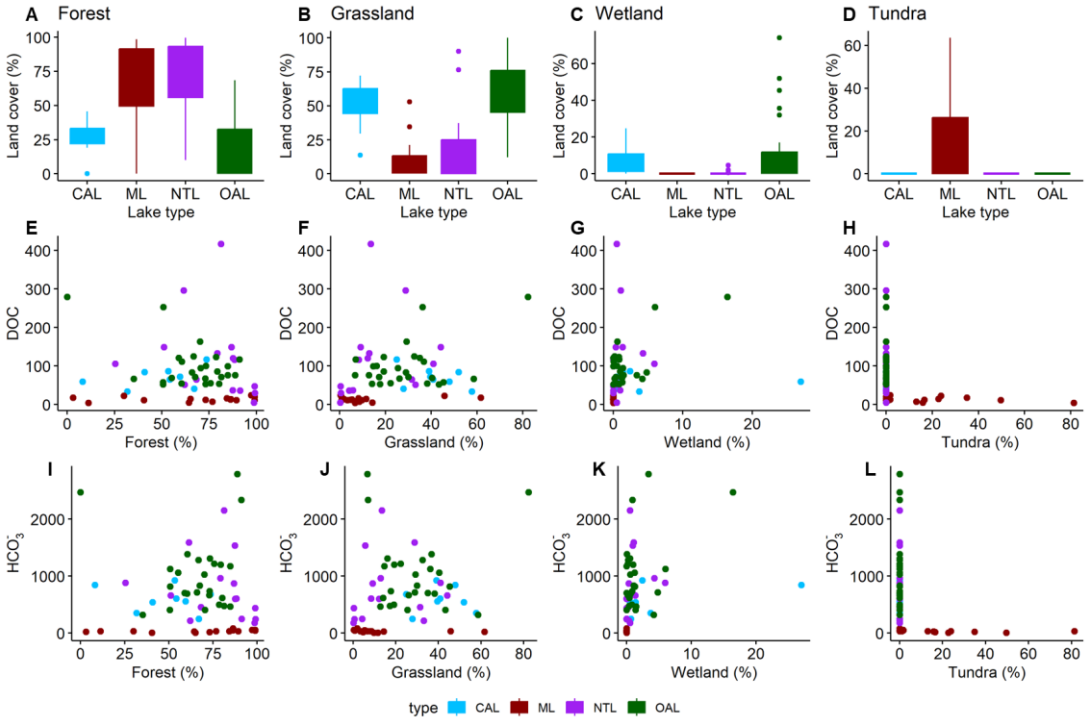


Figure A10. Percentage of satellite-derived land cover (50 m buffer zone) per lake type by land-cover category, shown as boxplots (A-D). Scatterplots display the relationship (E-H) between fractional forest land cover and DOC, and (I-L) between fractional forest land cover and HCO_3^-. DOC and HCO_3^- values are given in mg L^{-1}. Mountain lakes (ML) in brown, new thermokarst lakes (NTL) in purple, connected alaas lakes (CAL) in blue, and old alaas lakes (OAL) in green.

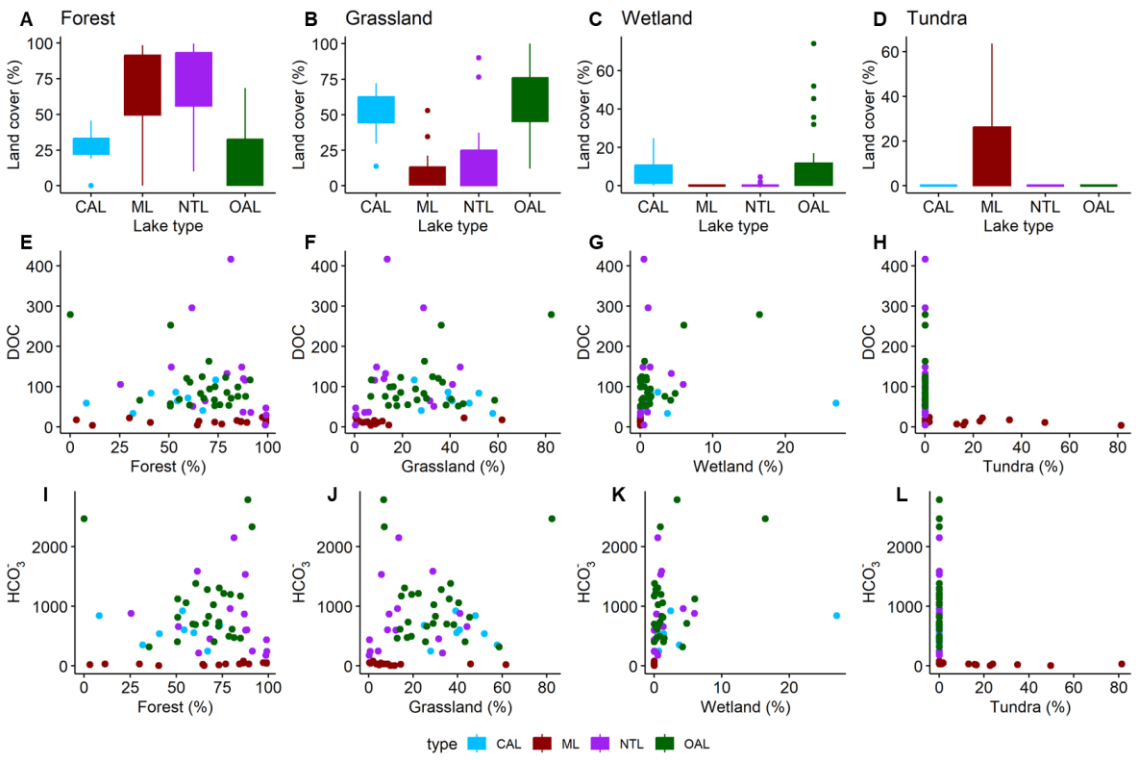


Figure A11: Percentage of satellite-derived land cover (360 m buffer zone) per lake type by land-cover category, shown as boxplots (A-D). Scatterplots display the relationship (E-H) between fractional forest land cover and DOC, and (I-L) between fractional forest land cover and HCO_3^-. DOC and HCO_3^- values are given in mg L^{-1}. Mountain lakes (ML) in brown, new thermokarst lakes (NTL) in purple, connected alaas lakes (CAL) in blue, and old alaas lakes (OAL) in green.

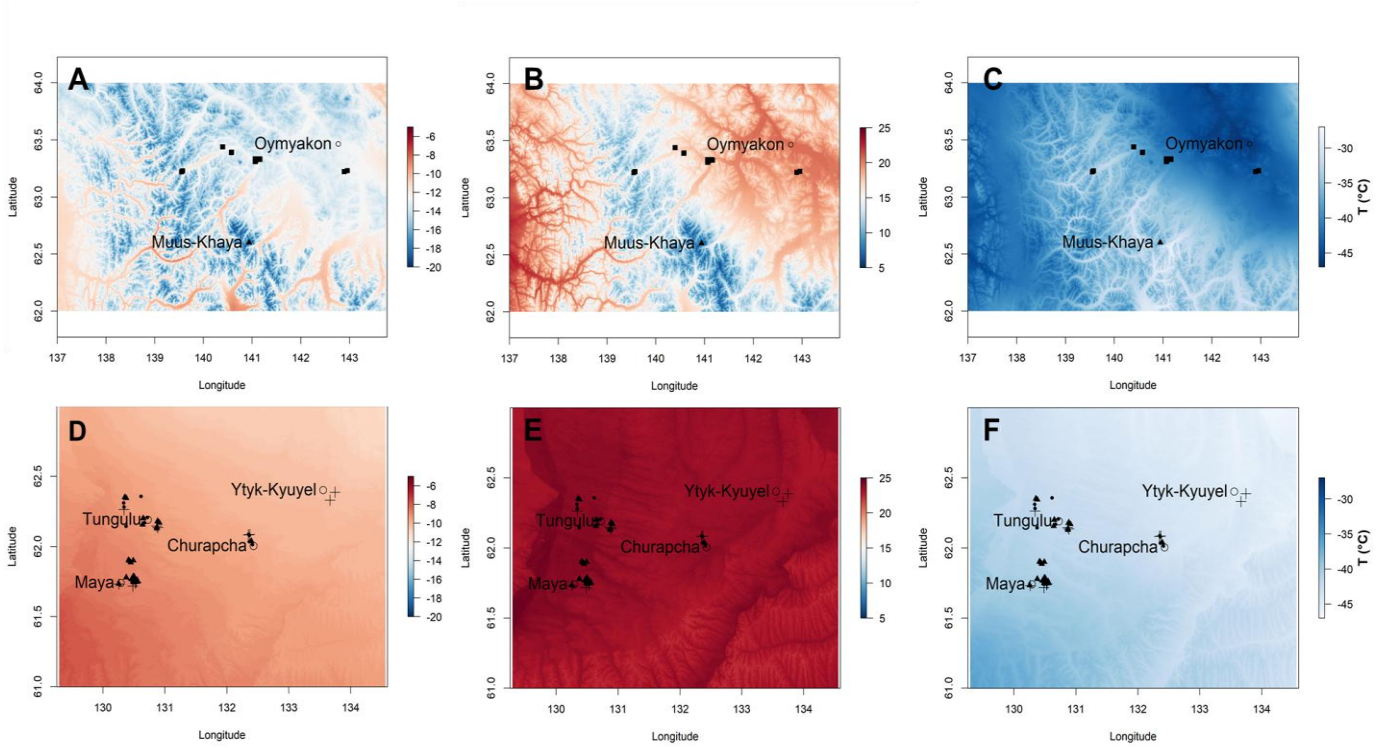


Figure A12: Temperature gradient extracted from CHELSA for the mountain region (upper row panels A-C) and the lowland region (lower row panels D-F). Left panel columns (A, D) display the mean annual temperature (MAT). Mid panel columns (B, E) display the maximum temperature of warmest month (Tmax). Right panel columns (C, F) display the minimum temperature of the coldest month (Tmin). Lake types are shown by different symbols: connected alaas lakes (filled circles), old alaas lakes (cubes), mountain lakes (triangles), new thermokarst lakes (crosses). Nearby settlements are given in circles, the highest mountain Muus Khaya is marked as a filled triangle.

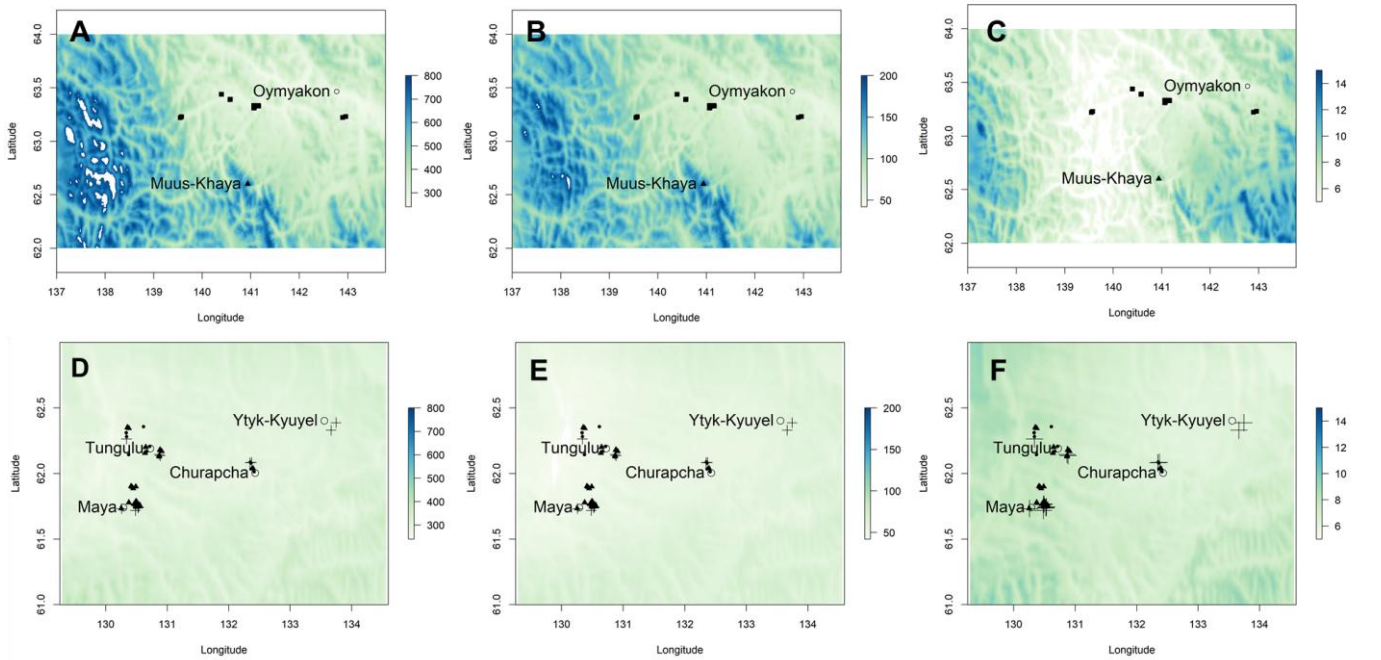


Figure A13: Precipitation gradient extracted from CHELSA for the mountain region (upper row panels A-C) and the lowland region (lower row panels D-F). Left panel columns (A, D) display the total annual precipitation (TAP, shown in kg m^{-2} $year^{-1}$ (=mm)). Mid panel columns (B, E) display the precipitation of the wettest month (Pwet, shown in kg m^{-2} (=mm) $month^{-1}$). Right panel columns (C, F) display the precipitation of the driest month (Pdry, shown in kg m^{-2} (=mm) $month^{-1}$). Lake types are shown by different symbols: connected alaas lakes (filled circles), old alaas lakes (cubes), mountain lakes (triangles), new thermokarst lakes (crosses). Nearby settlements are given in circles, the highest mountain Muus Khaya is marked as a filled triangle.

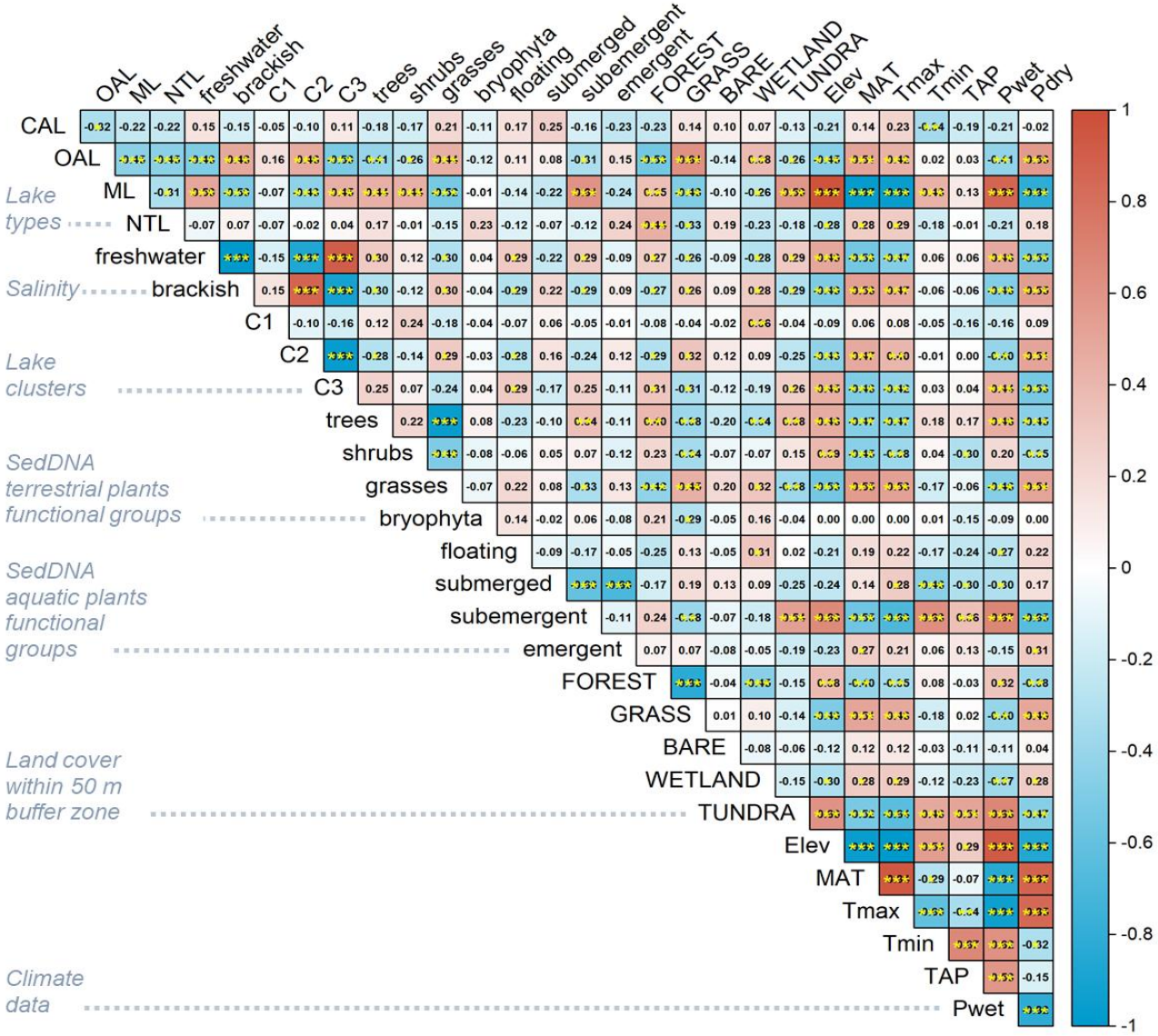


Figure A14: Correlation matrix for the main environmental variables (abbreviations see Table A6).

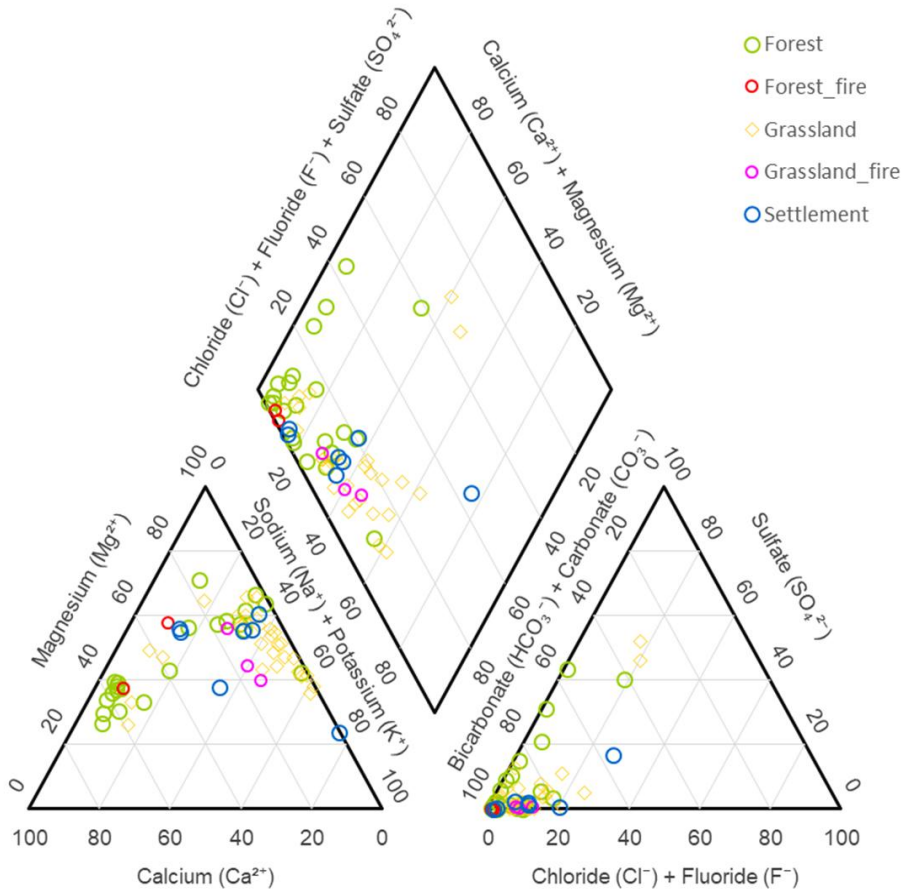


Figure A15: Hydrochemical facies of lakes linked to the dominant different land-cover type in a Piper diagram showing forest (green), forest fire-scars (red), grasslands (yellow), grasslands with fire-scars (pink), and settlements (blue).

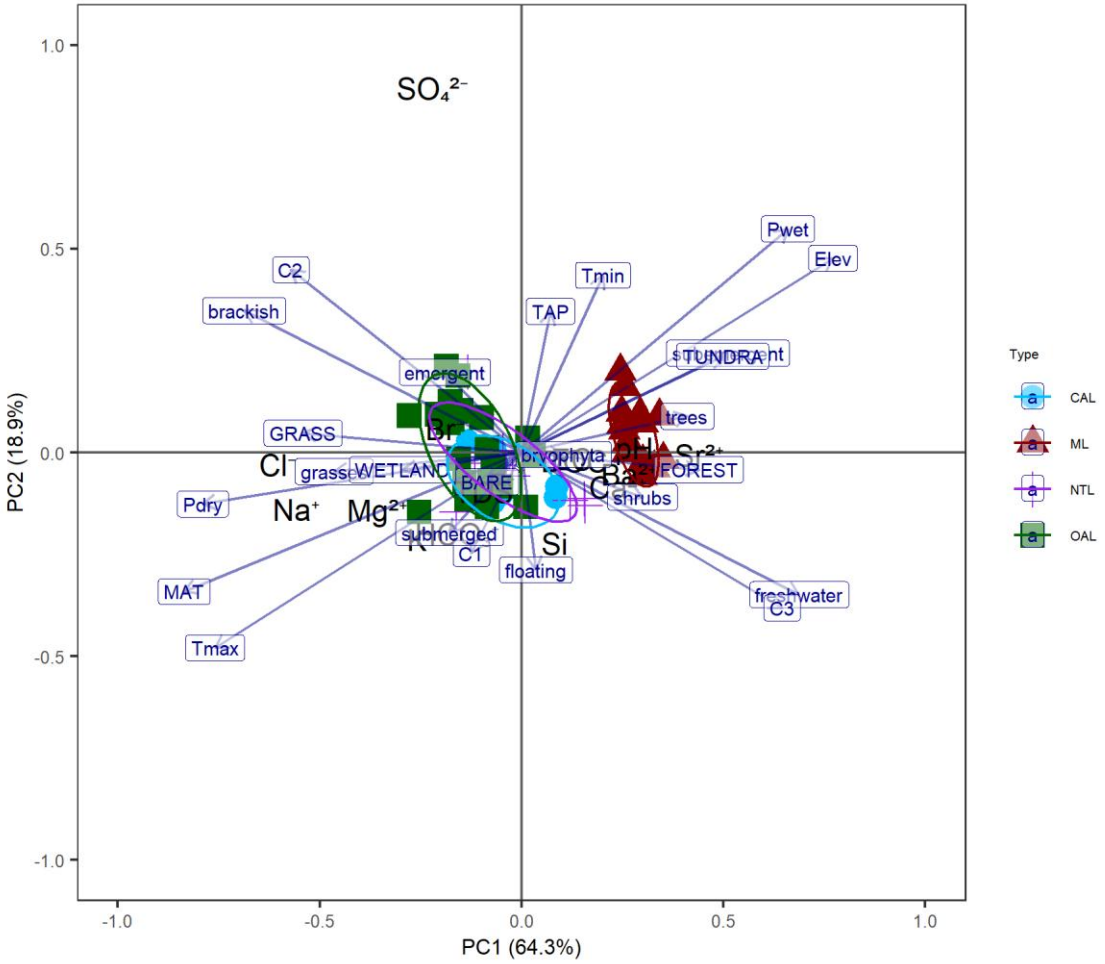


Figure A16: Principal component analysis (PCA) performed on all hydrophysical and hydrochemical and environmental variables related to all lakes. Arrows indicate the loadings of the different environmental variables. The colour legend shows the lake types: connected alaas lakes (CAL), old alaas lakes (OAL), new thermokarst lakes (NTL), mountain lakes (ML). For better visibility variable names have been abbreviated, please see Table A6.

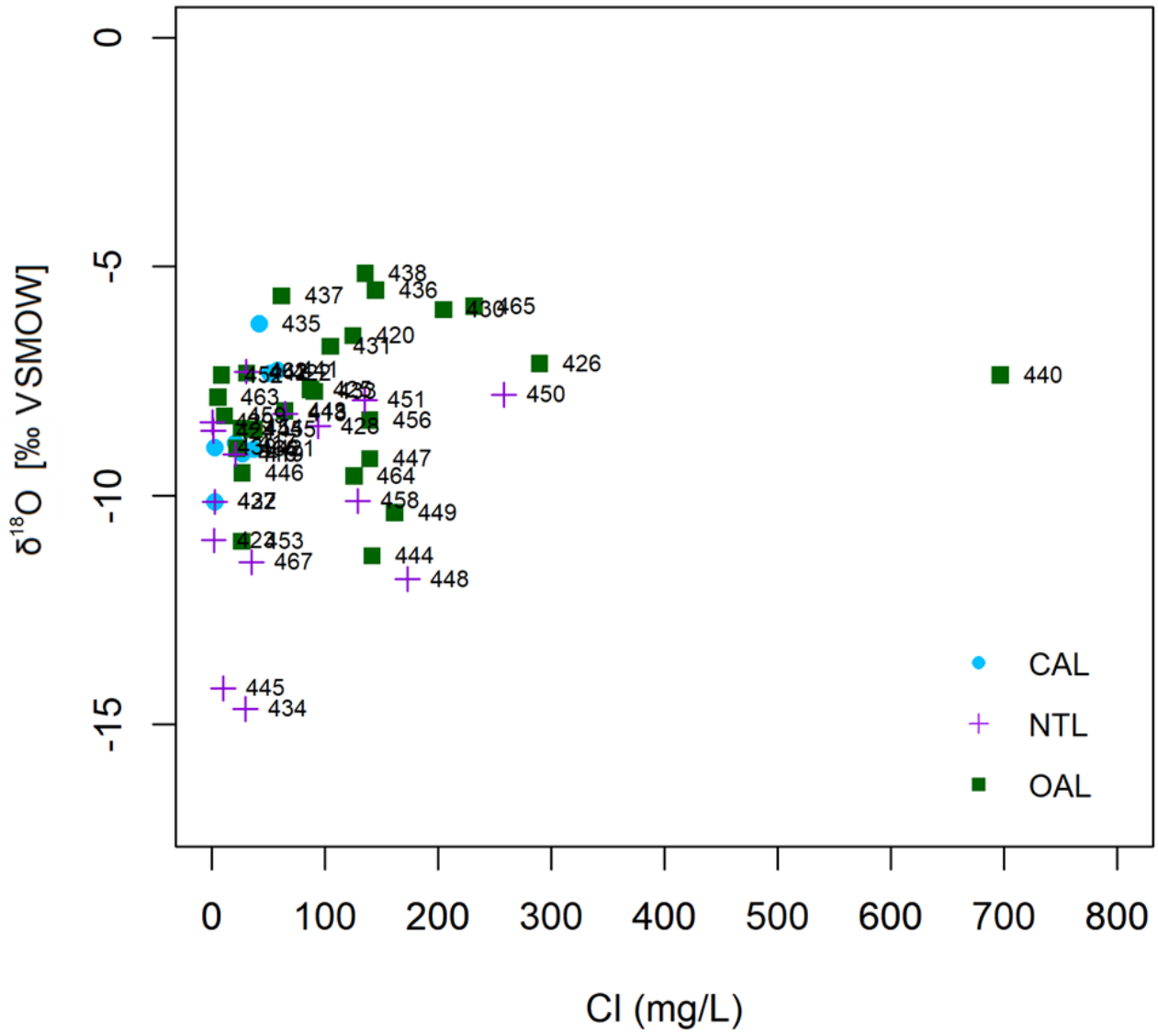


Figure A17: Scattergram of $\delta^{18}O$ versus chloride concentration (mg L^{-1}), for the group of lowland lakes only: old alaas lakes (OAL; green squares), connected alaas lakes (CAL; blue circles), and new thermokarst lakes (NTL; purple crosses).

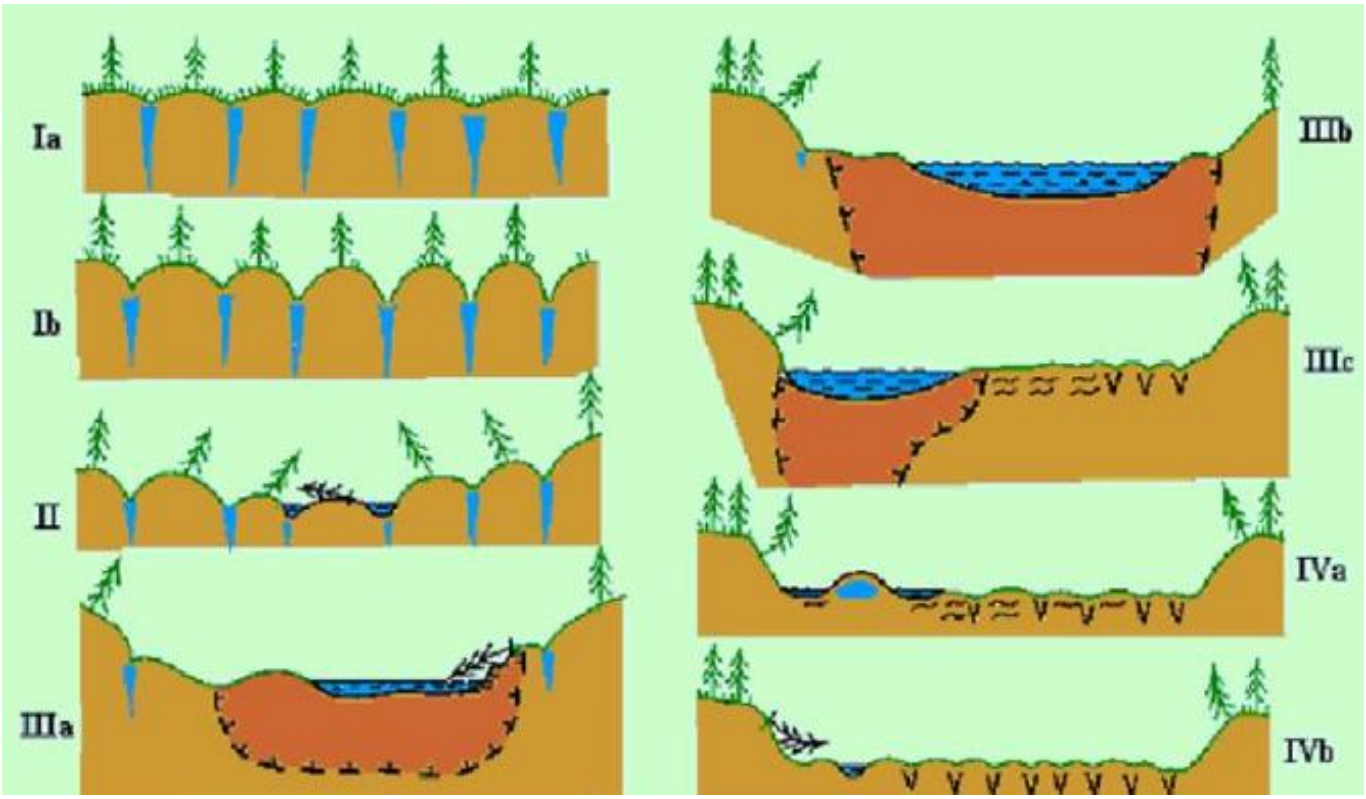


Figure A18: Scheme of the thermokarst lake stage development by Soloviev (1959) from Desyatkin and Desyatkin, 2006. Ia-forested lowland landscape with ground-ice rich (frozen pore water and Pleistocene ice wedges) subground (Pleistocene ice wedges filled with ground ice visualised in blue), such as the Yedoma sedimentary deposits; Ib-Byllar stage; II-Dyede lake stage; IIIa-Tyympy lake stage with unfrozen sediment (talik, visualised in orange) framing the water body and beneath; IIIb-alaas lake stage with unfrozen talik framing the water body and beneath; IIIc-mature alaas with a residual lake, a reduced talik beneath the water body and refreezing and formation and degradation of Holocene ice wedges on the alaas ground; IVa-old alaas with a pingo (ice hill with ice core visualised in blue) forming in the shallow residual alaas lake; IVb-old alaas with a very reduced residual alaas lake, degraded ice wedge geomorphology within the alaas and forest only on the upland.